VERIFICATION OF CFD PREDICTIONS FOR AIRFLOW VELOCITY AND PRESSURE THROUGH AN AIR FILTER

By

WAYNE GIMLIN

Bachelor of Science

University of Oklahoma

Norman, Oklahoma

1989

Submitted to the Faculty of the
Graduate College of
Oklahoma State University
in partial fulfillment of
the requirements of the
Degree of
MASTER OF SCIENCE
July, 1997

VERIFICATION OF CFD PREDICTIONS FOR AIRFLOW

VELOCITY AND PRESSURE THROUGH

AN AIR FILTER

Thesis Approved:

Thesis Adviser

Dean of the Graduate College

ACKNOWLEDGEMENTS

I would like to express my sincere appreciation to all those who supported, guided, and assisted me with this thesis. I would like to thank my advisor, Dr. Chambers for bringing me into the project and for guiding me throughout. I would like to thank Dr. Price for assisting me in enrolling at OSU.

I would also like to give my appreciation to my colleagues and friends, Scott Pickel, Francisco Canabal, Shenghong Yao, Sachin Anand, Fakhroddin Jadbabaei-Moghad, and Guojiang Liu who always had the time to assist me whenever I asked.

I would like to express my appreciation to Purolator Products, Inc. and the Oklahoma Center for the Advancement of Science and Technology for their financial support with this project.

I would especially like to thank my fiancee, Susanne, my parents, Richard and Joanne Gimlin, my siblings, Jennifer, Kenneth, and Janna, my grandparents, and the rest of my family for their constant love, support and encouragement throughout my life.

- This air filter filtration project is supported by Purolator Products Inc. and the Oklahoma Center for the Advancement of Science and Technology (OCAST)

TABLE OF CONTENTS

Chapter	Page
I. Introduction	1
1.1 Background	1
1.2 Objective	2
1.3 Filters	3
1.4 Modeling of Filters	4
1.4.1 Development of Equations	4
1.4.2 Pleat Modeling	7
1.5 Turbulence Modeling	8
1.5.1 Turbulent Flow Within Pleat Crevasse	8
1.5.2 Turbulent Flow Upstream and Downstream of Filter	13
1.6 Previous Computational Results	14
1.7 Experimental Verification	16
II. Numerical Method Derivation	19
2.1 Introduction	19
2.2 Conservation of Mass	19
2.3 Conservation of Momentum	22
2.3.1 Momentum Outside the Filter	24
2.3.2 Momentum Inside the Filter	25
2.4 Numerical Approximation	29
2.4.1 Discretized Continuity Equation	30
2.4.2 Discretized Momentum Equation in Non-Filter Region	30
2.4.2.1 Time Derivative	31
2.4.2.2 Pressure Derivative	31
2.4.2.3 Horizontal and Vertical Convective Derivatives	32
2.4.2.4 Viscous Diffusion Terms	33
2.4.3 Discretized Momentum Equation in the Filter Region	33
2.4.3.1 Darcy Diffusion Terms	34
2.4.3.2 Inertial Term	34
2.4.4 Pressure Iteration	34
2.4.5 Stability Considerations	37
III. Numerical Method Application	39
3.1 Introduction	39
3.1.1 Computational Simulation of an A13192 Filter Pleat	39
3.1.2 Computational Simulation of an Experimental Flow	40
3.2 Determination of Filter Inertial Resistance and Permeability	41

3.3 Determination of Generalized Node Matrix 42
3.4 Intra-Filter Modeling 45
3.5 Boundary and Initial Conditions 46
3.5.1 Initial Conditions 47
3.5.2 Inlet Boundary 47
3.5.3 Outlet Boundary 47
3.5.4 Side Boundaries 48
3.6 Specific Parameters of the A13192 Pleat Configuration 49
3.7 Specific Parameters of the Experimental Flow Configuration 51
3.8 Time Constraints 53
3.9 Summary of Parameters 54
IV. Verification Experiment 56
4.1 Introduction 56
4.2 Experimental Setup 56
4.3 Experimental Parameters 63
4.3.1 Laminar and Turbulent Flow 64
4.3.2 Measurement Location 66
V. Computational and Experimental Results 69
5.1 Experimental Results 69
5.1.1 Experimental Results: Tabular Representation 69
5.1.2 Experimental Results: Graphical Representation 72
5.1.3 Turbulence Intensity 73
5.1.4 Repeatability 75
5.2 Computational Results 75
5.2.1 Grid Density Study 75
5.2.2 Flow Domain Study 79
5.2.3 Permeability Study 81
5.2.4 Inertial Resistance Study 83
5.2.5 Porosity Study 85
5.2.6 Filter Thickness Study 86
5.2.7 Standard Experimental Configuration 87
5.2.8 A13192 Configuration Results 102
VI. Discussion 104
6.1 Analysis of Experiment 104
6.2 Comparison between Computational and Experimental Data 105
VII. Conclusions and Recommendations 109
7.1 Conclusions 109
7.2 Recommendations 110
References 112
Appendix A Experimental Configuration Results 115
Appendix B Experimental Derivation of Inertial Resistance and Permeability 128

LIST OF TABLES

Table	Page
3.1 Permeability and Inertial Resistance Terms	42
3.2 Summary of Parameters	55
5.1 Pressure Across Filter Medium and Grid Density	76
5.2 Pressure and Flow Domain	79
B.1 Filter Constant Experimental Results	130

LIST OF FIGURES

Figure Page

1.1 Cross Section of a Typical Pleated Air Filter 3

1.2 Typical Flow Through a Crevasse and Filter Pleat 10

1.3 Schematic of Filter Pleat Velocity Test 18

2.1 Arbitrary Finite Region 20

2.2 Finite Difference Control Node 29

3.1 Previous Computational Flow Simulations 40

3.2 Computational Flow Domain 41

3.3 General Matrix Description 44

3.4 Imposition of Rectangular Nodes Upon a Slanted Filter 45

3.5 Typical Flow Field Through an A13192 Air Filter 49

4.1 Experimental Flow Apparatus 58

4.2 Test Housing and Filter 59

4.3 Schematic of the Measurement System 61

4.4 Probe Volume 62

4.5 Boundary Layer Growth Within the Test Housing 65

4.6 Laser Beam Entry into Test Housing 66

4.7 Location of Measurement Points 67

5.1 U-Velocity Measurements 70

5.2 V-Velocity Measurements 71

5.3 Experimental Vertical Velocity (U-Velocity) vs. Scaled Horizontal and Vertical Position: L1=101.6 mm, L2=50.8 mm 72

5.4 Experimental Horizontal Velocity (V-Velocity) vs. Scaled Horizontal and Vertical Position: L1=101.6 mm, L2=50.8 mm 73

5.5 Turbulence Intensity vs. Scaled Horizontal and Vertical Position x/L1=101.6 mm, L2=50.8 mm 74

5.6 Pressure Through Filter Medium vs. Grid Density 77

5.7 U-Velocity Profile and Grid Density: x/L1=0.5, L1=101.6 mm, L2=50.8 mm 78

5.8 U-Velocity Profile and Vertical Flow Domain: x/L1=0.5, L2=50.8 mm 80

5.9 Pressure vs. Permeability 81

5.10 U-Velocity Profile and Permeability x/L1=0.5, L1=143.9 mm, L2=50.8 mm 82

5.11 Pressure Through Filter vs. Inertial Resistance 83

5.12 U-Velocity Profile and Inertial Resistance: x/L1=0.5, L1=143.9 mm, L2=50.8 mm 84

5.13 Pressure Through Filter vs. Porosity 85

5.14 U-Velocity Profile and Porosity x/L1=0.5, L1=143.9 mm, L2=50.8 mm 86

5.15 U-Velocity Profile and Filter Thickness x/L1=0.5, L1=101.6 mm, L2=50.8 mm 87

5.16 Comparison of Computational and Experimental U-Velocity Profile Experimental L1=101.6 mm, Computational L1=143.9 mm, L2=50.8 mm Profile 50.8 mm (2 in) Upstream of Filter Center 89

5.17 Comparison of Computational and Experimental U-Velocity Profile Experimental L1=101.6 mm, Computational L1=143.9 mm, L2=50.8 mm Profile 25.4 mm (1 in) Upstream of Filter Center 90

5.18 Comparison of Computational and Experimental U-Velocity Profile
Experimental L1=101.6 mm, Computational L1=143.9 mm, L2=50.8 mm
Profile 12.7 mm (0.5 in) Upstream of Filter Center 91

5.19 Comparison of Computational and Experimental U-Velocity Profile
Experimental L1=101.6 mm, Computational L1=143.9 mm, L2=50.8 mm
Profile at Filter Center 92

5.20 Comparison of Computational and Experimental U-Velocity Profile
Experimental L1=101.6 mm, Computational L1=143.9 mm, L2=50.8 mm
Profile 12.7 mm (0.5 in) Downstream of Filter Center 93

5.21 Comparison of Computational and Experimental U-Velocity Profile
Experimental L1=101.6 mm, Computational L1=143.9 mm, L2=50.8 mm
Profile 25.4 mm (1.0 in) Downstream of Filter Center 94

5.22 Comparison of Computational and Experimental U-Velocity Profile
Experimental L1=101.6 mm, Computational L1=143.9 mm, L2=50.8 mm
Profile 50.8 mm (2.0 in) Downstream of Filter Center 95

5.23 Comparison of Computational and Experimental V-Velocity Profile
Experimental L1=101.6 mm, Computational L1=143.9 mm, L2=50.8 mm
Profile 50.8 mm (2.0 in) Upstream of Filter Center 96

5.24 Comparison of Computational and Experimental V-Velocity Profile
Experimental L1=101.6 mm, Computational L1=143.9 mm, L2=50.8 mm
Profile 25.4 mm (1.0 in) Upstream of Filter Center 97

5.25 Comparison of Computational and Experimental V-Velocity Profile
Experimental L1=101.6 mm, Computational L1=143.9 mm, L2=50.8 mm
Profile 12.7 mm (0.5 in) Upstream of Filter Center 98

5.26 Comparison of Computational and Experimental V-Velocity Profile
Experimental L1=101.6 mm, Computational L1=143.9 mm, L2=50.8 mm
Profile at Filter Center 99

5.27 Comparison of Computational and Experimental V-Velocity Profile
Experimental L1=101.6 mm, Computational L1=143.9 mm, L2=50.8 mm
Profile 12.7 mm (0.5 in) Downstream of Filter Center 100

5.28 Comparison of Computational and Experimental V-Velocity Profile
Experimental L1=101.6 mm, Computational L1=143.9 mm, L2=50.8 mm
Profile 25.4 mm (1.0 in) Downstream of Filter Center 101

5.29 Comparison of Computational and Experimental V-Velocity Profile Experimental L1=101.6 mm, Computational L1=143.9 mm, L2=50.8 mm Profile 50.8 mm (2.0 in) Downstream of Filter Center 102

NOMENCLATURE

A(x)	duct cross sectional area	m^2
A_o	inlet cross sectional area	m^2
b	inertial resistance	m^{-1}
d	fringe spacing	m
E	redefined porosity	
f	Doppler frequency	s^{-1}
F	function term based on permeability, permeability based Reynolds number and filter geometry	
ibar	number of cells within the flow field in the x-direction	
i	cell counter in x-direction; tensor index in the x-direction	
i_i	tensor unit vector	
im1	imax-1	
imax	number of cells in the x-direction including boundaries	
j	cell counter in y-direction; tensor index in the y-direction	
jbar	number of cells within the flow field in the y-direction	
jm1	jmax-1	
jmax	number of cells in y-direction including boundaries	

K	filter medium permeability	m^2
K_{crit}	turbulent relaminarization criteria	
L	duct length	m
L	momentum	kg·m/s
n	indicates variable calculated at non-updated time n	
n+1	indicates variable calculated at updated time n+1	
n	unit normal vector	
nfilx	number of nodes spanning the filter medium in the x-direction	
nfily	number of nodes spanning the filter medium in the y-direction	
P	mean pressure	Pa
p	pressure divided by density	m^2/s^2
$p_{i,j}$	pressure index notation	m^2/s^2
Q	flow rate	m^3/s
Qe(x)	flow rate within a narrowing pleat crevasse	m^3/s
Qe_o	entrance flow rate into a narrowing pleat crevasse	m^3/s
Re	Reynolds Number	
Re_D	Reynolds Number based on fiber density	
$Re_{\sqrt{K}}$	Reynolds Number based on permeability	
t	time	s
t_n	filter thickness	mm
t_x	filter thickness in x-direction	mm
t_y	filter thickness in y-direction	mm

U	mean velocity in flow direction (x-direction)	m/s
$Ue(x)$	velocity along a narrowing crevasse	m/s
Ue_o	inlet velocity into a narrowing crevasse	m/s
$u_{i,j}$	velocity in x direction in index notation	m/s
V_i	flow velocity in the i direction	m/s
$\mathbf{V}$	flow velocity vector	m/s
$\mathbf{V_D}$	Darcy velocity vector	m/s
$v_{i,j}$	velocity in y-direction in index notation	m/s
W	pleat space	m
x_i	spatial direction, tensor notation	m
α	upstream differencing coefficient	
δ	porosity	
Γ	arbitrary boundary surface area	m^2
μ	dynamic viscosity	kg/m·s
σ_{ij}	stress tensor	Pa
$\sigma_{ij,i}$	gradient of stress tensor	Pa/m
ν	kinematic viscosity	m^2/s
ρ	density	kg/m^3
Ω	volume of arbitrary region	m^3
$\langle\rangle$	volume averaged variable	
,	tensor spatial derivative; also used in index notation	

CHAPTER I

INTRODUCTION

1.1 Background

Due to their importance as an integrated system in the automobile air intake system, air filters have been the focus of multiple engineering studies. The key role of an automobile air filter is the efficient removal of particles from the air used for the internal combustion process. Secondary requirements of the filter and filter housing include a low cost, compact space for packaging efficiency, durability, and a low resistance to the delivery of air to the engine.

Several of these requirements relate directly to the airflow through the filter. For example, a large delivery of air with low flow resistance is desirable for high engine performance. Obviously, a flow directed through an air filter will reduce this airflow rate which is characterized by a pressure drop through the filter. Additionally, experimental and computational studies [Duran, 1995; Newman, 1994] show that for larger particles a uniform air velocity profile across the filter can produce a higher removal of particulates along with changes in filter life and pressure drop effects.

To understand the airflow through an air filter, several studies using both computational and experimental methods have been performed. Recent work completed at the OSU Mechanical Engineering Laboratory used computational fluid dynamics (CFD) to

determine the velocity and pressure distribution of air through an air filter. These works [Cai,1993; Tebbutt, 1995; and Liu, 1995] simulate different aspects of the flow but use similar modeling techniques. Each of these works described the resulting distribution of velocity and the characteristic pressure drop as the flow passed through a simulated air filter. However, due to experimental complexities, no work was completed to verify these results by experimentation. This thesis was completed to further develop the existing computational models and verify these models with direct experimentation. This was accomplished with the creation of a CFD model and the use of a Laser Doppler Velocimetry (LDV) system which measures flow velocity on a point by point basis.

1.2 Objective

The objective of this research is to computationally model air flow through an air filter and verify this model through direct experimentation. Computational modeling techniques previously developed [Gurumoothy, 1990; Cai,1993; Tebbutt, 1995; and Liu, 1995] will be employed. Some of these techniques include the finite difference equation (FDE) staggered grid method used to discretize the Navier-Stokes governing fluid equations and the characterization of the filter as a porous medium employing Darcy's law, both of which are described in detail in subsequent sections.

To verify the computations, an experiment will be created to measure flow velocity and pressure change through a filter with the use of an LDV system and manometer. Once the CFD model is verified, past, present, and future results of computational research using similar modeling techniques can be given a higher level of confidence.

1.3 Filters

Automotive filters are used to remove particulates from the air being delivered to the engine. In general, air filters are made up of a non-woven cellulose fibrous mat that is pleated. These filters must provide a high dust removal efficiency and dust holding capacity while restricting the flow as little as possible. Normally, the filters are in a pleated shape so as to provide a maximum surface area for the airflow. This is advantageous because the higher surface area creates a greater filtration capability and lessens the pressure drop through the filter. Previous work in this project has examined the flow field and filtration of a typical production filter, the Purolator A13192. The pleats for this filter are approximately 3 cm high with a 3 mm pitch. The medium thickness is about 0.6 mm. Figure 1.1 shows a cross section of a pleated air filter. Note that in a real air filter, the corners are not sharp but rather rounded.

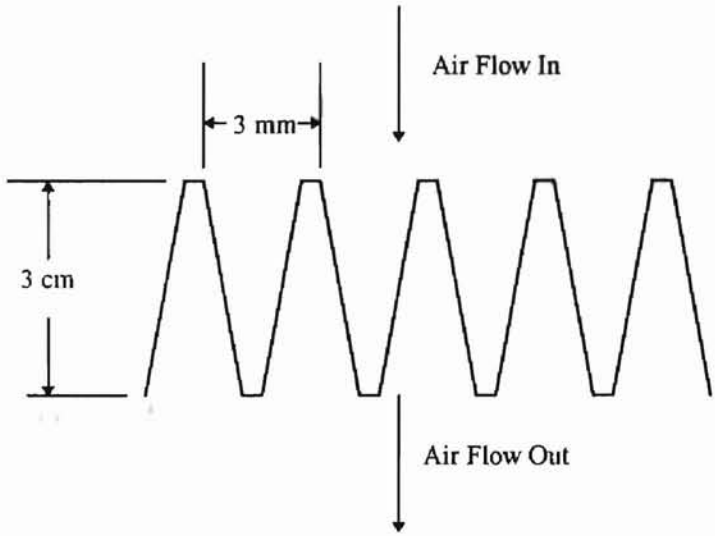

Figure 1.1 Cross Section of a Typical Pleated Air Filter

1.4 Modeling of Filters

1.4.1 Development of Equations

To model a filter using computational fluid dynamics requires certain assumptions. Typically, the Navier-Stokes equations are employed and configured in finite-difference form. Depending on the flow rate, the laminar equations can be utilized, or time-averaged Reynolds modeling can be applied to solve for turbulent flow. This was the approach used by Gurumoothy [1990]. Gurumoothy used a CFD code called PHOENICS which incorporated the transient viscous flow equations with a k-ε model for turbulence outside the filter. With this model, Gurumoothy modeled an entire air induction system (AIS) which included the filter.

It should be noted that in the modeling of the flow within the filter medium, the standard Navier-Stokes equations are not employed. The use of these equations would be exceedingly difficult because of the excessive number of fibers in the flow path. For an accurate model, a finite-difference node size on the order of microns would be needed.

To avoid this problem, a macroscopic description of the flow of air through a filter medium can be assumed by treating it as flow through a porous medium. The simplest porous flow description is known as Darcy's law which relates the pressure drop to the velocity [Vafai and Tien, 1980].

$$\nabla P = -\frac{\mu}{K} V_D \qquad (1.1)$$

Here the change in pressure through a porous medium is proportional to the fluid viscosity and the permeability of the medium (K) which is a macroscopic quantity. The velocity is represented as the Darcian velocity which is a value averaged over the cross sectional area of the medium. This velocity is averaged between the true velocity of the moving fluid between the solid fibers called the pore velocity and the "zero" velocity contribution from the area consisting of the solid fibers. The pore velocity, V_p, can be related to the Darcian velocity with the introduction of the medium porosity, δ, where $V_D = V_p\delta$.

An extended form of the Darcy equation utilized by Gurumoothy [1990] and Tebbutt [1995] includes an inertial resistance, b. According to Vafai and Tien [1980], the inertia of the flow is appreciable as the velocity of the flow increases. This inertial resistance is a function of the permeability, and another function F which itself is a function of the permeability, Reynolds number, and the medium geometry relating the layout of filter fibers.

$$b = \frac{2 \cdot F(K, Re_k, Geometry)}{\sqrt{K}} \qquad (1.2)$$

It can be added to the Darcy equation to form the extended Darcy equation.

$$\nabla P = -\frac{\mu}{K}\mathbf{V}_D - \frac{b\rho}{2}(\mathbf{V}_D \cdot \mathbf{V}_D)\frac{\mathbf{V}_D}{|\mathbf{V}_D|} \qquad (1.3)$$

Vafai and Tien [1980] also offered an equation that includes additional viscous and convective effects usually associated with the standard Navier-Stokes momentum equation. This approach utilizes a volume averaging technique over the pore and medium space to obtain a macroscopic velocity similar to the Darcian velocity but not the same.

Using this volume averaging technique, another extended form of Darcy's law can be formulated.

$$\rho\langle \mathbf{V}\cdot\nabla\mathbf{V}\rangle + \nabla\langle P\rangle = \mu\nabla^2\langle \mathbf{V}\rangle - \frac{\mu\delta}{K}\langle \mathbf{V}\rangle - \frac{b\rho\delta^2}{2}(\langle \mathbf{V}\rangle\cdot\langle \mathbf{V}\rangle)\frac{\langle \mathbf{V}\rangle}{|\langle \mathbf{V}\rangle|} \qquad (1.4)$$

Note that the angle brackets imply the volume averaging, but will be left out for convenience throughout this document. It should be noted that in the analyses by Cai [1993] and Liu [1995], the porosity δ is assumed to be 1. This implies that the fluid space within the filter is much larger than the solid space of the fibers within the filter leaving $\mathbf{V}_P$ approximately equal to $\mathbf{V}_D$ which is approximately equal to $\langle \mathbf{V}\rangle$.

It should be noted that Tebbutt utilized Eq. (1.3) for his analysis of porous media. However, Cai [1993] and Liu [1995] utilized Eq. (1.4) for their porous media analysis after it had been modified for transient flow. The details of this modification will be described later in this thesis. It should further be noted that in the works by Cai and Liu, the theoretical presentation of the term $-\frac{b}{2}(\mathbf{V}\cdot\mathbf{V})\frac{\mathbf{V}}{|\mathbf{V}|}$ is presented as $+b(\mathbf{V}\cdot\mathbf{V})\frac{\mathbf{V}}{|\mathbf{V}|}$. However in their numerical calculations the former term as provided by Eq. (1.4) is utilized. Based on this, the term $-\frac{b}{2}(\mathbf{V}\cdot\mathbf{V})\frac{\mathbf{V}}{|\mathbf{V}|}$ was included in this simulation.

Once the governing differential equations describing the flow through a filter are obtained, they cannot be solved directly due to their mathematical complexity. Thus, the need for computational fluid dynamics which converts the exact differential equations into a system of algebraic finite difference equations. For this thesis, an algorithm called SOLA

(Solution Algorithm) developed by Hirt et al., [1975] is employed. This FORTRAN code models the two-dimensional unsteady Navier-Stokes equations and provides a transient output of velocity and pressure for a particular flow field. The SOLA routine was utilized for CFD filter research both by Cai [1993] and Liu [1995]. Modifications of the SOLA routine to incorporate Eq. (1.3) are necessary to describe the flow within the filter.

1.4.2 Pleat Modeling

One of the major concerns in the design of filters is the pressure drop developed. As noted in Figure 1.1, the flow through the crevasses of the filter can be considered channel flow which contains strong viscous effects creating a pressure drop. The flow through the filter medium also creates a pressure drop due to the permeability and inertial effects. Changing the pleat count or frequency of pleats influences these pressure drops in opposite ways. In general, an increasing pleat count will lower the pressure drop due to the increasing medium cross sectional area and increase the pressure drop due to the viscous effect caused by a more constricted channel flow. The ratio of these two pressure drops can be expressed algebraically [Chen et al., 1993].

$$\frac{\Delta P_{viscous}}{\Delta P_{medium}} = \frac{\dfrac{\mu \cdot V_{mean}}{W}}{\dfrac{\mu \cdot V_{medium}^{\,2}}{K}\, t} = \left(\frac{\mu}{2K}\right)\left(\frac{L}{W}\right)\left(\frac{1}{W}\right)\left(\frac{1}{E}\right) \qquad (1.5)$$

Here, K is the a redefined permeability divided by the medium thickness and viscosity, W is the pleat space, t is the filter thickness, and E is a redefined porosity value based upon the filter thickness and pleat spacing.

$$E = 1 - \frac{t}{W} \qquad (1.6)$$

To optimize the pressure drop through a filter, the correct amount of pleats should be chosen so that $\Delta P_{viscous}$ is significant as compared to ΔP_{medium} [Chen et al., 1993]. This optimal pressure drop is called the minimal pressure drop or ΔP_{min}. $\Delta P_{viscous}$ and ΔP_{medium} should sum to ΔP_{min} with each providing a significant part. Chen calculated the pressure drop through a series of six simulated commercial filters as a function of pleat count and determined which pleat count created the minimum pressure drop ΔP_{min}. With the assumption of a low Stokes number regime utilized in their study, the results show that the optimum pleat count per inch can vary from 5 counts/in. to 20 counts/in. depending upon the type of filter and the pleat height.

1.5 Turbulence Modeling

Turbulence modeling was incorporated by Gurumoothy [1990], Cai [1993], Tebbutt [1995], and Liu [1995] to describe the flow outside the filter. In these analyses, it was reasonably assumed that the flow upstream and downstream of the filter would be turbulent. In Gurumoothy's, Cai's, and Liu's research, the k-ε approach to turbulent modeling was utilized while Tebbutt utilized the turbulent mixing length approach [Hinze, 1975].

1.5.1 Turbulent Flow Within the Pleat Crevasse

Due to the constricted space and the associated high viscous region between the fibers of the filter, it is assumed that the flow within the filter medium is laminar requiring no

turbulence modeling. As described by Tebbutt [1995], the Reynolds number within the filter can be calculated utilizing the filter fiber diameter, flow speed, and the fluid viscosity. At normal flow speeds, Tebbutt calculated Reynolds numbers on the order of 10 which is clearly laminar.

However, an examination of Figure 1.1 shows the existence of a flow space within the confined crevasse between the filter pleats. Here, Tebbutt [1995] assumed in his numerical calculations that the flow was also turbulent even though he theorizes in his conclusions that it is probably laminar. Cai [1993] simply assumed a turbulent flow within this crevasse of the pleat. Investigation of the turbulent flow assumption is necessary.

Examining Figure 1.1 shows that a pitch angle for the flow filter pleat is less than 5°. This means that the filter pleats are nearly parallel to the incoming roughly uniform flow. The analyses by Cai [1993] and Tebbutt [1995] show that the flow within the filter medium itself is almost directly perpendicular to the filter surface. As the flow approaches 3 m/s, the inertia of the flow within the filter medium can draw the flow parallel to the filter surface but not by much.

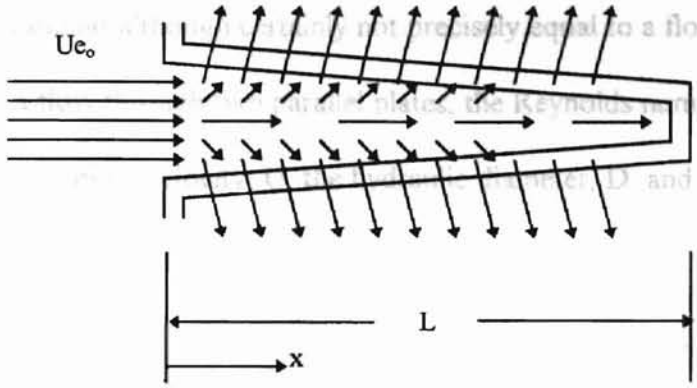

Figure 1.2 Typical Flow Through a Crevasse and Filter Pleat

Within the open crevasse, the flow turns to direct itself through the pleat. At the boundary between the filter medium and the open crevasse, the flow is nearly perpendicular to the filter medium with the parallel velocity very nearly zero. For a porous medium-open flow interface, the no-slip usually assigned to a flow on the boundary of a solid surface is changed to a velocity that matches the parallel flow within the medium [Brown, 1993].

Although the flow is not assigned a no-slip condition, the very low velocity flow parallel to the pleat and within the medium causes the parallel flow in the open crevasse to be very low at the boundary. This boundary condition is approximately 0.01 - 0.02 m/s for an incoming flow of 3 m/s [Tebbutt, 1995]. Furthermore, this condition within such a confined space causes a high viscous stress-gradient for the flow within the crevasse.

This type of flow is similar although certainly not precisely equal to a flow between parallel plates. For a flow through two parallel plates, the Reynolds number can be calculated with the incoming velocity, U, the hydraulic diameter, D, and the kinematic viscosity ν.

$$Re = \frac{UD}{\nu} \tag{1.7}$$

For a fully developed parallel plate flow with incoming velocity of 3 m/s and a hydraulic diameter of 3 mm, the Reynolds number is 600 well below the turbulent Reynolds number standard of 2300. Although this implies a laminar flow, the flow pattern within the pleat crevasse is different enough from a fully-developed parallel plate flow not to guarantee that laminar flow is present.

According to White [1991], a duct flow can relaminarize as the flow changes velocities due to a gradual contraction. This is similar to the situation in Figure 1.2. Referring to the downstream velocity as Ue, the critical relaminarization criteria can be calculated.

$$K_{crit} = \frac{\nu}{Ue^2}\frac{dUe}{dx} \approx 3E-6 \tag{1.8}$$

Assuming a uniform flow at the inlet, Ue_o, and the assumption of no flow within the filter, the ratio of the crevasse cross sectional area and velocity (A(x), Ue(x)) relative to the inlet cross sectional area and velocity (A_o, Ue_o) can be calculated.

$$\frac{A(x)}{A_o} = \frac{L-x}{L} \tag{1.9}$$

$$\frac{Ue(x)}{Ue_o} = \frac{A_o}{A(x)} \tag{1.10}$$

By substituting of Eq. (1.9) into Eq. (1.10) and taking the derivative of Eq. (1.10) with respect to x, the following expression can be derived.

$$\frac{dU_e}{dx} = Ue_o L(L-x)^2 \qquad (1.11)$$

By substituting Eq. (1.11) into Eq. (1.8), the criteria, K can be evaluated.

$$K = \frac{\nu}{Ue^2}\frac{dUe}{dx} = \frac{\nu}{Ue_o^2(\frac{L}{L-x})^2}\frac{Ue_o L}{(L-x)^2} = \frac{\nu}{Ue_o L} \qquad (1.12)$$

For the A13192 filter, the length, L, is 0.03 m, the inlet velocity, Ue_o, can vary from 1 m/s to 5 m/s, and the kinematic viscosity, ν, is approximately 1.5×10^{-5} m^2/s. Substituting these values into Eq. (1.12) provides values of K varying from 4.667e-04 to 9.33e-05. These values are well above the critical value of 3×10^{-6} indicating even if the flow is turbulent entering the crevasse, a strong relaminarization occurs as the flow moves toward the filter media. However, one must recall that this analysis is based upon the assumption of no flow through the filter media. The addition of consideration of this through-flow would reduce the value of K.

In reality, the flow rate through the crevasse decreases in the x-direction as flow is continually diverted through the filter and out of the crevasse. One can assume that the flow rate, Qe(x) is related to the flow rate at the entrance Qe_o.

$$\frac{Qe(x)}{Qe_o} = \frac{L-x}{L} \qquad (1.13)$$

$$Qe(x) = Ue(x)A(x) \qquad (1.14)$$

$$Qe_o = Ue_o A_o \qquad (1.15)$$

Substituting the expression for A(x) in Eq. (1.9) into Eq. (1.14) and then substituting Eq. (1.14) and Eq. (1.15) into Eq. (1.13), the crevasse velocity is found to remain constant at all values of x.

$$Ue(x) = Ue_o \qquad (1.16)$$

This implies that the relaminarization criteria K is 0 with the result that the flow does not become laminar within the crevasse if it is already turbulent at the entrance. For an accurate determination of the relaminarization criteria, it is seen that a good estimate of the reduction of flow rate by the filter is needed. Eq. (1.13) was utilized as a rough approximation. More complex expressions for the flow rate would result in varying estimates for the relaminarization criteria.

1.5.2 Turbulent Flow Upstream and Downstream of Filter

Upstream and downstream of the filter, the flow can be either turbulent or laminar. As with all turbulent calculations, this is determined by flow conditions such as Reynolds number, flow geometry, inlet, and boundary conditions. Flow through a car engine air intake system is generally assumed turbulent, [Cai ,1993]. However, previous simulations by Cai utilizing turbulent flow models concluded that turbulent modeling near the filter provides little effect on the flow through the pleat.

Since one of the objectives of this thesis is to determine the accuracy of modeling porous flow with the extended form of the Darcy's equation, Eq. (1.4), the simplifying assumption of laminar flow was employed. Therefore, for both the computational simulation and the experimental flow introduced in the next section, flow parameters were

chosen which allowed a laminar assumption. Details of the validity of this assumption are provided in Section 4.4.

1.6 Previous Computational Results

With the use of the porous medium governing equations and modeling techniques developed in Sections 1.4 and 1.5, many different simulations of air flow through air filters have previously been created providing various results [Gurumoothy, 1990; Cai,1993; Chen et al., 1993; Tebbutt, 1995; Liu, 1995].

Several significant conclusions have been determined from these past simulations. One is that the flow through a filter pleat is not normal to the pleat face. Inertia draws the flow vectors toward the downstream direction [Cai, 1993; Tebbutt, 1995].

It was found that an air filter creates a strong drop in pressure through the porous medium but that the viscous drag within the pleat also significantly affects the pressure drop at small pleat angles [Cai, 1993; Tebbutt, 1995]. This is the situation found in the A13192 filter. As noted in Section 1.4, Chen et al. [1993] determined that the effect of increasing pleat count for a filter provided an optimum pressure drop through a pleat. As the pleat count was increased, the cross sectional filter area was increased thereby decreasing the pressure drop due to permeability. However, the viscous effect was increased within the folds of the pleat crevasse. This lead to an optimum pleat count of approximately 5 to 20 pleats per inch depending on the permeability of the filter, pleat height, and flow rate.

As noted in Section 1.5, one parameter typically investigated for its effect on a filter is turbulence. Tebbutt [1995] reasoned that turbulence cannot be found within the filter medium while turbulence within the crevasse of the filter pleats could have a significant viscous effect if it exists. As noted in Section 1.5, Cai [1993] reasoned that the turbulence modeling upstream and downstream of the filter medium had a negligible effect on the velocity and Liu [1995] stated that the turbulence upstream and downstream of a porous medium created little pressure drop when compared to the pressure drop found through the medium.

Variations in the values of permeability and the inertial constant have shown various results. Liu [1995] found that the permeability distribution can significantly alter the flow pattern through a porous medium. However, although Cai [1993] did not experimentally determine the value of the permeability and inertial resistance, he parametrically determined that the inertial constant and permeability did not strongly affect the velocity magnitude variation through the filter. As described in a later section, Tebbutt [1995] determined experimentally the permeability and inertial resistance and found them to be significantly different from those assumed by Cai [1993].

One of the more troubling results found from past simulations is the instability of some CFD flow geometries utilizing the porous flow equations. Tebbutt [1995] determined that the mixing of porous and nonporous governing equations created these instabilities. This was especially true for configurations involving a rectangularly shaped pleated filter as represented by Figure 1.1. The Newton method of solving a set of nonlinear equations

utilized by Tebbutt is highly sensitive to initial conditions chosen for the significant variables. In the finite element simulation developed by Chen et al. [1993], a square shaped pleated filter was analyzed. However, problems of stability were not reported which could warrant further investigation of the use of the finite element method in analyzing filter flow.

1.7 Experimental Verification

To verify the finite difference models by experimentation, some method of velocity and pressure measurements is needed. The velocity measurement can be supplied by a Laser Doppler velocimetry (LDV) system which measures the velocity of an airflow on a point by point basis. The OSU Mechanical Engineering Laboratory has been provided a filter test stand by Purolator Inc. With the use of this test stand, an air flow experiment can be created to enable measurements of pressure and velocity changes through an air filter. Details of the test stand are included in Chapter IV.

The LDV system is used to measure the velocity of the airflow. A laser beam is created and directed to a fiber drive. This fiber drive splits the beam into two sets of blue and green shifted and unshifted beams with the use of a Bragg cell. A transceiver receives the four beams from the fiber drive through fiber optic cables and projects them in perpendicular planes through a lens with a focal length of 500 mm. The beams are focused to a focal point producing a probe volume within the flow. Seeding particles are introduced into the flow by an aerosol generator. As seed particles pass through the probe volume, a reflected "Doppler burst" of light is modulated at the Doppler frequency and is

collected by the transceiver. This burst is focused on another fiber optic cable and transmitted to the photodetector. The photodetector converts the optical signal to an analog electrical signal and passes it to the Doppler Signal Analyzer (DSA). The DSA filters the signal through a high pass filter and low pass filter. The DSA uses a 1-bit analog-to-digital converter to convert the complex, filtered, sampled signal to a square wave representation of the input signal. The Digital Signal Processor (DSP) is used to perform a discrete Fourier transform (DFT) using a fast Fourier transform (FFT), algorithm. System software is then utilized to perform statistical analysis and presentation of velocity information of the particles in histogram form. Details of these components are provided in Chapter IV.

To verify the CFD model described in the previous section, a specific filter velocity test as illustrated by Figure 1.3 was created using the process previously described. Since a typical filter has pleats only millimeters apart, velocity measurements near the filter and within pleat folds are very difficult. Therefore, filter paper was utilized to create a large simulated pleat with a width and height of 50.8 mm (2 in.). This experimental pleat was located within a 50.8 mm x 254 mm Plexiglas duct designed specifically to obtain flow velocity data. Flow was directed through the experimental pleat and the velocity data was obtained near the pleat by the LDV system at various locations. Results of the CFD simulation and experiment are presented in Chapter V. If the results are in close agreement, confidence can be given to the computational modeling approach utilized.

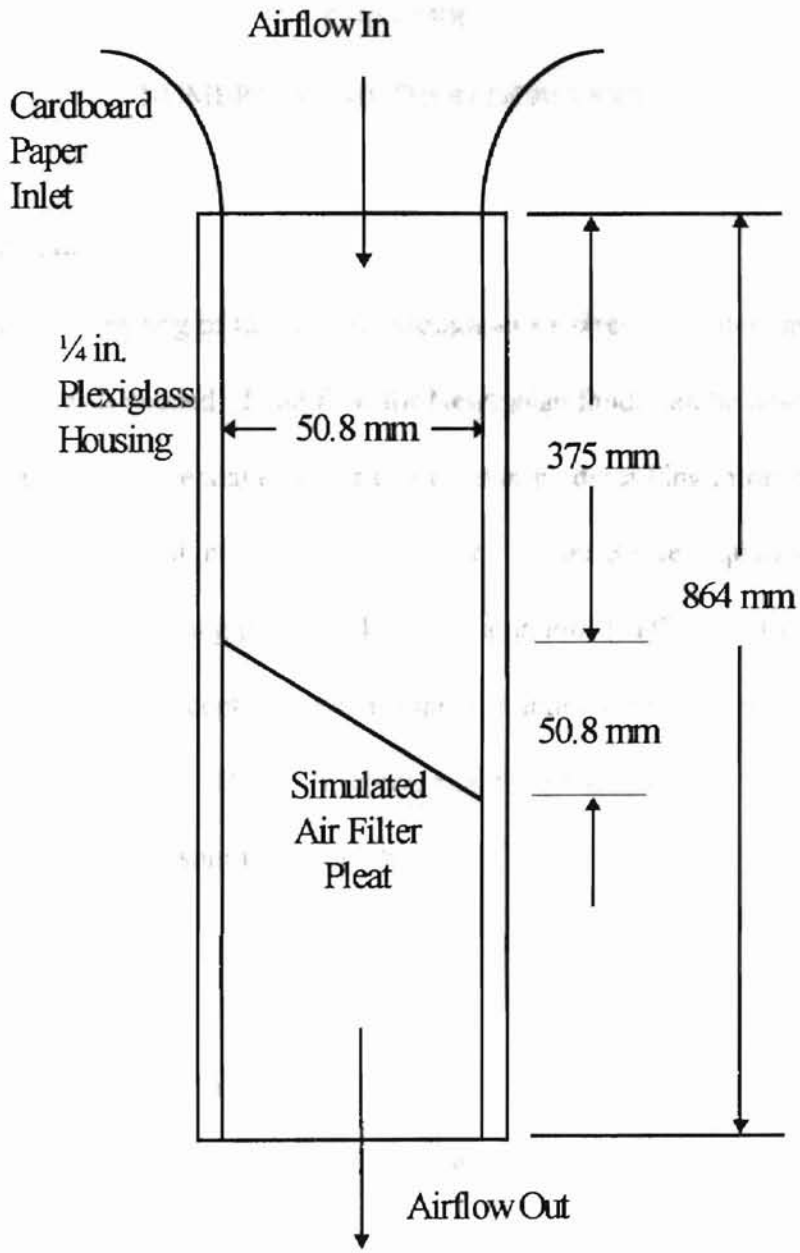

Figure 1.3 Schematic of Filter Pleat Velocity Test

CHAPTER II

NUMERICAL METHOD DERIVATION

2.1 Introduction

To understand the modeling of the airflow through an air filter, an understanding of the governing equations is needed. Fluid flow for Newtonian fluids can be described with the Navier-Stokes partial differential equations. However by describing intrafilter flow as flow through a porous medium, modifications of the Navier-Stokes equations are necessary. Once the governing partial differential equations (PDEs) are formed, they cannot be directly solved except for several simple situations due to their complex mathematical characteristics. However, converting the PDEs to finite difference equations (FDEs) allows a numerical solution to be obtained.

2.2 Conservation of Mass

A standard theorem of mechanics is that the mass of an object is independent of time. This concept can be applied to a fluid flow through an arbitrary finite region of space with boundary surface area Γ and volume Ω. For this region, $\mathbf{n}$ represents the unit normal vector to the surface and ρ is the density.

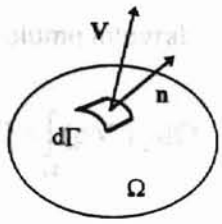

Figure 2.1 Arbitrary Finite Region

The integral summation of the mass rate of flow out of an infinitesimal area $d\Gamma$ provides the total mass flow.

$$\dot{m} = \int_{\Gamma} \rho \mathbf{V} \cdot \mathbf{n} d\Gamma = \int_{\Gamma} \rho V_i n_i d\Gamma \qquad (2.1)$$

Note that tensor component notation is used with V_1, V_2, and V_3 representing components of velocity in the x_1, x_2, and x_3 directions. Normal rules for free index and summation of repeating indices are applied [Chung, 1994].

The change of mass within the region Ω is summed from the change of mass for each region $d\Omega$.

$$\dot{m} = -\int_{\Omega} \frac{\partial \rho}{\partial t} d\Omega \qquad (2.2)$$

Since mass must be conserved, Eqs. (2.1) and (2.2) must be equal.

$$-\int_{\Omega} \frac{\partial \rho}{\partial t} d\Omega = \int_{\Gamma} \rho V_i n_i d\Gamma \qquad (2.3)$$

Applying the Green-Gauss theorem [Chung,1994] on the right hand side of Eq. (2.3) converts the surface integral to a volume integral.

$$\int_{\Gamma} \rho V_i n_i d\Gamma = \int_{\Omega} \frac{\partial}{\partial x_i}(\rho V_i) d\Omega = \int_{\Omega} (\rho V_i)_{,i} \, d\Omega \qquad (2.4)$$

Note that the comma is used as a shorthand for the derivative with respect to a tensorial spatial derivative. Substituting Eq. (2.4) into Eq. (2.3) provides one equation.

$$\int_{\Omega} \left(\frac{\partial \rho}{\partial t} + (\rho V_i)_{,i} \right) d\Omega = 0 \qquad (2.5)$$

For the above integral equation to remain valid for all arbitrary volumes, it is necessary for the integrand to vanish so that:

$$\frac{\partial \rho}{\partial t} + (\rho V_i)_{,i} = 0 \qquad (2.6)$$

In vector notation, Eq. (2.6) can be expressed by:

$$\frac{\partial \rho}{\partial t} + \nabla \cdot (\rho \mathbf{V}) = 0$$
$$\text{where } \nabla = \mathbf{i}_i \frac{\partial}{\partial x_i} \qquad (2.7)$$

Either Eq. (2.6) or Eq. (2.7) is known as the continuity equation which represents the conservation of mass in a flow. For incompressible flow (ρ=constant) this equation can be simplified.

$$\nabla \cdot \mathbf{V} = V_{i,i} = 0 \qquad (2.8)$$

2.3 Conservation of Momentum

Another theorem in mechanics is the conservation of momentum. In general, for any arbitrary object of mass M, the momentum , **L**, can be defined by the velocity multiplied by the infinitesimal mass, dm.

$$\mathbf{L} = \int_m \mathbf{V} dm = \int_\Omega \rho \mathbf{V} d\Omega \tag{2.9}$$

The time rate of change of linear momentum is then defined by the resulting forces

$$\dot{\mathbf{L}} = \frac{D}{Dt}\int_\Omega \rho \mathbf{V} d\Omega = \int_\Omega \rho \mathbf{F} d\Omega + \int_\Gamma \sigma(n) d\Gamma \tag{2.10}$$

Note that the material or Eulerian derivative is employed which takes into account both the spatial and time derivative of a quantity in a given region and is defined by:

$$\frac{D}{Dt} = \frac{\partial}{\partial t} + \mathbf{V} \cdot \nabla \tag{2.11}$$

In Eq. (2.10), **F** is an arbitrary body force per unit mass and σ (n) is the stress vector normal to the body surface Γ.

Note that the stress vector can be redefined in tensor notation [Canabal, 1992].

$$\sigma(n) = \sigma_i n_i = \sigma_{ij} \mathbf{i}_j n_i \tag{2.12}$$

where n_i is a component of a vector normal to the surface and σ_{ij} is the stress tensor. Applying the Green-Gauss theorem [Chung, 1994], the stress vector can be rewritten

$$\int_\Gamma \sigma_{ij} \mathbf{i}_j n_i d\Gamma = \int_\Omega \frac{\partial \sigma_{ij}}{\partial x_i} \mathbf{i}_j d\Omega \tag{2.13}$$

Also note that the following notation can be included for convenience.

$$\frac{\partial \sigma_{ij}}{\partial x_i} = \sigma_{ij,i} \tag{2.14}$$

By using the definition of the material derivative, the left side of Eq. (2.10) can be rearranged.

$$\int_{\Omega} \frac{D}{Dt}(\rho \mathbf{V} d\Omega) = \int_{\Omega} d\Omega \frac{D}{Dt}(\rho \mathbf{V}) + \int_{\Omega} \rho \mathbf{V} \frac{D}{Dt}(d\Omega) \tag{2.15}$$

which rearranges to:

$$\int_{\Omega} \frac{D}{Dt}(\rho \mathbf{V}) d\Omega + \int_{\Omega} \rho \mathbf{V} \frac{D}{Dt}(d\Omega) = \int_{\Omega} \frac{D}{Dt}(\rho \mathbf{V}) d\Omega \tag{2.16}$$

Note that the second term of Eq. (2.16) is zero for incompressible flow.

$$\frac{D}{Dt}(d\Omega) = 0 \tag{2.17}$$

By applying the definition of the material derivative, Eq. (2.11), to Eq. (2.16) and by substituting Eq. (2.16) and Eq. (2.13), into Eq. (2.10) the following is obtained.

$$\int_{\Omega} \left(\frac{\partial(\rho \mathbf{V})}{\partial t} + (\mathbf{V} \cdot \nabla)(\rho \mathbf{V}) - \rho \mathbf{F} - \sigma_{ij,i} \mathbf{i}_j\right) d\Omega = 0 \tag{2.18}$$

For the integral to be valid for all arbitrary volumes, it is necessary for the integrand to vanish.

$$\frac{\partial(\rho \mathbf{V})}{\partial t} + (\mathbf{V} \cdot \nabla)(\rho \mathbf{V}) - \rho \mathbf{F} - \sigma_{ij,i} \mathbf{i}_j = 0 \tag{2.19}$$

Note the following vector notation can be utilized [Chung, 1994].

$$\begin{aligned} \mathbf{V} &= V_j \mathbf{i}_j \\ \nabla &= \mathbf{i}_i \frac{\partial}{\partial x_i} \\ (\mathbf{V} \cdot \nabla)\mathbf{V} &= V_i V_{j,i} \mathbf{i}_j \end{aligned} \tag{2.20}$$

For ρ=constant or incompressible flow, Eq. (2.19) can be rewritten as:

$$\rho\frac{\partial V_j}{\partial t}\mathbf{i}_j + \rho V_i V_{j,i}\mathbf{i}_j - \rho F_j \mathbf{i}_j - \sigma_{ij,i}\mathbf{i}_j = 0 \qquad (2.21)$$

The vector summation can be divided through leaving only the tensor components.

$$\rho\frac{\partial V_j}{\partial t} + \rho V_i V_{j,i} - \rho F_j - \sigma_{ij,i} = 0 \qquad (2.22)$$

Equation (2.22) is the incompressible momentum equation.

2.3.1 Momentum Outside the Filter

To use the momentum equation, the stress tensor σ_{ij} must be defined. The scope of this work is restricted to laminar flow of Newtonian fluids. Under these restrictions, the constitutive law governing the relation between velocity gradients and the stress tensor [Chung, 1994] can be established.

$$\sigma_{ij} = -P\delta_{ij} + \mu\left[\left[\frac{\partial V_i}{\partial x_j} + \frac{\partial V_j}{\partial x_i}\right] - \frac{2}{3}\frac{\partial V_k}{\partial x_k}\delta_{ij}\right] \qquad (2.23)$$

where δ_{ij} is the Kronecker delta, μ is the dynamic viscosity, and P is the hydrostatic pressure. However, it should be noted that for incompressible flow, Eq. (2.8) can be substituted into Eq. (2.23) to eliminate the term $V_{k,k}$. Also, for this analysis the dynamic viscosity is assumed constant. By using these substitutions and taking the spatial derivative of Eq. (2.23), an expression for the gradient of the stress tensor, $\sigma_{ij,i}$ is developed.

$$\sigma_{ij,i} = -\frac{\partial P}{\partial x_j} + \mu\frac{\partial}{\partial x_i}\left(\frac{\partial V_i}{\partial x_j} + \frac{\partial V_j}{\partial x_i}\right) \qquad (2.24)$$

Furthermore, using the assumption that no body forces are significant and by substituting, Eq. (2.24) into Eq. (2.22), the incompressible Navier-Stokes momentum equation used for the nonfilter region in this analysis is obtained.

$$\rho\frac{\partial V_j}{\partial t}+\rho V_i V_{j,i}=-\frac{\partial P}{\partial x_j}+\mu\frac{\partial}{\partial x_i}\left(\frac{\partial V_i}{\partial x_j}+\frac{\partial V_j}{\partial x_i}\right) \qquad (2.25)$$

The equation can be written in equivalent vector form.

$$\rho\frac{\partial \mathbf{V}}{\partial t}+\rho(\mathbf{V}\cdot\nabla)\mathbf{V}=-\nabla P+\mu(\nabla^2\mathbf{V}) \qquad (2.26)$$

2.3.2 Momentum Inside the Filter

To describe the momentum equation within the region of the filter medium requires modifications of the Navier-Stokes momentum equation, Eq. (2.25). These modifications assume that the filter can be described as a porous medium. The simplest of the alternate momentum equations is Darcy's law which assumes that the pressure drop through a porous medium is proportional to the velocity. It can be expressed in tensor notation.

$$\sigma_{ij,i}=\frac{\partial P}{\partial x_j}+\frac{\mu}{K}V_j=0 \qquad (2.27)$$

In vector form this equation was presented previously in Section 1.4 using the Darcian velocity.

$$\nabla P=-\frac{\mu}{K}\mathbf{V}_D \qquad (1.1)$$

Darcy's law represents a simple description of a flow through a porous medium, K is the permeability of the porous structure. The velocity V_j is the macroscopic velocity of a flow through a medium and not the actual velocity of the flow through the individual pores.

Instead of employing the Darcian velocity V_D which was described in Section 1.4, a volume averaging technique is utilized to characterize the velocity and pressure provided by Eq. (2.27). This technique [Vafai and Tien, 1980] averages any physical quantity over the volume in which it is being measured.

$$\langle \Psi \rangle = \frac{1}{\Omega} \int_{\Omega} \Psi d\Omega \tag{2.28}$$

With this technique, quantities such as pressure and velocity are averaged within a space that includes both filter and nonfilter regions. It should be noted that by utilizing the volume averaging technique coupled with Darcy's law, the filter is mathematically simulated as one homogeneous region. Although the Navier-Stokes momentum equation, Eq. (2.25) is still valid on a small scale, a redefinition of the extremely complex porous flow as one homogeneous field is assumed. By doing so, a redefinition of the stress gradient tensor $\sigma_{ij,i}$ is required. This is what is done by Darcy's law, Eq. (2.27).

Darcy's law exists only for flow with low inertia which is defined as Stokes flow. A Stokes flow condition exists if the Reynolds number for the flow is less than 1. For a porous medium, the Reynolds number is defined by either the fiber diameter or the permeability K, the velocity V, and the kinematic viscosity.

$$\mathbf{Re}_D = \frac{VD}{\nu} \tag{2.29}$$

$$\mathbf{Re}_{\sqrt{K}} = \frac{V\sqrt{K}}{\nu} \tag{2.30}$$

Velocities for the flow in this research were approximately 1 m/s. The permeability K was measured at 6.72e-11 m^2 (See Appendix B for details of measurements used to determine

K). The fibers in the filter are approximately 40 μm in diameter, [Sabnis, 1993, Tebbutt, 1995], and the kinematic viscosity of air used is 1.5e-05 m^2/s. Using these values, the Reynolds number based upon fiber diameter and the Reynolds number based upon filter permeability is calculated to be 2.66 and 0.546, respectively. This indicates that a Stokes flow might or might not exist. Prudence would dictate that a term describing the inertial resistance through the filter should be included.

Vafai and Tien [1980] postulated that the inertial resistance through a porous medium was dependent upon a function F based upon the permeability, the geometry, and the permeability based Reynolds number as well as the velocity, density, the permeability, and porosity. Vafai and Tien described this inertial resistance and the accompanying pressure drop with either the Darcian velocity or the volume averaged velocity as described with Eq. (2.28).

$$\nabla P = -F\left(K, Re_{\sqrt{K}}, \text{Geometry}\right)\frac{\rho}{\sqrt{K}}\delta^2 \cdot \left(\langle \mathbf{V} \rangle \cdot \langle \mathbf{V} \rangle\right)\frac{\langle \mathbf{V} \rangle}{|\langle \mathbf{V} \rangle|} \qquad (2.31)$$

The function term F and the permeability K can be rearranged into one inertial resistance term b/2. Note that in the research by Cai [1993], Tebbutt [1995], and Liu [1995] the term b/2 was employed although Cai's and Liu's research did not include the ½ factor in their derivation, only in their calculations. Furthermore, no mention of a factor of ½ is mentioned in Vafai and Tien [1980]. However, it should be noted that the ½ term was legitimately incorporated by Cai [1993], Tebbutt [1995], and Liu [1995] in their calculations as long it is recognized that the inertial resistance term b that they utilized is twice the product of the coefficients in Eq. (2.31).

$$b = \frac{2 \cdot F(K, Re_k, Geometry)}{\sqrt{K}} \qquad (1.2)$$

With this redefined inertial resistance term b, a form of Darcy's law can expressed which includes the inertial resistance, the resistance due to viscosity and permeability, and the standard viscous diffusion employed in flow outside of a porous medium.

$$\sigma_{ij,i} = -\frac{\partial P}{\partial x_j} + \mu \frac{\partial}{\partial x_i}\left\langle \frac{\partial V_i}{\partial x_j} + \frac{\partial V_j}{\partial x_i} \right\rangle - \frac{\mu\delta}{K} V_j - 0.5\rho\delta^2 b V_j (V_i V_i)^{0.5} = 0 \qquad (2.32)$$

By examining Eq. (2.32), one can see that it very similar to the Navier-Stokes momentum equation, Eq. (2.25). However, Eq. (2.32) assumes that the stress gradient, $\sigma_{ij,i}$ is 0. By assuming that this stress gradient is not zero but rather equating it to the full Eulerian derivative of the velocity as done by the momentum equation, Eq. (2.22), a redefined form of the Navier-Stokes equation for transient porous flow is developed. Also, by dividing Eq. (2.32) by ρ, the kinematic viscosity ν can be utilized.

$$\frac{\partial V_j}{\partial t} + V_i V_{j,i} = -\frac{1}{\rho}\frac{\partial P}{\partial x_j} + \nu \frac{\partial}{\partial x_i}\left\langle \frac{\partial V_i}{\partial x_j} + \frac{\partial V_j}{\partial x_i} \right\rangle - \frac{\nu\delta}{K} V_j - 0.5 b\delta^2 V_j (V_i V_i)^{0.5} \qquad (2.33)$$

This is very similar to the extended form of Darcy's law as given by Eq. (1.4). The difference is that Eq. (2.33) includes the full material derivative of the velocity, Eq. (2.11), while Eq. (1.4) only utilizes the convective term.

$$\rho\langle \mathbf{V} \cdot \nabla \mathbf{V} \rangle + \nabla\langle P \rangle = \mu \nabla^2 \langle \mathbf{V} \rangle - \frac{\mu\delta}{K}\langle \mathbf{V} \rangle - \frac{b\rho\delta^2}{2}(\langle \mathbf{V} \rangle \cdot \langle \mathbf{V} \rangle)\frac{\langle \mathbf{V} \rangle}{|\langle \mathbf{V} \rangle|} \qquad (1.4)$$

Eq. (2.33) represents the transient extended form of the Darcy's law utilized for this analysis.

2.4 Numerical Approximation

To solve the governing partial differential equations for this analysis, Eqs. (2.8, 2.25,& 2.33), finite differencing is employed. As stated in Section 1.4, a routine called SOLA by Hirt et al., [1975] uses finite differencing of the momentum and continuity equations. The finite differencing method is used widely in CFD calculations and divides the flow domain into a set of nodes. For this analysis, a grid of two-dimensional nodes was chosen for a two-dimensional analysis. If the analysis had been configured as three-dimensional, the nodes would be considered control volumes. Figure 2.2 shows the arrangement of a typical two-dimensional node.

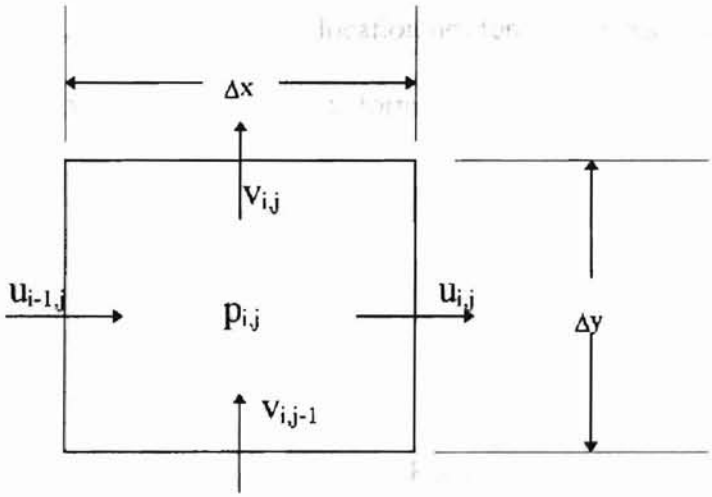

Figure 2.2 Finite Difference Control Node

Note that the subscripts do not indicate tensor indices as utilized in Sections 2.1-2.3 but rather subscripts denoting the node location. Note that the control node need not be a square even though it can be. Also note that the staggered grid approach [Patankar, 1980], is used with the velocities represented at the edge of the node while the pressure is provided at the center. The velocities u and v are employed which are the horizontal and

vertical components respectively of the velocity vector **V** as described in previous sections. Also note that u and v correspond to the V_1 and V_2 tensor components described previously.

2.4.1 Discretized Continuity Equation

By applying upstream differencing to Eq. (2.8), a finite difference form of the continuity equation is obtained. The superscript 'n+1' indicates that the value is determined at the future or updated time level, $t+\Delta t$. A superscript 'n' indicates that the time value is determined at the old or nonupdated time value, t. It should once again be noted that the subscripts i and j only determine the node location not tensor indices. The continuity equation takes the following finite difference form.

Continuity: $$\frac{u_{i,j}^{n+1} - u_{i-1,j}^{n+1}}{\Delta x} + \frac{v_{i,j}^{n+1} - v_{i,j-1}^{n+1}}{\Delta y} = 0 \qquad (2.34)$$

2.4.2 Discretized Momentum Equation in Non-Filter Region

A finite difference discretization of the nonfilter momentum equation, Eq. (2.25) requires a mixture of upstream and central differencing. Discretization of the various terms of Eq. (2.25) can be written for the horizontal and vertical momentum equations to produce two finite difference momentum equations.

u-momentum equation

$$u_{i,j}^{n+1} = u_{i,j}^{n} + \Delta t[\frac{1}{\Delta x}(p_{i,j}^{n} - p_{i+1,j}^{n}) - fux - fuy + visx] \qquad (2.35)$$

v-momentum equation

$$v_{i,j}^{n+1} = v_{i,j}^{n} + \Delta t[\frac{1}{\Delta y}(p_{i,j}^{n} - p_{i,j+1}^{n}) - fvx - fvy + visy] \qquad (2.36)$$

Each of these terms is subsequently explained.

2.4.2.1 Time Derivative

The time derivative of Eq. (2.3.17), $\frac{\partial V_j}{\partial t}$, is transformed into the time difference forms

$\frac{u_{i,j}^{n+1} - u_{i,j}^{n}}{\Delta t}$ and $\frac{v_{i,j}^{n+1} - v_{i,j}^{n}}{\Delta t}$ for the u-momentum and v-momentum equations respectively.

Note that these terms have been algebraically rearranged in Eqs. (2.35 & 2.36)

2.4.2.2 Pressure Derivative

The pressure derivative $-\frac{1}{\rho}\frac{\partial P}{\partial x_j}$ appearing in Eq. (2.25) is represented in finite difference form for the u-momentum and v-momentum by $\frac{1}{\Delta x}(p_{i+1,j}^{n} - p_{i,j}^{n})$ and $\frac{1}{\Delta y}(p_{i,j+1}^{n} - p_{i,j}^{n})$ respectively. This is a forward or downstream difference representation. Note that the pressure terms are the initial terms p^n not the updated pressure p^{n+1}. Obtaining the updated pressure will be described in a subsequent section. Also note that the smaller case p represents a density modified pressure $\frac{P}{\rho}$ for simplicity.

2.4.2.3 Horizontal and Vertical Convective Derivatives

The terms fux, fuy, fvx, and fvy are the finite difference approximations of the term $V_iV_{j,i}$ as it appears in Eq. (2.25). To approximate the convective terms a mixture of upstream and central differencing is applied. The control variable α is utilized to determine the proportion of upstream differencing used. Although upstream differencing alone would ensure stability, central differencing is needed to prevent numerical smoothing, [Hirt et al., 1975]. The complicated combination of central and upstream differencing was developed specifically for the SOLA routine. Note that all velocity terms are values of u^n and v^n.

Eq. (2.37)

$$V_1 V_{1,1} \cong \text{fux} = \frac{1}{4\Delta x}\left[\begin{array}{l}\left(u_{i,j}+u_{i+1,j}\right)^2+\alpha\left|u_{i,j}+u_{i+1,j}\right|\left(u_{i,j}-u_{i+1,j}\right)-\left(u_{i,j}-u_{i+1,j}\right)^2- \\ \alpha\left|u_{i-1,j}+u_{i,j}\right|\left(u_{i-1,j}-u_{i,j}\right)\end{array}\right]$$

Eq. (2.38)

$$V_2 V_{1,2} \cong \text{fuy} = \frac{1}{4\Delta y}\left[\begin{array}{l}\left(v_{i,j}+v_{i+1,j}\right)\left(u_{i,j}+u_{i,j+1}\right)+\alpha\left|v_{i,j}+v_{i+1,j}\right|\left(u_{i,j}-u_{i+1,j}\right)-\left(v_{i,j}+v_{i+1,j}\right) \\ \left(u_{i,j}+u_{i,j-1}\right)-\alpha\left|v_{i,j-1}+v_{i+1,j-1}\right|\left(u_{i,j-1}-u_{i,j}\right)\end{array}\right]$$

Eq. (2.39)

$$V_1 V_{2,1} \cong \text{fvx} = \frac{1}{4\Delta x}\left[\begin{array}{l}\left(u_{i,j}+u_{i,j+1}\right)\left(v_{i,j}+v_{i+1,j}\right)+\alpha\left|u_{i,j}+u_{i,j+1}\right|\left(v_{i,j}-v_{i+1,j}\right)-\left(u_{i-1,j}+u_{i-1,j+1}\right) \\ \left(v_{i-1,j}+v_{i,j}\right)-\alpha\left|u_{i-1,j}+u_{i+1,j-1}\right|\left(v_{i-1,j}-v_{i,j}\right)\end{array}\right]$$

Eq. (2.40)

$$V_2 V_{2,2} \cong fvy = \frac{1}{4\Delta y}\begin{bmatrix}\left(v_{i,j}+v_{i,j+1}\right)^2+\alpha\left|v_{i,j}+v_{i,j+1}\right|\left(v_{i,j}-v_{i,j+1}\right)-\left(v_{i,j-1}v_{i,j}\right)^2\\-\alpha\left|v_{i,j-1}+v_{i,j}\right|\left(v_{i,j-1}-v_{i,j}\right)\end{bmatrix}$$

2.4.2.4 Viscous Diffusion Terms

The terms visx and visy are the finite difference approximations of the viscous diffusion term $\nu\frac{\partial}{\partial x_i}\left(\frac{\partial V_j}{\partial x_i}+\frac{\partial V_i}{\partial x_j}\right)$ from Eq. (2.25). Central differencing is utilized for these terms.

Note that all velocity terms are the nonupdated time terms u^n and v^n.

Eq. (2.41)

$$\nu\left(V_{1,11}+V_{1,22}\right) \cong visx = \nu\left(\frac{1}{\Delta x^2}\left(u_{i+1,j}-2u_{i,j}+u_{i-1,j}\right)+\frac{1}{\Delta y^2}\left(u_{i,j+1}-2u_{i,j}+u_{i,j-1}\right)\right)$$

Eq. (2.42)

$$\nu\left(V_{2,11}+V_{2,22}\right) \cong visy = \nu\left(\frac{1}{\Delta x^2}\left(v_{i+1,j}-2v_{i,j}+v_{i-1,j}\right)+\frac{1}{\Delta y^2}\left(v_{i,j+1}-2v_{i,j}+v_{i,j-1}\right)\right)$$

2.4.3 Discretized Momentum Equation in the Filter Region

The discretized finite difference momentum equations approximating Eq. (2.33) are very similar to the nonfilter equations, Eqs. (2.35 & 2.36). However, they include the additional terms to describe the momentum lost due to the filter.

u-momentum equation

$$u_{i,j}^{n+1} = u_{i,j}^n + \Delta t[\frac{1}{\Delta x}(p_{i,j}^n - p_{i+1,j}^n) - fux - fuy + visx + Dar_x + In_x] \qquad (2.43)$$

v-momentum equation

$$v_{i,j}^{n+1} = v_{i,j}^{n} + \Delta t[\frac{1}{\Delta y}(p_{i,j}^{n} - p_{i,j+1}^{n}) - fvx - fvy + visy + Dar_y + In_y] \qquad (2.44)$$

2.4.3.1 Darcy Diffusion Term

The Darcy diffusion term in Eq. (2.33), $-\frac{\nu\delta}{K}V_j$, is represented by the term Dar_x and Dar_y. As previously stated, this term represents the momentum lost due to the permeability, K. Note that finite differencing is not needed but rather a direct substitution for the velocity.

$$Dar_x = -\frac{\nu\delta}{K}u_{i,j}^{n} \qquad (2.45)$$

$$Dar_y = -\frac{\nu\delta}{K}v_{i,j}^{n} \qquad (2.46)$$

2.4.3.2 Inertial Term

The inertial term in Eq. (2.33), $-0.5b\delta^2 V_j(V_i V_i)^{0.5}$ is represented by In_x and In_y. Note that these terms do not require finite differencing but rather direct substitution. Note also that the velocity terms are utilized at the nonupdated time, u^n and v^n.

$$In_x = -0.5b\delta^2 u_{i,j}\sqrt{u_{i,j}^2 + v_{i,j}^2} \qquad (2.47)$$

$$In_y = -0.5b\delta^2 v_{i,j}\sqrt{u_{i,j}^2 + v_{i,j}^2} \qquad (2.48)$$

2.4.4 Pressure Iteration

By examining the finite difference momentum equations, Eqs. (2.35, 2.36, 2.43, & 2.44), one should note that updated time values are obtained for the velocities u^{n+1} and v^{n+1}, but

nothing is said about an updated pressure, p^{n+1}. The SOLA routine obtains these values for velocity without a corresponding value for pressure. However, since the pressure is not correct, the continuity equation, Eq. (2.34), will not be satisfied although the momentum equations are. To correct this problem, the dilatation, D, is defined.

$$D = \frac{u_{i,j}^{n+1} - u_{i-1,j}^{n+1}}{\Delta x} + \frac{v_{i,j}^{n+1} - v_{i,j-1}^{n+1}}{\Delta y} \tag{2.49}$$

Once the dilatation is defined, adjusting the pressure of the cell (i,j) should drive the dilatation to zero satisfying the continuity equation. To do so a highly linearized form of the momentum equation is applied [Hirt et al., 1975].

$$\frac{\partial V_j}{\partial t} = \pm \frac{\partial p}{\partial x_j} \tag{2.50}$$

By adjusting the pressure an amount Δp to a given cell (i,j), and applying finite difference approximations to Eq. (2.50), the following expressions involving Δp can be derived.

$$\frac{u_{i,j}^{n+1} - u_{i,j}^{n}}{\Delta t} = +\frac{\Delta p}{\Delta x} \tag{2.51}$$

$$\frac{u_{i-1,j}^{n+1} - u_{i-1,j}^{n}}{\Delta t} = -\frac{\Delta p}{\Delta x} \tag{2.52}$$

$$\frac{v_{i,j}^{n+1} - v_{i,j}^{n}}{\Delta t} = +\frac{\Delta p}{\Delta y} \tag{2.53}$$

$$\frac{v_{i,j-1}^{n+1} - v_{i,j-1}^{n}}{\Delta t} = -\frac{\Delta p}{\Delta y} \tag{2.54}$$

Substituting these expressions for the updated velocities into Eq. (2.49) provides an expression for Δp.

$$\Delta p = \frac{-\omega \cdot D}{\left(2\Delta t\left(\frac{1}{\Delta x^2} + \frac{1}{\Delta y^2}\right)\right)} \qquad (2.55)$$

Note that an iteration value, ω, is introduced. Updating the value of Δp causes the value of the dilatation to approach zero but only after several iterations. The iteration value, ω, is utilized to more quickly drive the value of D to zero. To summarize the process, SOLA proceeds by the following.

1. Finds the updated velocity values, $u_{i,j}^{n+1}$ and $v_{i,j}^{n+1}$ for all the cells with the discretized momentum equations, Eqs. (2.35, 2.36, 2.43, & 2.44).
2. Determines the value of the dilatation D with Eq. (2.49). As stated, this value should be near zero within a certain amount for the continuity equation, Eq. (2.34) to be satisfied.
3. If the dilatation is too large, the routine determines an adjustment to the cell pressure with Eq. (2.55). Equation (2.55) merely provides an estimation of what the pressure should be to satisfy both the momentum equations and the continuity equation. If the dilatation is close to zero, the continuity equation, Eq. (2.34), and the momentum equations, Eqs. (2.35, 2.36, 2.43, & 2.44), are already satisfied and the sequence is ended.
4. New velocity values are obtained utilizing estimated pressure from Step 3. This is done by utilizing Eqs. (2.51, 2.52, 2.53, & 2.54). SOLA then returns to Step 2.
5. Repeats Steps 1-4 for each new solution in time.

2.4.5 Stability Considerations

In general, for a numerical model to work, the algorithm must converge to a stable solution. Important factors for the solution of this study are the time increment, Δt, space increments, Δx and Δy, and the upstream difference parameter α. For a finite difference routine like SOLA, certain guidelines should be considered.

First, since material should not move more than one cell size (Figure 2.2) in a given time step, Δt can be related to Δx , Δy, u, and v.

$$\Delta t < \min\left[\frac{\Delta x}{|u|}, \frac{\Delta y}{|v|}\right] \tag{2.56}$$

Second, the kinematic viscosity requires that the momentum diffusion cannot transfer through one cell size in a given time step.

$$\Delta t < \frac{1}{2\nu}\left(\frac{\Delta x^2 \Delta y^2}{\Delta x^2 + \Delta y^2}\right) \tag{2.57}$$

Furthermore, the upstream difference coefficient α applied to the convection terms of the momentum equation should satisfy the following criteria.

$$1 \geq \alpha \geq \max\left[\left|\frac{u\Delta t}{\Delta x}\right|, \left|\frac{v\Delta t}{\Delta y}\right|\right] \tag{2.58}$$

The value for α should be in the range 0 to 1. The case of α equal to 0 is equivalent to a full central difference while a value of 1 is equivalent to the fully upwind difference.

Equations (2.56), (2.57), and (2.58) represent general rules in determining the time increment and upstream difference coefficient. For this study, other parameters

influencing the stability include the permeability K, and the inertial term b. In general, these two coefficients force the time increment to be much smaller than Eqs. (2.56), (2.57), and (2.58). This will be further discussed in a later section.

Determination of all the parameters introduced in Chapter II will be specified in Chapter III for the specific flow experiment of this study.

CHAPTER III

NUMERICAL METHOD APPLICATION

3.1 Introduction

The generalized development of the finite difference method provided in Chapter II was specifically created to simulate the flow through a filter. To do so, a particular flow configuration must be chosen to simulate. This configuration includes parameters such as geometry, size, boundary conditions, and fluid properties.

3.1.1 Computational Simulation of an A13192 Filter Pleat

Referring to Figure 1.1, it is seen that the flow through an air filter is on a very small scale. Previous work by Cai [1993] and Tebbutt [1995] created computational models to simulate this type of flow. Instead of modeling the entire filter, these simulations modeled a single or half-pleat describing the flow within the porous filter, flow within the upstream and downstream crevasse, and the open duct flow upstream and downstream of the filter. These computational domains were chosen because they could represent the small scale flow through the filter pleats of a standard A13192 filter. Figure 3.1 describes the computational flow domains previously developed.

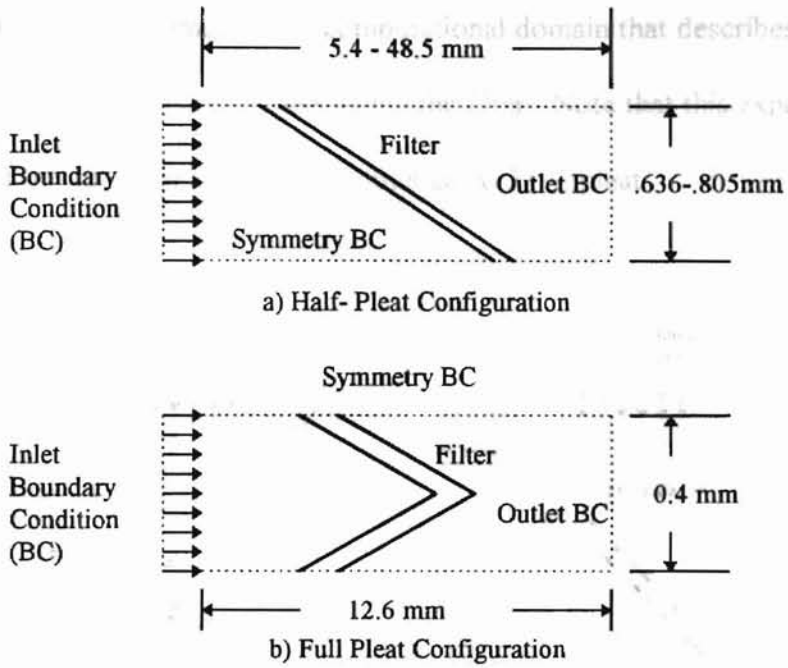

Figure 3.1 Previous Computational Flow Simulation

The flow configuration used for this study will be similar to Tebbutt's half-pleat configuration utilizing the SOLA computational routine. Like Tebbutt's analysis, a small scale simulation describing the flow through a pleat of the A13192 Filter will be investigated. Afterward a large scale filter simulation will be created specifically for verification by experimental methods.

3.1.2 Computational Simulation of an Experimental Flow

This large scale filter flow simulation will attempt to model a portion of an experimental flow created specifically for verification. As described in Section 1.4 and Figure 1.3, the experimental flow is directed through a rectangular duct with a cross section of 50.8 mm x 254 mm. The flow is forced through filter paper slanted 45° to the incoming flow which is then exhausted from the test housing to a constant area duct. The computational flow

model simulating this experiment has a computational domain that describes only a portion of the flow upstream, downstream, and within the filter. Note that this experimental flow is similar to but not the same as a flow through an A13192 pleat.

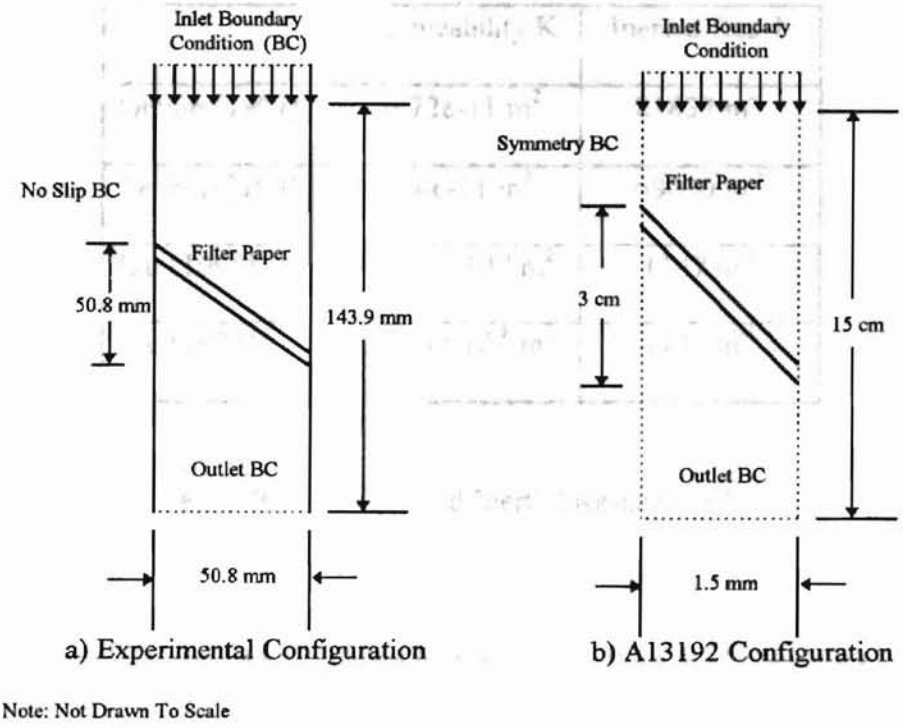

Figure 3.2 Computational Flow Domain

3.2 Determination of Filter Inertial Resistance and Permeability

Many parameters must be chosen to complete the simulations of the filter flow introduced in Section 3.1. Among the most important are the constants used to describe the resistive characteristics of the filter to the flow. Section 1.4 introduced the two constants that determine these characteristics. These are the inertial resistance, b, and the permeability, K. These values are incorporated into the intra-filter momentum equation, Eq. (2.33), and are critical in determining the flow field through and around an air filter. The values K and

b are different for different types of filter media and can vary even for different samples of a given type of filter. Previous studies have utilized varying values. These previously used values and those values used by this study are provided by the following table.

	Permeability K	Inertial Res. b
Gimlin [1997]	6.72e-11 m^2	81833 m^{-1}
Tebbutt [1995]	7.4e-11 m^2	68000 m^{-1}
Liu [1995]	10^{-4} to 10^{-8} m^2	1147 m^{-1}
Cai [1993]	10^{-4} to 10^{-8} m^2	1147 m^{-1}

Table 3.1 Permeability and Inertial Resistance Terms

It should be noted that the values utilized by Liu [1995] and Cai [1993] were based upon a resistance through an entire filter as shown by Figure 1.1. This includes the space occupied by the filter medium and the empty space within the pleat crevasse. The values by Tebbutt [1995] and the current study were determined for the filter medium only which is why the values are very different. Appendix B describes the method of the derivation of these two constants.

3.3 Determination of Generalized Node Matrix

Figure 3.2 represents the two-dimensional computational flow field developed for this study. What is lacking from the geometry of Figure 3.2 is the finite difference control nodes and the definition of the computational boundary conditions.

The determination of the finite difference control node system is an important factor in determining the flow solution. The SOLA routine imposes a two-dimensional rectangular node matrix upon a real flow. An example of one control node is provided in Figure 2.2. Important points to remember when choosing a control node system is that its size is critical to the results. In general, the smaller node size provides a more accurate solution. The problem with this concept is that smaller nodes tend to create a higher computer usage time. As explained in the following sections, varying node configurations were utilized. Additionally, the flow domain was divided into filter and nonfilter regions. Computationally, this means that the nodes outside the filter were guided by the nonfilter finite difference momentum equations, Eq. (2.35) and Eq. (2.36), while the nodes within the filter were guided by the filter finite difference momentum equations, Eq. (2.43) and Eq. (2.44).

As noted by Tebbutt [1995], the mixture of filter and nonfilter momentum equations tends to create unstable solutions. This was found to be true especially if the filter thickness was represented by only one node in the downstream direction. Therefore, it is necessary to include several nodes for the intra-filter representation in the downstream or x-direction. Figure 3.3 shows a generic configuration of the computational domain and control node system.

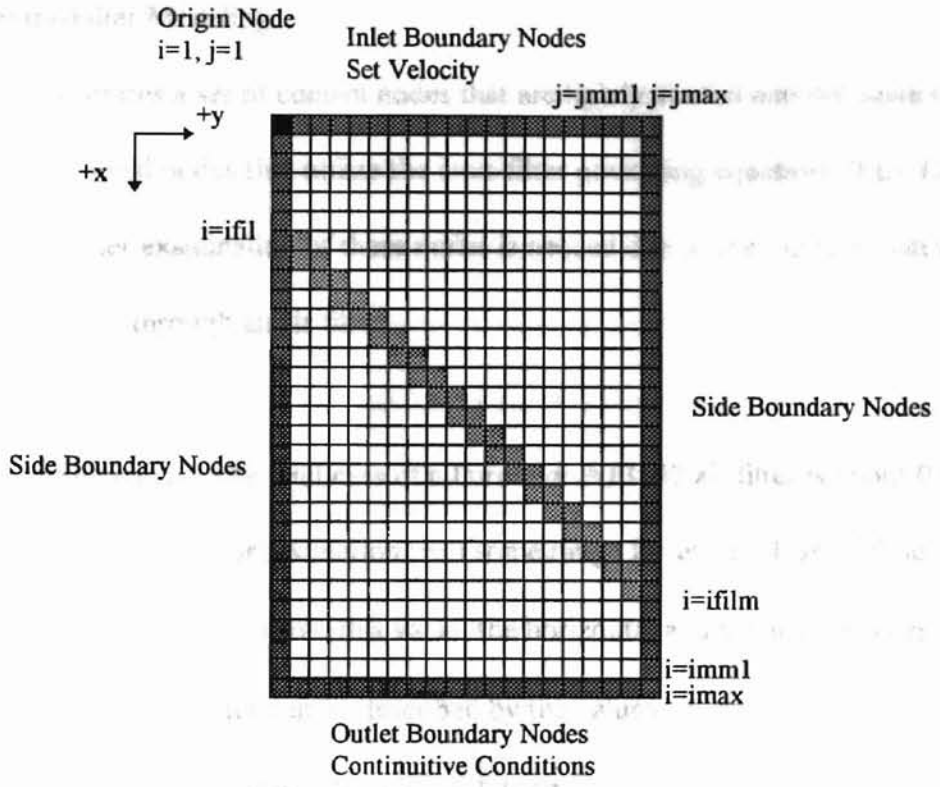

Figure 3.3 General Matrix Description

The control nodes in Figure 3.3 are numbered by an ordered pair (i,j). With this system, the i represents the x-value location and j represents the y-value location. As shown, the computational nodes for which the SOLA routine is obtaining a solution have (i,j) values ranging from i=2 to "imm1" and j=2 to "jmm1". Note that "imm1" and "jmm1" are short for "imax" and "jmax" minus 1. The nodes on the edge of the matrix (i=1, i=imax, j=1, or j=jmax) are boundary nodes to which boundary conditions are applied. Also, the x-value location of the furthest upstream filter node is denoted by "ifil", short for i-filter. The x-value location of the furthest downstream filter node is denoted by "ifilm", short for i-filter max.

3.4 Intra-Filter Modeling

Figure 3.3 illustrates a set of control nodes that are lightly shaded and delineate the intra-filter computational nodes that utilize the intra-filter governing equations, Eqs. (2.43) and (2.44). A further examination of these nodes is needed due to their critical nature in the analysis of a flow through an air filter.

As noted in Section 1.3, the thickness of a Purolator A13192 air filter is about 0.6 mm. Note that this is only an approximation with some range for error. This thickness can be represented by a value Δt_n. From this value, the horizontal and vertical thickness along the x and y axes through a filter can be described by the values Δt_x and Δt_y. The computational matrix of nodes illustrated by Figure 3.3 can be imposed upon a filter described by these values Δt_n, Δt_x, Δt_y.

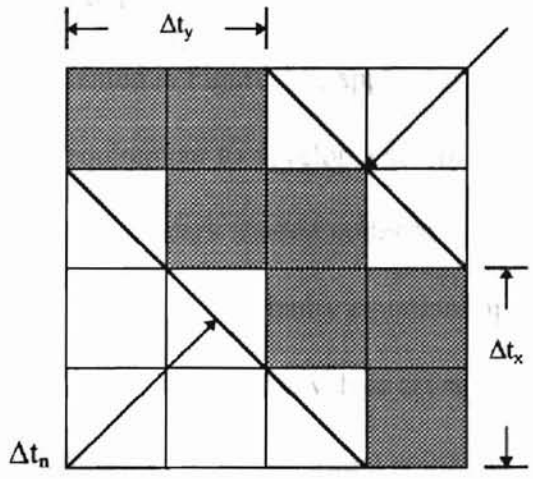

Figure 3.4 Imposition of Rectangular Nodes Upon a Slanted Filter

In Figure 3.4, the shaded nodes are the computational nodes that simulate the flow through the filter as governed by Eqs. (2.4.10) and (2.4.11). However, the physical shape of the filter is the complete area between the slanted rectangular lines a distance Δt_n apart. With this discrepancy between the area of the shaded rectangular computational nodes and the true area of a porous filter, some error must be assumed because some sections of nonfilter computational nodes are included in the area that should be the exclusive domain of the filter. This is a necessary approximation when imposing rectangular nodes upon a real geometric domain. However, it can be deduced from the geometry of Figure 3.4 that if the filter thickness is 0.6 mm and if the nodes are square, the value for Δt_x and Δt_y is $.67\sqrt{2}\ \Delta t_n$ or .565 mm. Appropriate values for Δx and Δy can easily be chosen after the number of intrafilter nodes are chosen in the x and y directions.

3.5 Boundary and Initial Conditions

Figure 3.3 shows the general node configuration utilized for this analysis. For the two types of flow domains presented in Figure 3.2, application of boundary and initial conditions is a necessary requirement to develop a solution. The control nodes that represent boundary nodes are the dark shaded nodes at the edges of the matrix. These nodes do not have the momentum or continuity equations applied to them. Although their velocities and pressures are calculated, these values are not generally viewed as solutions but only as inputs to the continuity and momentum equations for the interior nodes. Note that the nodes on the corners (e.g. i=1, j=1) are unimportant and contribute nothing to the solution. The initial and boundary values are determined in the following way.

3.5.1 Initial Conditions (All nodes, Time=0)

To provide a quick convergence from the initial calculation to the steady-state solution, the initial conditions for all of the nodes were set in the following way.

$$u_{i,j}=1.0 \text{ m/s} \tag{3.5}$$

$$v_{i,j}= 0.0 \text{ m/s} \tag{3.6}$$

$$p_{i,j}= 0 \text{ Pa} \tag{3.7}$$

3.5.2 Inlet Boundary (i=1, j=1...jmax)

The upstream incoming flow for this analysis was chosen as a uniform inlet flow. Note that the pressures for these nodes are unimportant since the momentum equations, Eqs. (2.35, 2.36, 2.43, 2.44), utilize a forward difference scheme for the pressure.

$$u_{1,j} = 1.0 \text{ m/s} \tag{3.8}$$

$$v_{1,j} = 0.0 \text{ m/s} \tag{3.9}$$

3.5.3 Outlet Boundary (i=imax, j=1...jmax)

This boundary is a continuitive boundary outlet. Only the pressure is set, while the values for the velocities are determined from the nodes immediately upstream.

$$u_{imax,j} = u_{im1,j} \tag{3.10}$$

$$v_{imax,j} = v_{im1,j} \tag{3.11}$$

$$p_{imax,j} = 0 \text{ Pa} \tag{3.12}$$

3.5.4 Side Boundaries (i = 1...imax, j=1) (i=1...imax, j=jmax)

The boundary conditions for the left and right boundaries are very similar since they are both either nonpermeable walls, Figure 3.2(a), or no cross flow free-slip conditions, Figure 3.2(b). For the nonpermeable wall boundary, no flow crosses the wall and there is no slip parallel to the wall. The free slip boundary configures the flow to be symmetric with any flow to the right or left of the computational domain. No cross flow is allowed. Only the pressure of the right boundary is calculated due to the forward difference scheme for the pressure in the momentum equations, Eqs. (2.35, 2.36, 2.43, 2.44).

Right Boundary:

Nonpermeable Wall

$$u_{i,jmax} = -u_{im1,j} \tag{3.13}$$

$$v_{i,jm1} = 0 \text{ m/s} \tag{3.14}$$

$$p_{i,jmax} = p_{im1} \tag{3.15}$$

Symmetry

$$u_{i,jmax} = u_{im1,j} \tag{3.16}$$

$$v_{i,jm1} = 0 \text{ m/s} \tag{3.17}$$

$$p_{i,jmax} = p_{im1} \tag{3.18}$$

Left Boundary:

Nonpermeable Wall

$$u_{i,1} = -u_{i,2} \quad (3.19)$$

$$v_{i,1} = 0 \text{ m/s} \quad (3.20)$$

Symmetry

$$u_{i,1} = u_{i,2} \quad (3.21)$$

$$v_{i,1} = 0 \text{ m/s} \quad (3.22)$$

3.6 Specific Parameters of the A13192 Pleat Configuration

Figure 3.2.b illustrates the basic geometric domain of the A13192 half-pleat configuration. This domain is intended to simulate the flow of air through filter medium through half a pleat of an A13192 filter as illustrated by Figure 1.1. A half-pleat was chosen due to the symmetry of the flow.

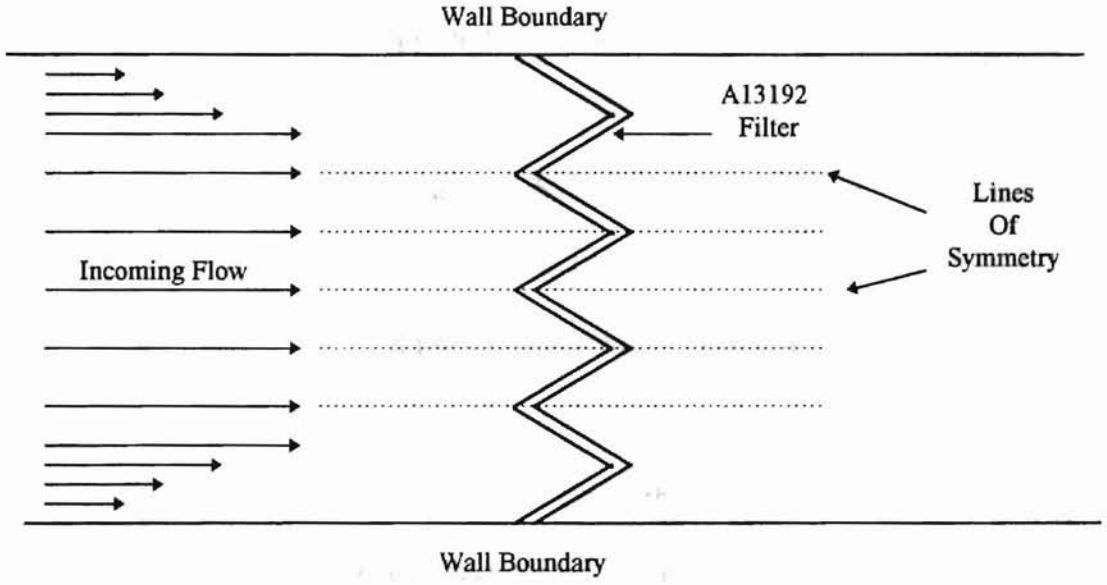

Figure 3.5 Typical Flow Field Through an A13192 Filter

The computational flow domain of Figure 3.2.b was developed from the assumptions of the larger flow field illustrated in Figure 3.5. In any real flow, the wall boundary will impose a no-slip condition thus creating an asymmetric flow near the wall. For a flow that is not fully developed, the core of the flow can still obtain a symmetrically uniform velocity at the inlet and thus create a line of symmetry along each half-pleat. Note however that near the pleat the vertical velocity, v, and the gradients of velocity, $\frac{\partial u}{\partial x}$ and $\frac{\partial v}{\partial y}$ are not zero.

What is necessary to complete the A13192 half-pleat configuration is the determination of the specific parameters illustrated by Figures 3.2, 3.3, and 3.4. The general boundary conditions were delineated in Section 3.5. The inlet velocity boundary condition was chosen as 1 m/s. Free slip or symmetry conditions were applied as side boundaries and continuitive conditions were applied to the exiting boundary conditions.

The size of the matrix and node size can be a strong determinant in the accuracy of the solution. Specific questions that should be addressed are the total amount of nodes throughout the grid matrix and the amount of nodes representing the filter in the x and y directions. Ideally, a very fine node with a large matrix would be chosen. However, computer usage time becomes a limiting factor if the node matrix is too fine.

To determine how large the node and matrix size should be, one can examine the size of the nodes needed to accurately describe the internal porous flow within the filter. For the A13192 filter, Δt_x and Δt_y are determined by the thickness of the filter paper and the angle

the paper is inclined with the incoming flow. The slope of the filter paper is 1.5 mm/30 mm so the pitch angle is 2.86°. From the geometry of Figure 3.2, the values for Δt_x and Δt_y are 12.0 mm and 0.6 mm, respectively. From these values the values of the rectangular node size (Δx and Δy) can be chosen. A determination of this value is based upon the amount of nodes properly needed to describe the thickness of the filter medium. Referring to Figure 3.2, it is seen that 2 nodes are utilized in the x and y directions to describe the filter medium. These values are referred to as "nfilx" and "nfily". If "nfilx" and "nfily" are both equal to 4 then the values for Δx and Δy are 3 mm and 0.15 mm respectively. This would set the total nodal matrix to 50 x 10 (imax=52, jmax=12) for a computational flow domain of 150 mm x 1.5 mm.

An alternate form for this configuration was analyzed also. This configuration utilizes a square node of 0.15 mm width in the x and y directions. As with the standard A13192 configuration, the values for nfilx and nfily are set to four. The total node matrix also remains at 50 x 10, however, the computational flow domain is now 7.5 mm x 1.5 mm.

3.7 Specific Parameters of the Experimental Flow Configuration

Parameters for the computational flow simulation for the experimental flow were developed in a similar manner as for the A13192 configuration except for a few variations. The inlet velocity was chosen as 1 m/s. As explained in Section 3.5, no slip wall boundary conditions were chosen for the side boundaries and continuitive conditions were chosen for the exit.

An examination of Figure 3.2 shows that the computational flow domain for the experimental configuration is quite a bit larger than for the A13192 configuration. However, the thickness of the filter medium is still approximately 0.6 mm. Ideally, a node size could be chosen that was small enough to describe the interior of the filter medium, and a matrix size could be chosen large enough to cover the entire domain. However, this is not possible due to restrictions on computer processing capacity.

As a standard, a 60 x 30 nodal matrix was chosen to cover the computational domain of 101.6 mm x 50.8 mm. This creates a square node size $\Delta x=\Delta y=$ 1.69 mm. Parametrics on these values will be investigated to determine solution sensitivity to the size of the nodes. Since the filter medium for the experiment was chosen to create a 45° angle with the incoming flow, the nodes are configured as squares similar to those in Figure 3.4. By setting "nfilx" and "nfily" equal to 4, the thickness of the filter medium in the x and y directions, Δt_x and Δt_y, become 10.16 mm with the total filter medium thickness, Δt_n=10.8 mm. This is much larger than the 0.6 mm thick filter used in the experiment.

By simulating a filter medium 10.8 mm thick, the parameters of the filter medium itself must be changed to reestablish the correct flow conditions. As derived in Section 3.2, the permeability, K, and the inertial resistance, b are 6.72e-11 m^2 and 81833 m^{-1} respectively. Parametrics for these values can be performed to determine what values are needed for the 10.8 mm simulated filter to match the flow field examined in the actual 0.6 mm experimental filter.

The simulation created therefore is not of the 0.6 mm thick filter but one that is much larger. However, by simulating a fictitious thick filter whose permeability and inertial resistance values have been significantly altered, it is hoped that the flow conditions of velocity and pressure developed by the thin 0.6 mm filter can be accurately matched. It is reasonable that the velocity gradient through the filter medium will not be represented. Neither will the pressure gradient. What is desired, is that the velocity and pressure distribution upstream and downstream of the filter can be accurately represented. This is one of the objectives of the verification experiment.

3.8 Time Constraints

As stated previously, SOLA solves the velocity and pressure field at time increments Δt, and the routine continues to do so until the results have converged. The Δt is specified by the programmer.

The choice of time increments is guided by need for solution stability and accuracy. The stability criteria equations, Eqs. (2.56 and 2.57), define a standard for the Δt for a given node size Δx by Δy.

Unfortunately, the Δt found by Eqs. (2.56 and 2.57) is still too large due to the influence of the permeability, K, and the inertial resistance, b. Noting from Section 3.2, that $K=6.72e\text{-}11\ m^2$ and $b=81833\ m^{-1}$, these terms have a heavy influence on the filter momentum equations, Eqs. (2.43 and 2.44). Without a smaller Δt, these terms destabilize the momentum equations such that there is no convergence. As noted by Cai [1993] and

Liu [1995], a good value for Δt is 1/100 the value calculated by the stability criteria. This would provide a value of about 10^{-8} s for the A13192 configuration and 10^{-5} s for the experimental configuration.

The program was allowed to continue until the pressure of selected nodes differed by less than 1 Pa in 500 time increments. For a pressure of 180 Pa, this corresponds to a difference of approximately 0.5%. Observation of the velocity results showed that they had converged to a difference of less than 1.0%

3.9 Summary of Parameters

Other parameters chosen for this analysis include the upstream differencing, the viscosity, the over-relaxation factor ω, the density ρ and others. Table 3.2 summarizes these values for the different configurations.

	A13192 Configuration	A13192 alt. Configuration	Experimental Configuration
Flow Domain, x-dir, L1 (mm)	150	7.5	143.9
Flow Domain y-dir, L2 (mm)	1.5	1.5	50.8
Nodes in x direction (imm2)	50	50	85
Nodes in y direction (jmm2)	10	10	30
Node Size Δx (mm)	3.0	.15	1.69
Node Size Δy (mm)	.15	.15	1.69
x-filter thickness Δt_x (mm)	12.0	.6	10.16
y-filter Thickness Δt_y (mm)	0.6	.6	10.16
Filter nodes x-direction	4	4	6
Filter nodes y-direction	4	4	6
Upstream Filter (ifil)	20	20	27
Downstream Filter (ifilm)	32	32	61
Inlet Velocity (m/s)	1.0	1.0	1.0
Permeability (m^2)	6.72e-11	6.72e-11	5.096e-10
Inertial Resistance (m^{-1})	81833	81833	10000
Porosity	1.0	1.0	1.0
Density kg/m^3	1.18	1.18	1.18
Viscosity (m^2/s)	1.59e-5	1.59e-5	1.59e-5
Time increment (s)	1.0e-08	1.0e-08	1.0e-05
Convergence criteria (Pa)	1 Pa	1Pa	1 Pa
Upstream Differencing	0.92	.92	0.92
Over-relaxation Factor	1.7	1.7	1.7

Table 3.2 Summary of Parameters

CHAPTER IV

VERIFICATION EXPERIMENT

4.1 Introduction

The configuration for the computational simulation described as the experimental configuration in Chapter III was created specifically for verification by a physical flow experiment. This experiment consisted of directing a flow of air through a single sheet of filter paper within a rectangular duct with a cross section of 50.8 mm x 254 mm. Measurements of velocity and pressure near the filter paper were gathered which could be compared to the velocity and pressure results obtained from the computational data. All results of both computational and experimental studies are provided in Chapter V.

4.2 Experimental Setup

Figure 3.2 illustrates the experimental configuration utilized for the computational simulation as described in Chapter III. In Figure 3.2, it is shown that air flows within a two-dimensional duct through a filter paper slanted 45°. Of course the computational domain illustrated by Figure 3.2 was only a small part of the entire flow created in the experiment. This complete flow field is illustrated by Figure 4.1. From Figure 4.1, it is shown that air was drawn through a test housing by a centrifugal multistage exhauster or blower. Upstream from the test housing, the flow was seeded with 0.966 μm Polystyrene Latex aerosol particles by a 6-Jet atomizer (TSI Incorporated Model 9306). The purpose of these particles was for velocity measurements by a Laser Doppler Velocimeter (LDV) system. To avoid introducing condensed water into the flow, a fan heater was utilized to

completely evaporate the water surrounding the particles. From the test housing, the flow was exhausted through PVC pipe through a flow meter and eventually through the blower.

The inlet and exhaust ducting consist of PVC tubing of various sizes. As shown in Figure 4.1, the inlet ducting is not connected to the test housing. Only a small portion of the flow introduced into the test housing comes from the inlet ducting. The majority of the flow in the test housing comes directly from the room.

The exhaust ducting is connected to the test housing and consists of Plexiglas and PVC tubing. Within the exhaust ducting is a TSI Series 2010 Mass Flowmeter which measures the flow rate. This flow sensor has a maximum measurable flow rate of approximately 0.23 m^3/s.

The complete automotive filter test stand consists of the multistage centrifugal blower, absolute filter, elevated test stand area, laminar flow element and control panel. It was produced in 1976 by Facet Enterprises, Inc. specifically for testing automotive air filters. The test stand has been transferred to the OSU Mechanical Engineering Laboratories from Purolator Products Inc. For this test, the centrifugal blower was utilized to pull approximately .011 m^3/s through the housing.

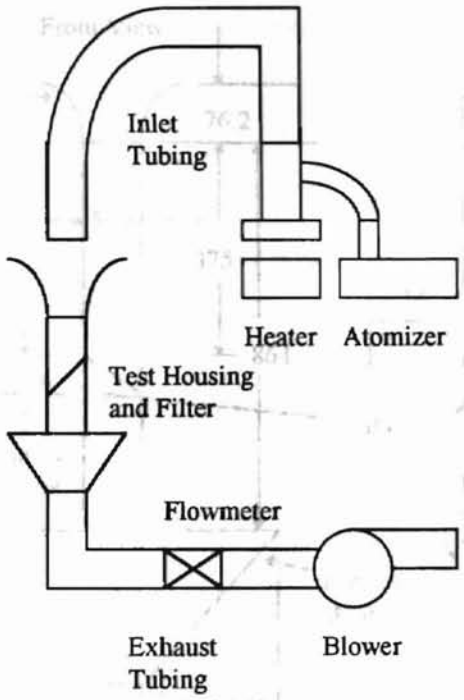

Figure 4.1 Experimental Flow Apparatus

The test housing with the filter is the critical component of the experiment. This test housing was created so that the CFD simulation domain illustrated in Figure 3.2, could be recreated experimentally. Figure 4.2 illustrates the test housing.

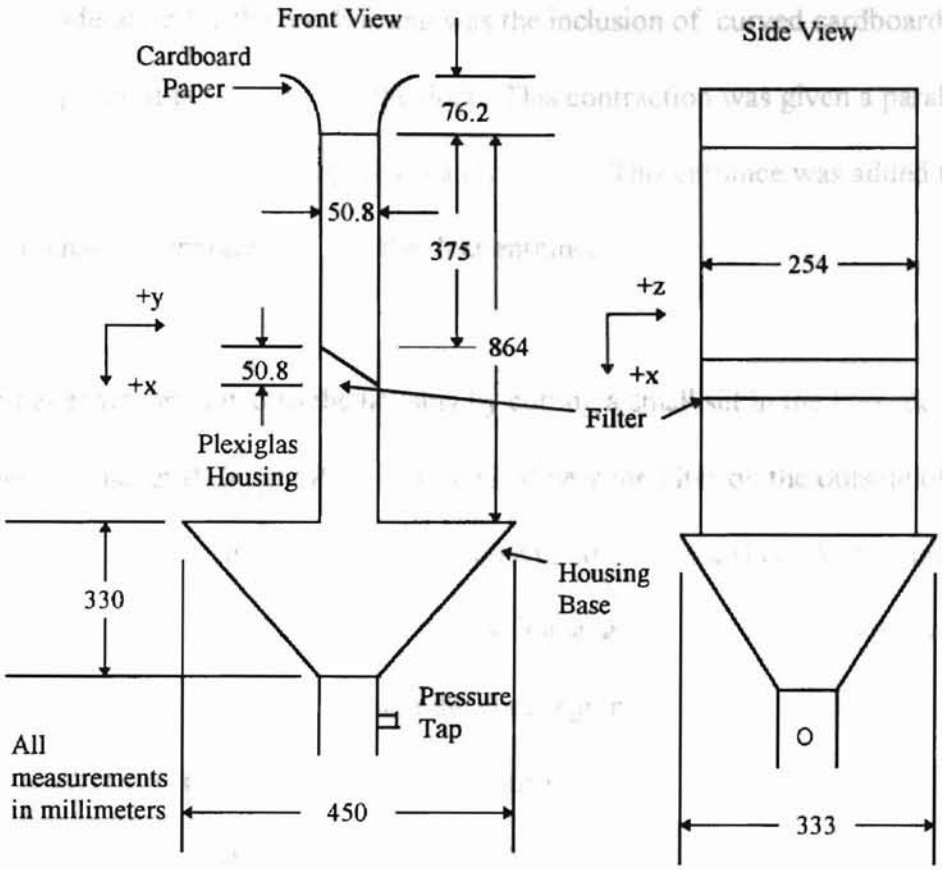

Figure 4.2 Test Housing and Filter

In this housing, air is drawn from the top inlet, directed through a single layer of filter paper, passed through the base, and then exhausted through a pipe to the blower. The housing is constructed with ¼ in. thick transparent Plexiglas enabling laser beams optical access for Laser Doppler Velocimeter velocity measurements. The test housing is divided into two parts. The first is a rectangular duct which holds the filter and has cross sectional dimensions of 254 mm by 50.8 mm . These dimensions provide a 5 to 1 ratio so as to create a nearly two-dimensional flow in the xy plane. The second part of the test housing is the base which is a plenum to exhaust the air after passing through the duct. This air plenum serves to isolate the duct from the exit piping.

Another consideration for the test housing was the inclusion of curved cardboard construction paper at the entrance of the duct. This contraction was given a parabolic shape and provided an area ratio approximately 4 to 1. This entrance was added to help maintain laminar, unseparated flow at the duct entrance.

The filter paper was mounted to the housing by cutting a small slit in the Plexiglas and pulling the filter paper through. Putty was applied near the filter on the outside of the housing to insure that no air leaked into the housing due to these slits. A manometer port was included downstream of the base of the test housing to determine the pressure difference between the ambient room and the duct region downstream of the filter. To measure the pressure effect of the filter, the experiment was first run at a specified flow rate without the filter installed. The pressure difference between the room and the duct was recorded. During the actual filter experiment with the filter installed, the experiment was run at the same flow rate and the pressure was once again recorded. By comparing the pressure in the duct between the run with the filter and the run without the filter, the pressure effect of the filter can be determined.

Velocity measurements were performed with a fiber optic LDV system with its transceiver mounted on a traverse table. A schematic of this system is provided in Figure 4.3.

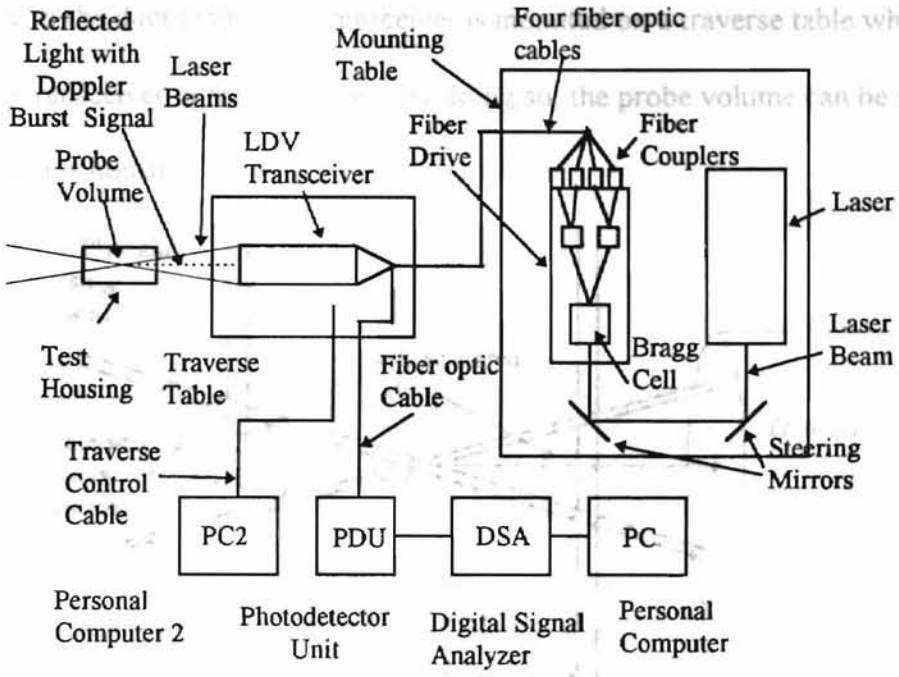

Figure 4.3 Schematic of the Measurement System

With this system, a Coherent Innova, 70-A, 4 watt, argon ion laser applies a beam to a fiber drive. A typical setting for the laser is 0.2 Watts during alignment of the fiber drive and 0.6 Watts for actual measurement operation. Within the fiber drive, a Bragg cell applies a frequency shift to the beam which produces a moving fringe pattern. Two beams are produced by this frequency shift which are then separately split into two blue and two green beams producing a total of four beams, one shifted and one unshifted for each color. These beams are focused from the fiber drive to four separate fiber optic cables with the fiber couplers. The beams are then transmitted through the cables to the fiber optic transceiver. The fiber optic transceiver focuses the four beams to create a probe volume within the test housing that is 737 μm in length and 66 μm in diameter. The green beams measure the velocity along the duct (±x) and the blue beams measure the velocity

crosswise to the duct (±y). The transceiver is mounted on a traverse table which can move the transceiver in any direction. By doing so, the probe volume can be moved within the test housing.

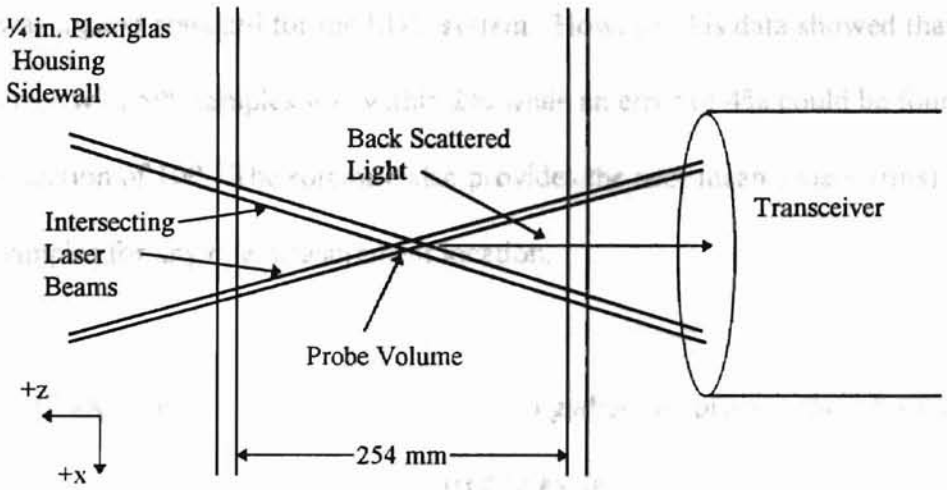

Figure 4.4 Probe Volume

The aerosol particles pass through the probe volume and produce a scattered light signal called a Doppler burst signal. Within the probe volume, the laser beams produce an interference fringe system with a fringe spacing, d. As a particle passes through these fringes, the Doppler burst signal is created. This signal is sensed through the scattered light collected by the transceiver and passed on to the photodetector unit (PDU), and the Digital Signal Analyzer (DSA). The DSA, with suitable signal processing, performs a Fast Fourier Transform, FFT, on the burst signal, providing a Doppler frequency, f. The velocity of the particle passing through the probe volume is a function of the frequency and the fringe spacing.

$$V = f\,d \qquad (4.1)$$

The number of samples to be gathered for one data point can be specified by the Aerometrics Data Collection Software. For this test, 500 samples were set as the standard amount of samples to be collected. Newman [1994] determined that a sample collection of 1000 was a good standard for the LDV system. However, his data showed that the velocity error with 500 samples was within 2% while an error of 4% could be found with a sample collection of 100. The software also provides the root mean square (rms) for the velocity samples for any one measurement location.

An Intel 486 DX/2 personal computer was used to gather and process the information from the DSA. The program software referred to as the DSA software performs a statistical analysis of the sample data sent from the DSA itself. Displays of mean velocity, rms velocity for the samples, and a velocity histogram are provided. Another 486 computer was used to control the traverse table driven by two stepping motors. The distance that the transceiver could be moved with the stepping motors was controllable from the software.

4.3 Experimental Parameters

The purpose of the experiment was to verify the CFD models developed in Chapter III. To do so, the experiment was set up with the apparatus described in Sections 4.1 and 4.2. Critical parameters for the equipment in this experiment are chosen in this section.

4.3.1 Laminar and Turbulent Flow

The flow speed through the housing was chosen to create a laminar flow within the test housing. To do so, the lowest setting for the blower was chosen. This setting created a flow of .01189 m^3/s through the test housing. Initial readings from the LDV indicated that this created an average velocity of 1m/s near the filter. Refer to Figure 4.2. The filter is located from 37.5 to 46 cm (14.75 to 16.75 in.) from the entrance of the Plexiglas housing duct. This distance from the inlet places the filter within the boundary layer entrance region for the housing. Recall that the flow through the test housing is treated as a two-dimensional flow between two parallel plates 50.8 mm apart.

Calculation of the flat plate Reynolds number can be done upstream of the filter assuming a zero pressure gradient. Of course, the actual pressure gradient is favorable between the entrance and the filter. Using a distance of 37.5 cm from the entrance to the filter, a velocity of 1 m/s, and a viscosity of 1.59e-05 m^2/s, the boundary layer Reynolds number is calculated to be 2.35×10^4 which is laminar.

The growing boundary layers can be considered laminar or turbulent. At a distance of 37.5 cm from the inlet, the boundary layer thickness can be calculated as either 11.8 mm or 14.1 mm depending on whether one assumes that the boundary layer is laminar or turbulent. Either way, it can be seen that with a wall 50.8 mm apart, the boundary layer is sufficiently thin to create a laminar core.

These calculations assume a zero pressure gradient whereas the situation with this flow is a favorable pressure gradient. This is more likely to create laminar flow with smaller boundary layers. However, any disturbances at the entrance such as a bump between the cardboard inlet to the duct could promote turbulence.

The assumption of laminar flow utilized in the CFD simulations was checked by measuring the rms value of the u-velocity. The vertical turbulence intensity can be found by dividing the local rms value of the local u-velocity by the mean u-velocity near the center of the duct. The turbulent intensity results are provided in Chapter V.

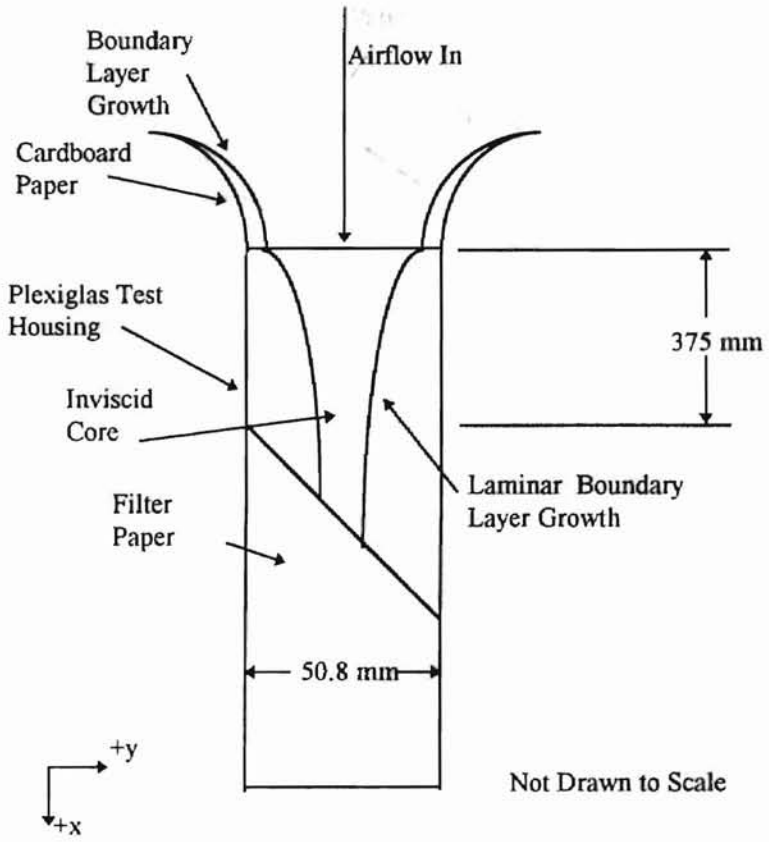

Figure 4.5 Boundary Layer Growth Within Test Housing

4.3.2 Measurement Location

The LDV measures the velocity of the airflow on a point by point basis. Although velocity measurements near the filter paper are taken, few can be taken very close to the filter due to the nature of the LDV system. As previously mentioned, in this system, 4 beams, 2 green and 2 blue, penetrate the ±z Plexiglas walls to create a probe volume inside the flow. Unfortunately, as the beams penetrate the Plexiglas sidewall, they cannot intersect with either the filter paper or the 6.35 mm (¼ in.) ±y Plexiglas sidewalls as they converge to form a probe volume. Figure 4.6 illustrates the situation.

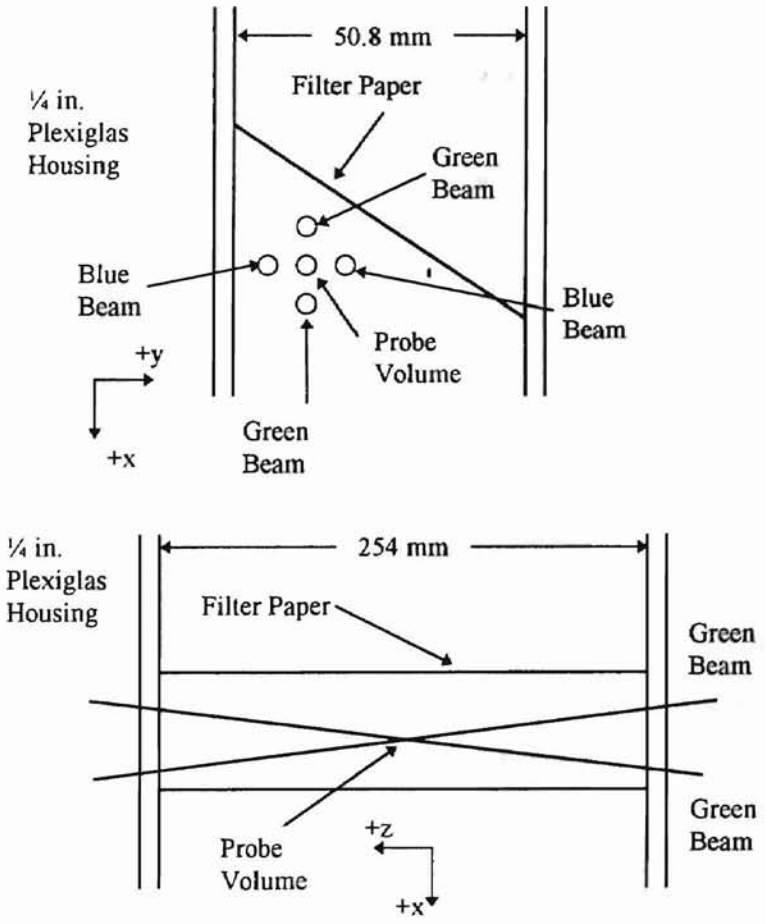

Figure 4.6 Laser Beam Entry into Test Housing

Blockage of the beam can occur if the probe location is chosen too close to either the sidewall or the filter. Figure 4.7 illustrates the position of the data points taken near the filter.

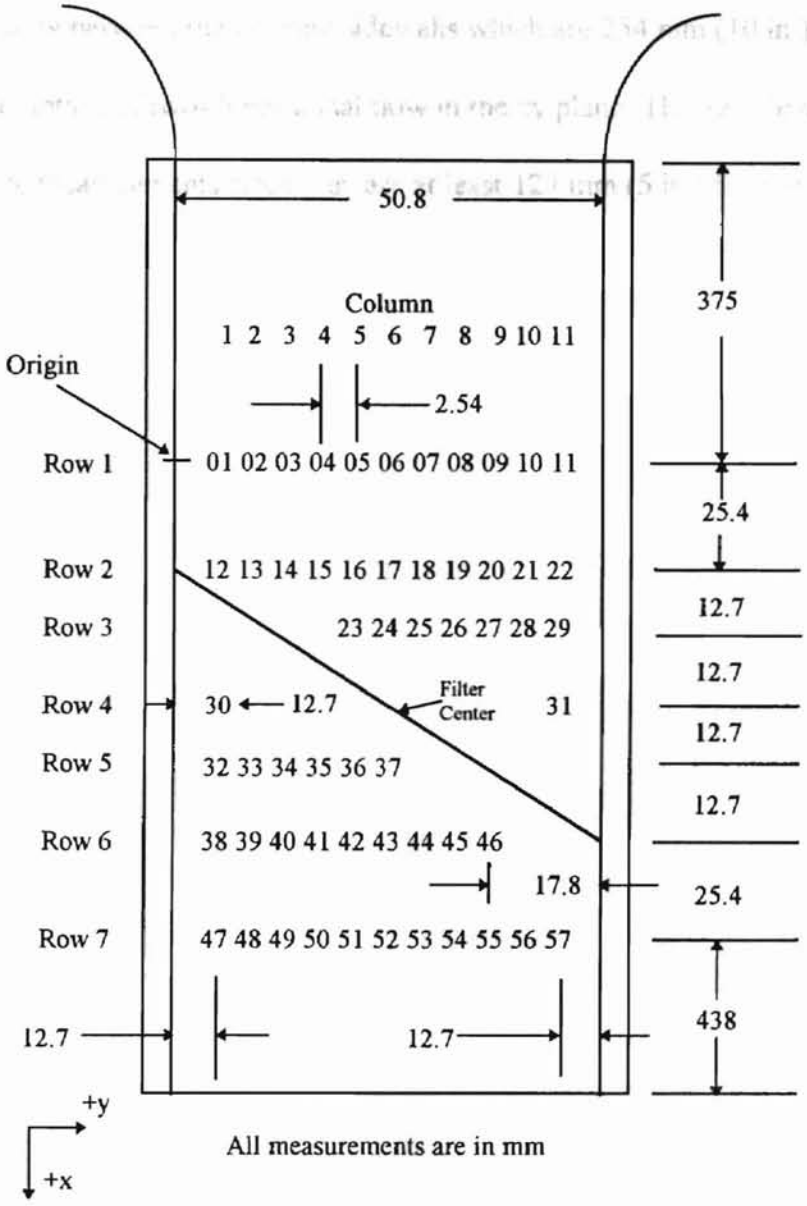

Figure 4.7 Location of Measurement Points

It should be noted that all of the measurement points are at least 12.7 mm (0.5 in). from the wall due to the 4 beam configuration as shown in Figure 4.6. Most of the interior data points are 2.54 mm (0.1 in.) apart. Note again that in the z direction, the probe volume is in the center exactly between the housing sidewalls which are 254 mm (10 in.) apart allowing an assumption of two-dimensional flow in the xy plane. The ±z sidewalls have little effect on the measurements since they are at least 127 mm (5 in.) from the probe volume.

CHAPTER V

COMPUTATIONAL AND EXPERIMENTAL RESULTS

5.1 Experimental Results

The results of the verification experiment consist of velocity and pressure measurements. The velocity is divided into the x-component or u-velocities and the y-component or v-velocities. The u and v velocity data is presented in Figures 5.1 and 5.2. The position of the velocity data is provided by Figure 4.7.

5.1.1 Experimental Results: Tabular Representation

Figures 5.1 and 5.2 provide the velocity data for the experiment in a tabular format. Graphical format is provided in the next section. The data is divided into rows and columns. The total length of the measurement field is 101.6 mm (4 in). The velocity was measured in a location near the filter to determine velocities induced on the flow by the filter. The region to the left of the filter is referred to as the downstream crevasse. The region to the right of the filter is referred to as the upstream crevasse.

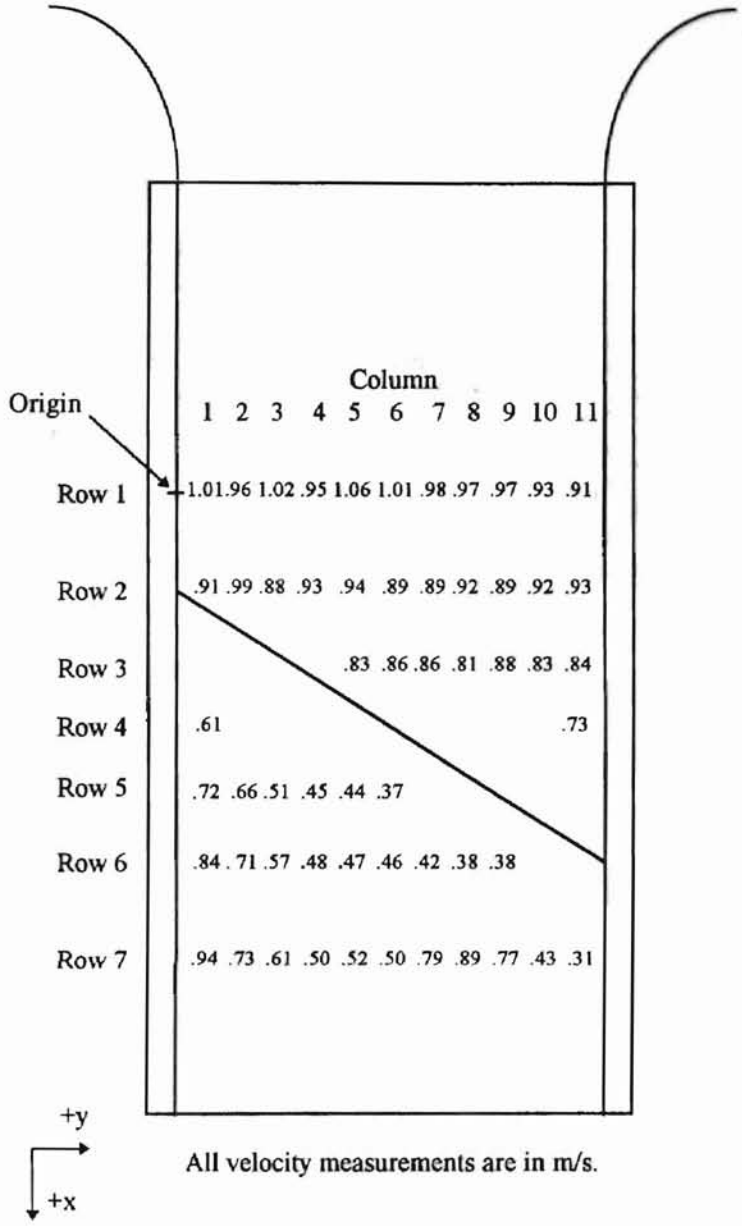

Figure 5.1 U-Velocity Measurements

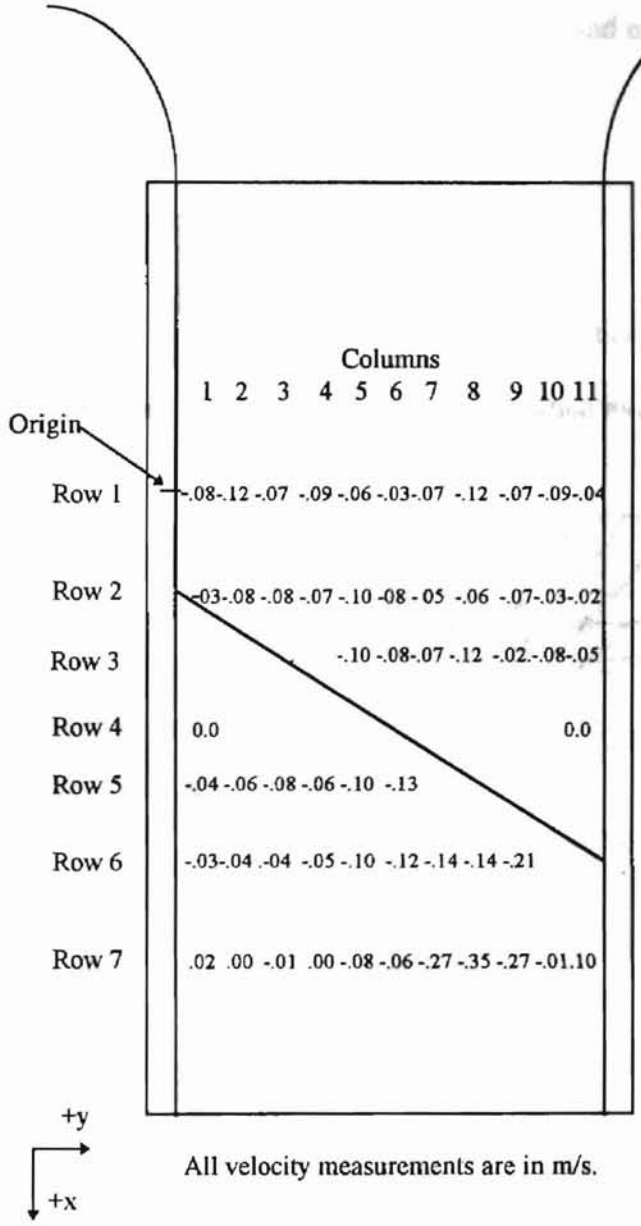

Figure 5.2 V-Velocity Measurements

The change of pressure through the filter was found to be 180 Pa as measured by the manometer. This was determined by first measuring the pressure between the downstream pipe and the ambient room without the filter installed. The filter was then added and the additional pressure drop induced by the filter was measured at the same flow rate. Note

that a superposition of the pressure drops of the filter, duct and exhaust plenum is assumed in this assessment.

5.1.2 Experimental Results: Graphical Representation

The data provided in the previous section is provided in graphical format in Figures 5.3 and 5.4. Reference to Figures 4.7, 5.1 and 5.2 is useful when interpreting these graphs.

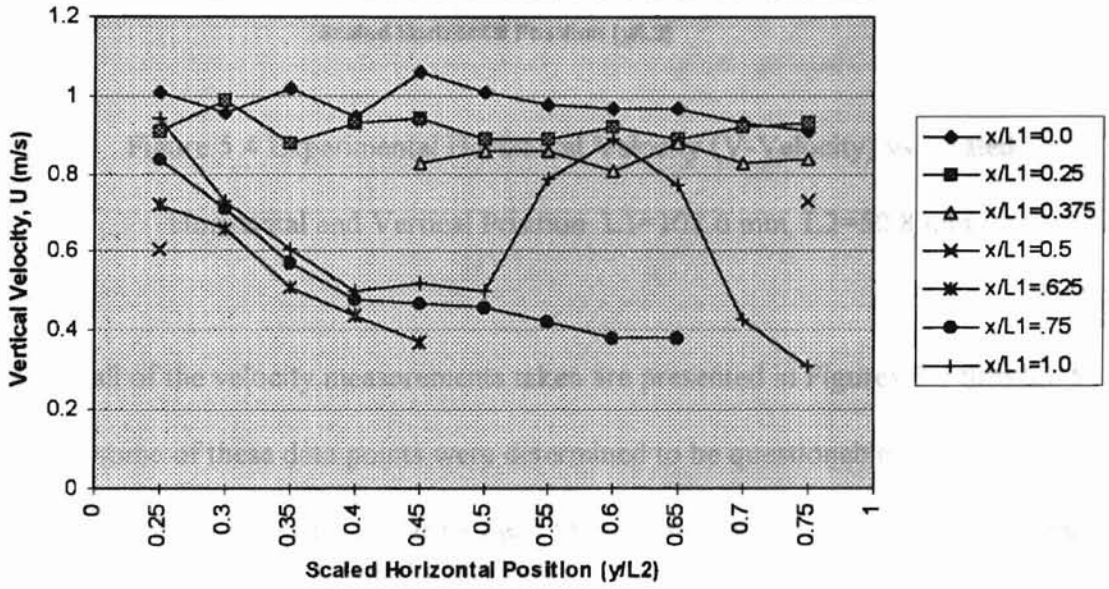

Figure 5.3 Experimental Vertical Velocity (U-Velocity) vs. Scaled Horizontal and Vertical Positions L1=101.6 mm, L2=50.8 mm

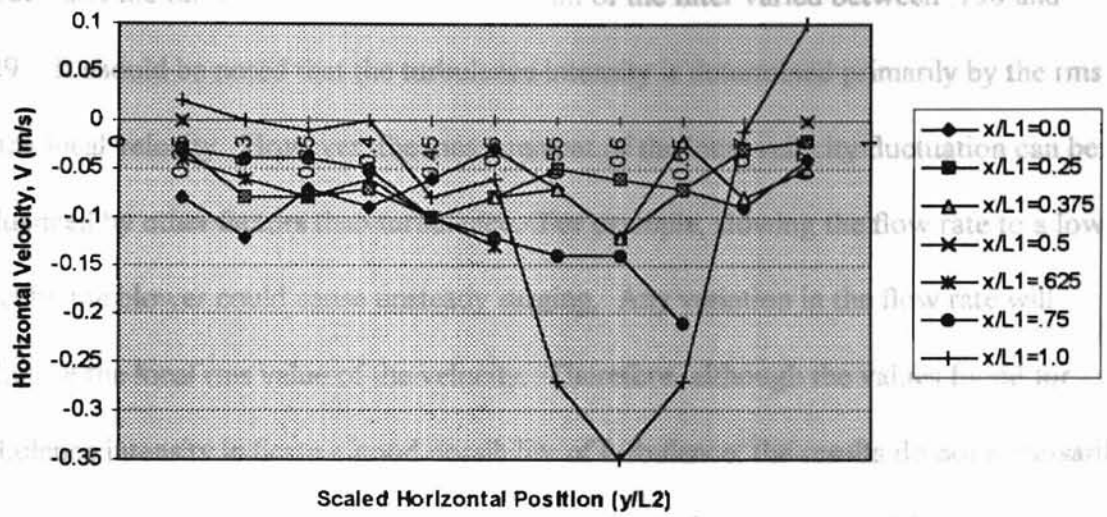

Figure 5.4 Experimental Horizontal Velocity (V-Velocity) vs. Scaled Horizontal and Vertical Position L1=101.6 mm, L2=50.8 mm

Note that all of the velocity measurements taken are presented in Figures 5.1 through 5.4. However, some of these data points were determined to be questionable measurements which should be noted when comparing them to the computational data as done in Section 5.6. Referring to Figure 4.7, these are points 12, 43, 46, 53, 54, 55, 56, and 57. Measurements of these points was characterized by a low particle count along with a scattered velocity histogram. Further explanation of these data points is provided in Chapter VI.

5.1.3 Turbulence Intensity

The turbulence intensity for the vertical velocity of each measurement was determined by dividing the rms of the local vertical velocity by the average mean velocity at the center of the duct. It was found that upstream of the filter the turbulence intensity varied from .208

to .287 and the turbulence intensity downstream of the filter varied between .198 and .429. It should be noted that the turbulence intensity is determined primarily by the rms of the local velocity. However, the measurement of the local velocity fluctuation can be influenced by other factors than turbulence. For example, slowing the flow rate to a low level by the blower could cause unsteady surging. Any variation in the flow rate will influence the local rms value of the velocity. Therefore, although the values found for turbulence intensity indicate a good possibility of turbulence, the results do not necessarily ensure that turbulence was present particularly in the region upstream of the filter.

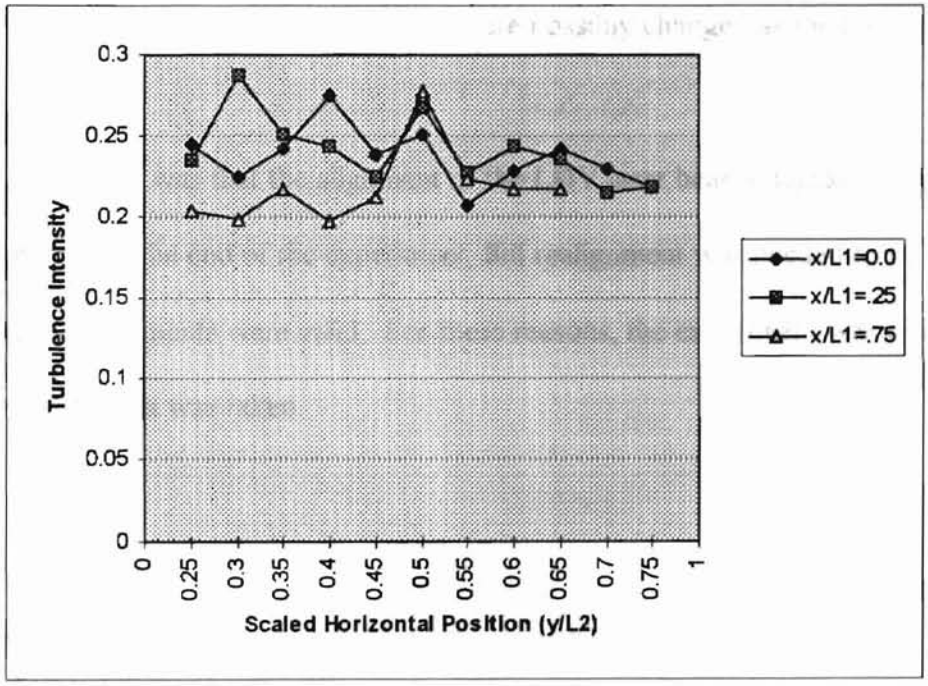

Figure 5.5 Turbulence Intensity vs. Scaled

Horizontal and Vertical Position L1=101.6 mm, L2=50.8 mm

5.1.4 Repeatability

Several practice runs of the experimental data were performed before the complete experiment was completed. During these practice runs, several factors were noted that could possibly affect the repeatability of the experiment.

One was that the filter became increasingly wet due to humidity. Although the vapor from the atomizer was fully heated before being introduced into the filter duct, the system was an open system as illustrated in Figure 4.1 allowing some humidity into the system. Subsequently, the characteristics of the filter were possibly changed as the test proceeded.

Another event noted was that the alignment of the LDV laser beams degraded throughout the experiment. By the end of the experiment, full realignment was needed to ensure that the velocity measurements were valid. For these reasons, the experiment was not repeated once the velocity data was taken.

5.2 Computational Results

The computational results are presented mostly in graphical format. This is due to the large data size. References to Figure 3.2 for the correct flow configuration are helpful when examining the results.

5.2.1 Grid Density Study

One of the important parameters investigated in computational simulations is the density of the grid. More accurate solutions are the typical result of an increasing grid size.

However, these are obtained at a cost of computer usage time. With the standard experimental configuration provided by Table 3.2, the size of the grid was varied. Changing the grid density also changes the number of nodes used to describe the filter medium. These parametric variations are provided by Table 5.1. The most drastic change noticed by changing the grid density is the total change of pressure from the inlet to the outlet of the flow field. Velocity can also be affected. Table 5.1 and Figure 5.6 show the variation of pressure with grid density. Figure 5.7 shows how the velocity profile changes with grid density.

Grid Density	Filter nodes x and y dir.	Node size (mm)	Pressure (Pa)
20 x 10	2	5.08 x 5.08	118
30 x 15	3	3.38 x 3.38	152
40 x 20	4	2.54 x 2.54	169
50 x 25	5	2.03 x 2.03	178
60 x 30	6	1.69 x 1.69	180

Table 5.1 Pressure Across Filter Medium and Grid Density

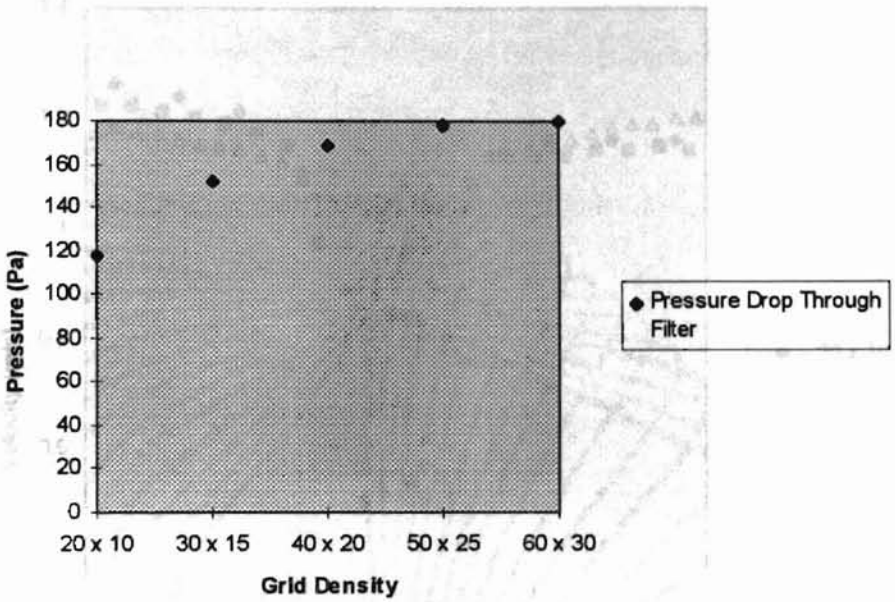

Figure 5.6 Pressure Through Filter Medium vs. Grid Density

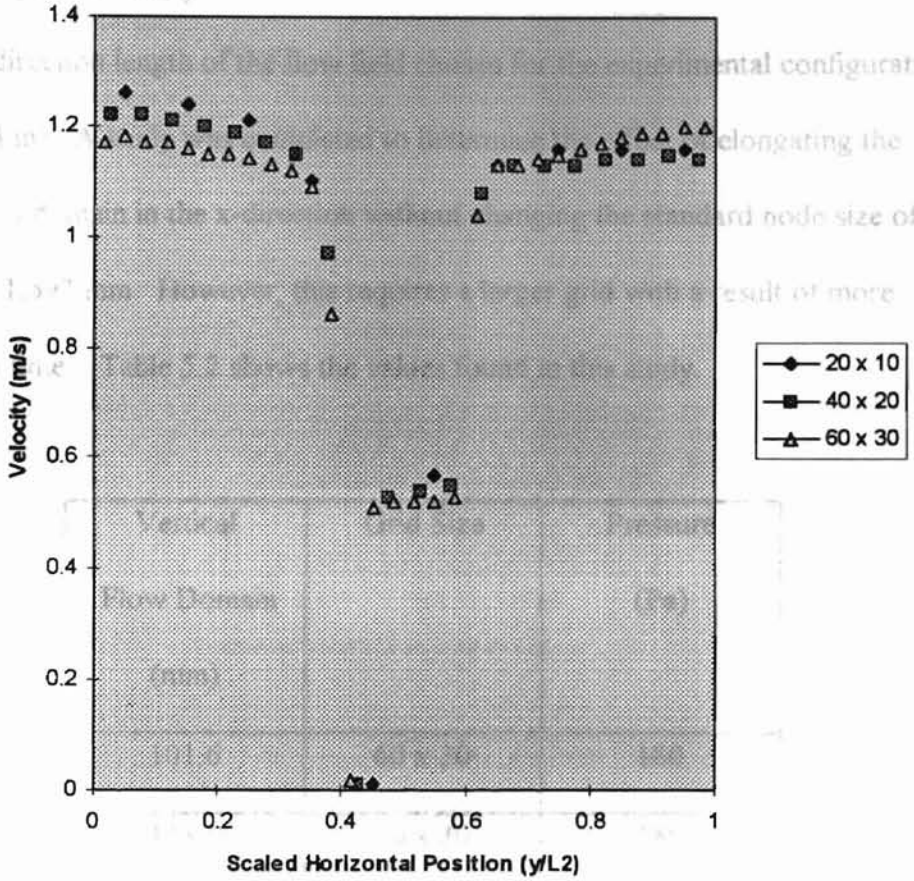

Figure 5.7 U-Velocity Profile and Grid Density

x/L1=0.5, L1=101.6 mm, L2=50.8

An examination of Figure 5.6 shows that the overall pressure difference is a nonlinear function of grid density. As the grid becomes denser, the pressure continues to increase but decreasingly so. The velocity profile in Figure 5.7 shows how the velocity varies with grid density. From these parametrics, a node size of 1.693 mm x 1.693 mm was chosen although the grid was expanded to 85 x 30 to increase the flow domain as explained in the next section.

5.2.2 Flow Domain Study

The total x-direction length of the flow field chosen for the experimental configuration is 101.6 mm (4 in). A study was completed to determine the effect of elongating the computational domain in the x-direction without changing the standard node size of 1.693 mm x 1.693 mm. However, this requires a larger grid with a result of more computation time. Table 5.2 shows the values found in this study.

Vertical Flow Domain (mm)	Grid Size	Pressure (Pa)
101.6	60 x 30	180
118.3	70 x 30	180
143.9	85 x 30	180

Table 5.2 Pressure and Flow Domain

Table 5.2 shows that the overall pressure change due to the filter is not affected by the flow length. Also, the effect on the velocity for the varying flow lengths is small as shown by Figure 5.8. Here, the u-velocity profile is shown not to vary significantly with the overall flow length. However, for the experimental configuration, the longest flow domain length of 143.9 mm with a corresponding grid size of 85 x 30 is utilized to ensure the most accurate results.

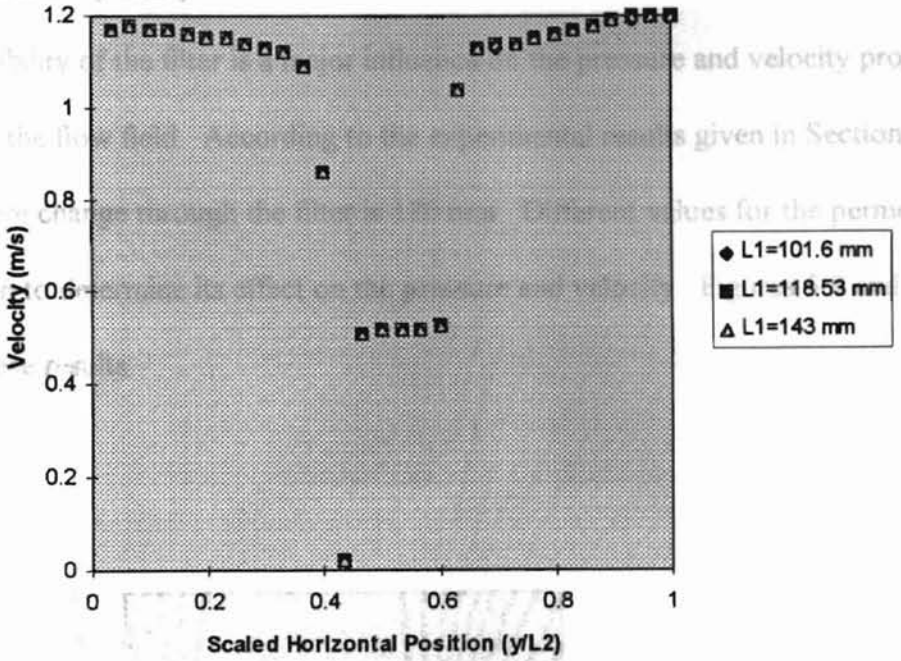

Figure 5.8 U-Velocity Profile and Vertical Flow Domain

x/L1=0.5, L2=50.8 mm

5.2.3 Permeability Study

The permeability of the filter is a major influence on the pressure and velocity profile throughout the flow field. According to the experimental results given in Section 5.1, the total pressure change through the filter is 180 mm. Different values for the permeability were chosen to determine its effect on the pressure and velocity. Figures 5.9 and 5.10 describe these results.

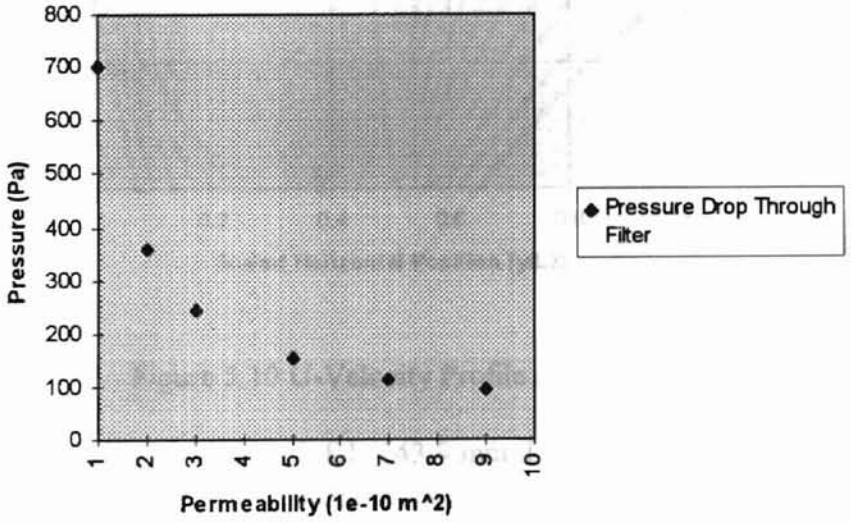

Figure 5.9 Pressure Vs. Permeability

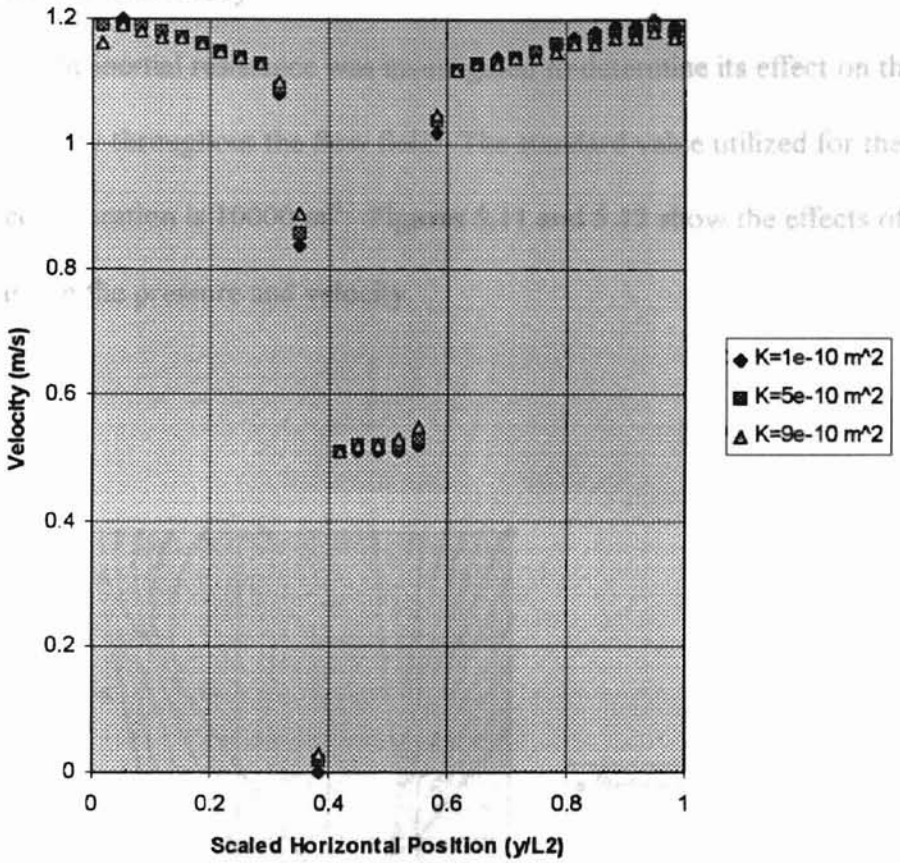

Figure 5.10 U-Velocity Profile and Permeability

x/L1=0.5, L1=143.9 mm, L2=50.8 mm

It is seen from Figure 5.9, that the pressure is a nonlinear function of the permeability. By iterating on the value of the permeability and observing the total pressure difference through the filter, a permeability of 5.096e-10 m^2 was chosen producing a total pressure change of 180 Pa through the filter. As previously explained, this was the pressure drop that was observed through the filter in the verification experiment.

5.2.4 Inertial Resistance Study

The variation of the inertial resistance was investigated to determine its effect on the pressure and velocity throughout the flow field. The standard value utilized for the experimental configuration is 10000 m^{-1}. Figures 5.11 and 5.12 show the effects of the inertial constant on the pressure and velocity.

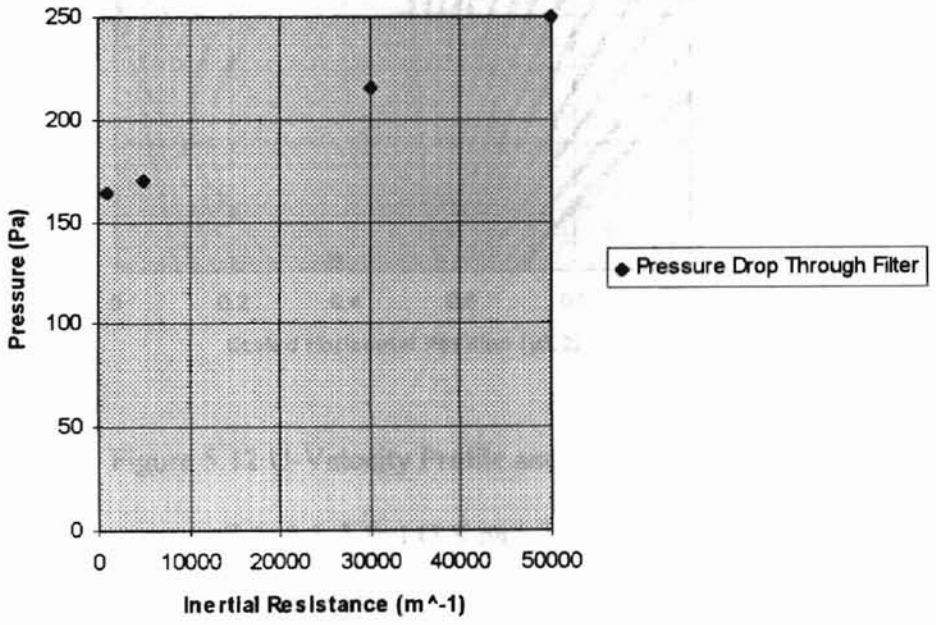

Figure 5.11 Pressure Through Filter vs. Inertial Resistance

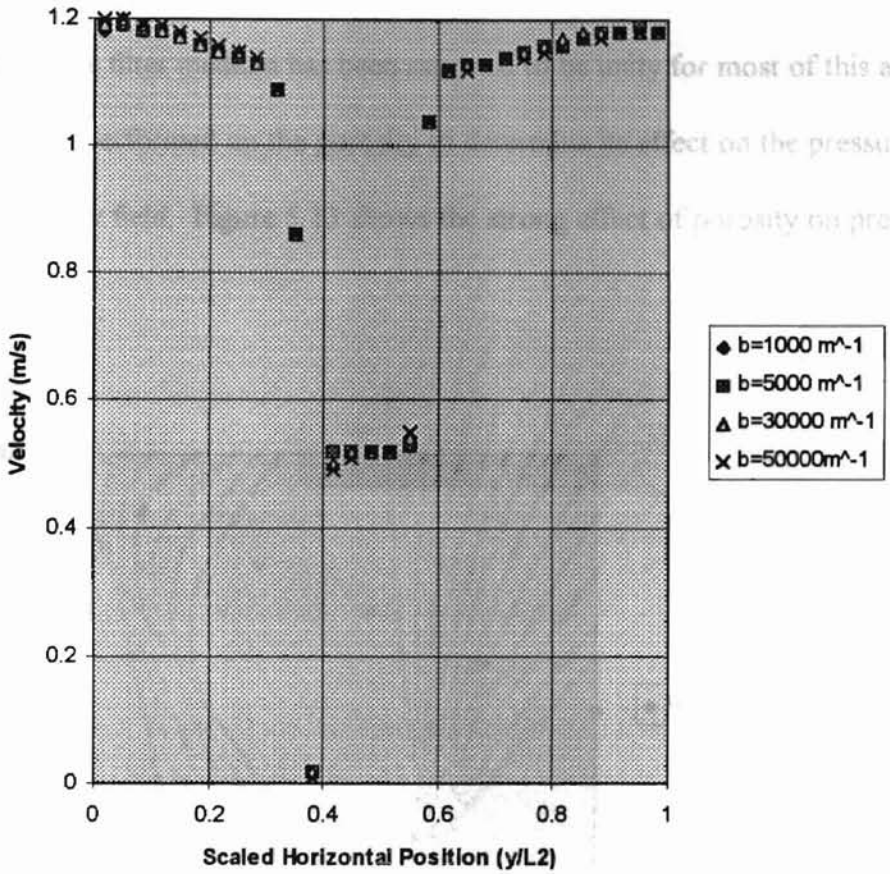

Figure 5.12 U-Velocity Profile and Inertial Resistance

x/L1=0.5, L1=143.9 mm, L2=50.8 mm

It is seen from Figure 5.11, that the inertial resistance can influence the pressure through the filter and that that influence is fairly linear. However, Figure 5.12 shows that the velocity of the flow through the filter is only weakly affected by changes in inertial resistance.

5.2.5 Porosity Study

The porosity of the filter medium has been assumed to be unity for most of this analysis. Parametrics were performed on the porosity to determine its effect on the pressure and velocity of the flow field. Figure 5.13 shows the strong effect of porosity on pressure.

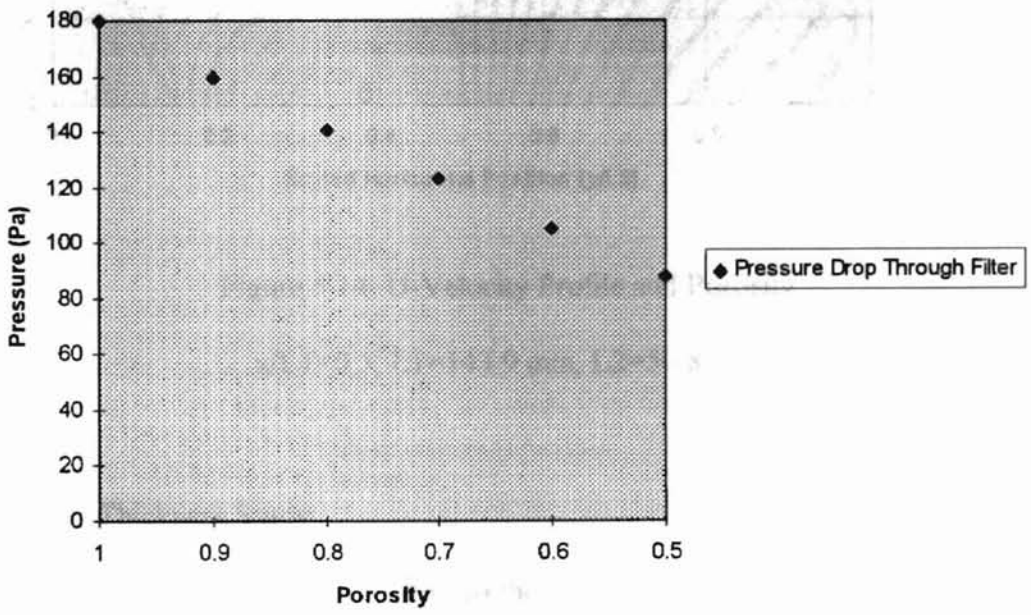

Figure 5.13 Pressure Through Filter Vs. Porosity

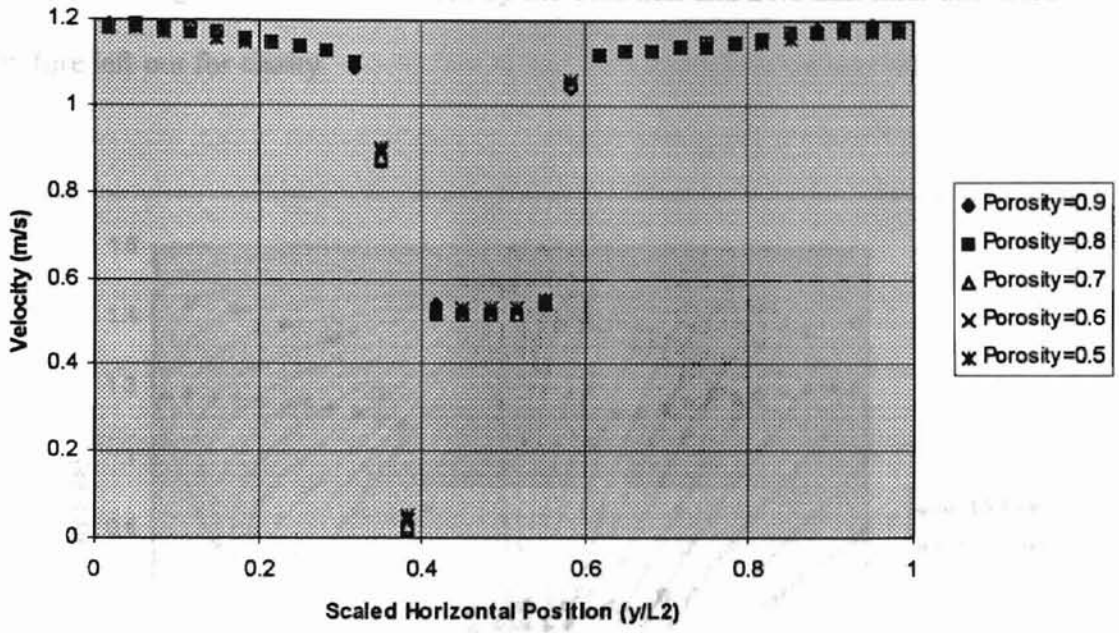

Figure 5.14 U-Velocity Profile and Porosity

x/L1=0.5, L1=143.9 mm, L2=50.8 mm

5.2.6 Filter Thickness Study

The sensitivity of the velocity of the filter to the filter thickness was examined. The filter thickness was varied which required a changing grid size so as to utilize six nodes to describe the filter in the x and y direction while maintaining a constant computational domain. Filter thickness was varied from 10.8 mm to 21.6 mm. The flow domain was maintained at 101.6 mm x 50.8 mm. Additionally, the permeability was adjusted for each case so as to allow the pressure drop through the filter to remain a constant 180 Pa for each case. Figure 5.15 shows the effect of filter thickness on velocity. Cases for filter thickness of 12.9 mm and 16.2 mm were also completed but their velocity results all fell

between the range of velocities induced by the 10.8 mm and 21.6 mm filter and were therefore left out for clarity.

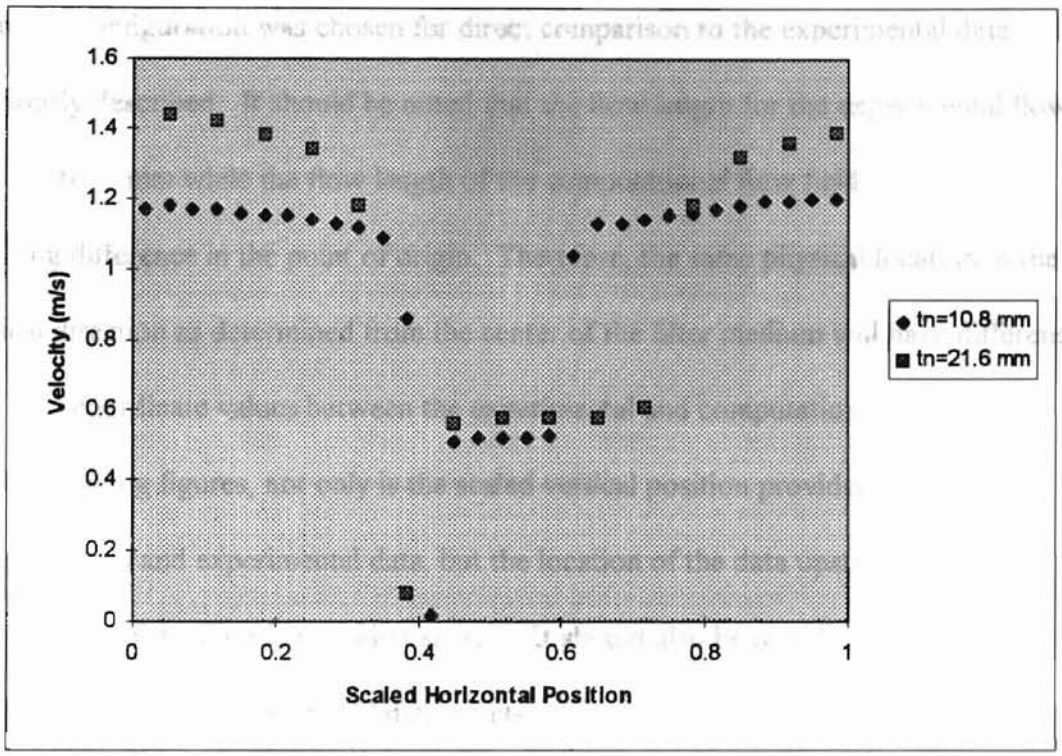

Figure 5.15 U-Velocity Profile and Filter Thickness

x/L1=0.5, L1=101.6 mm, L2=50.8 mm

These results show that a changing filter thickness induces a different velocity upon the flow near the filter even though the permeability was adjusted to maintain a constant pressure drop.

5.2.7 Standard Experimental Configuration

The table of velocity results for the standard experimental configuration as described by Table 3.4 is provided in Appendix A. Including the boundary nodes, this configuration

has 87 rows and 32 columns of data to describe the flow field. Each data point is spaced 1.693 mm apart from the adjoining data point. This configuration was the one chosen for verification with the experimental data as provided by Figures 5.1 and 5.2. Velocity data from this configuration was chosen for direct comparison to the experimental data previously described. It should be noted that the flow length for the experimental flow field is 101.6 mm while the flow length of the computational flow field is 143.9 mm with a resulting difference in the point of origin. Therefore, the same physical location in the vertical direction as determined from the center of the filter medium will have different x-direction coordinate values between the experimental and computational data. Therefore, in the following figures, not only is the scaled vertical position provided for the computational and experimental data, but the location of the data upstream and downstream of the filter is provided as well. It should also be noted that in the following figures, some of the experimental data points were determined to be questionable. These include points 12, 43, 46, 53, 54, 55, 56, and 57. Further explanation of this is provided in Chapter VI.

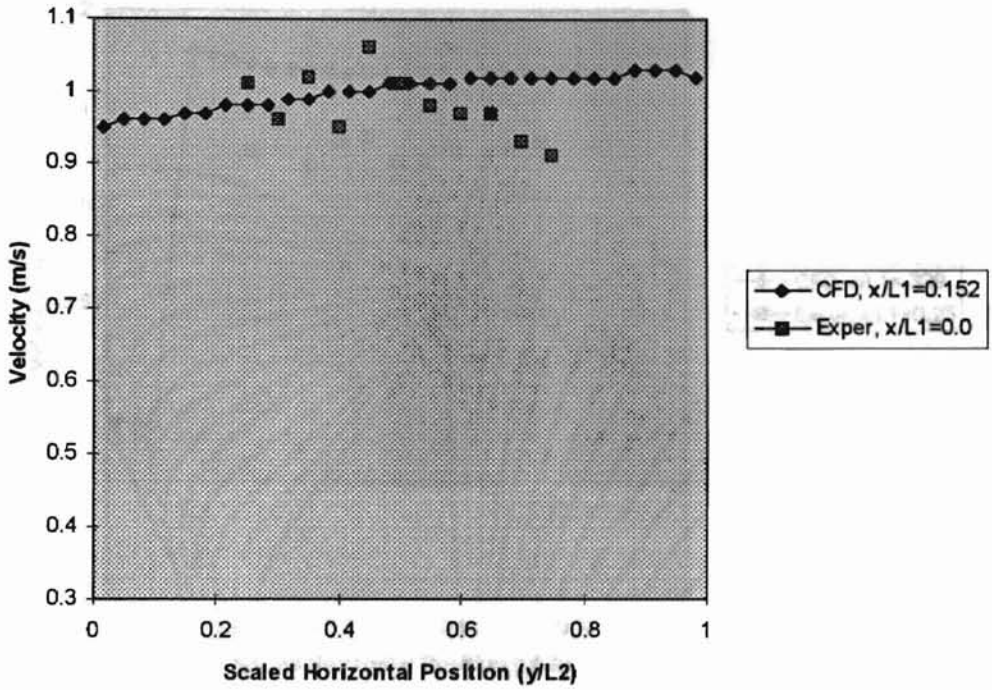

Figure 5.16 Comparison of Computational and Experimental U-Velocity Profile; Experimental L1=101.6 mm, Computational L1=143.9 mm, L2=50.8 mm; Profile 50.8 mm (2 in) Upstream of Filter Center

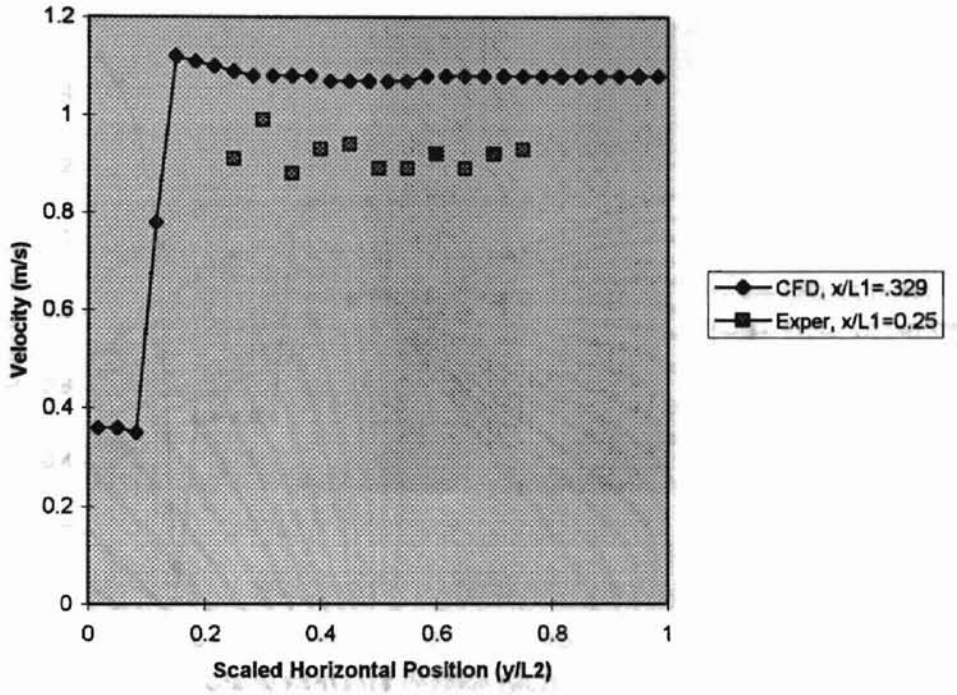

Figure 5.17 Comparison of Computational and Experimental U-Velocity Profile; Experimental L1=101.6 mm, Computational L1=143.9 mm, L2=50.8 mm; Profile 25.4 mm (1 in) Upstream of Filter Center

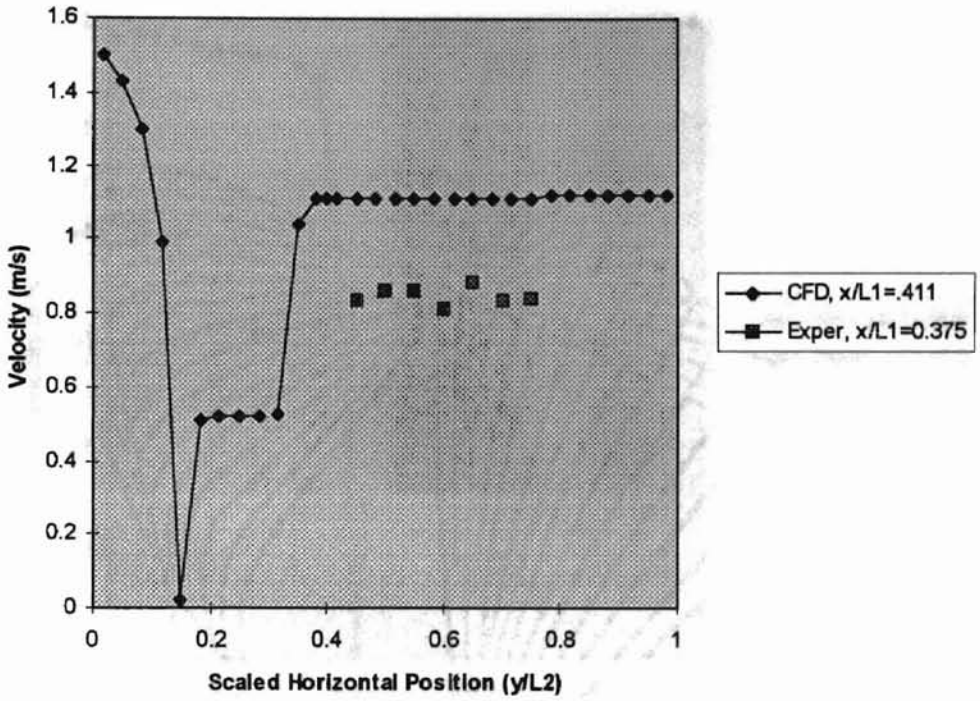

Figure 5.18 Comparison of Computational and Experimental U-Velocity Profile; Experimental L1=101.6 mm, Computational L1=143.9 mm, L2=50.8 mm; Profile 12.7 mm (0.5 in) Upstream of Filter Center

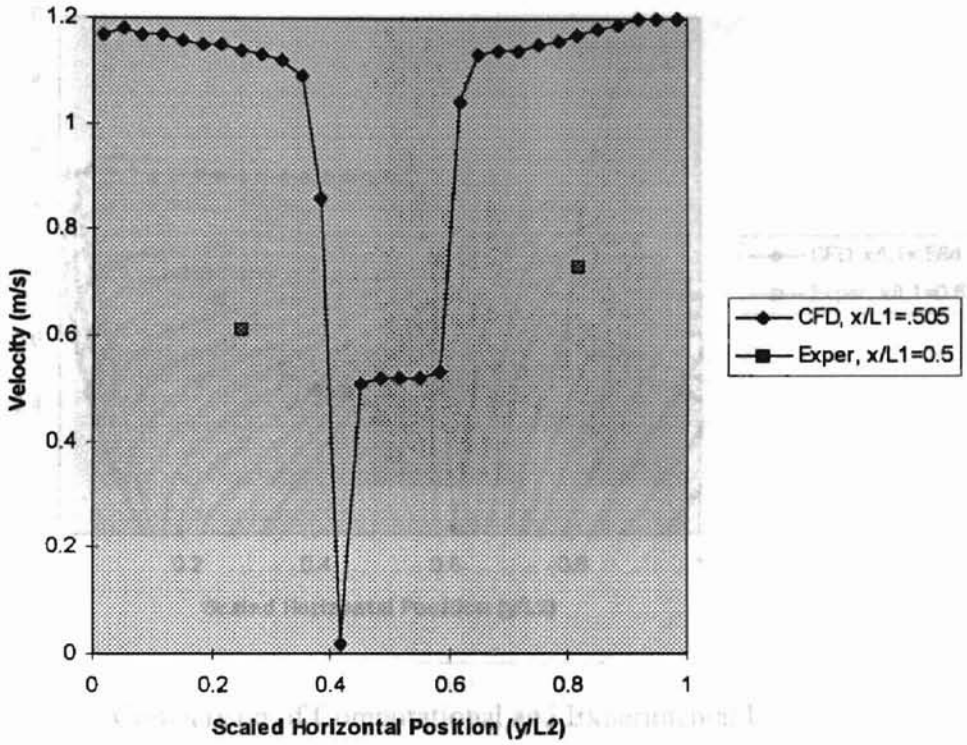

Figure 5.19 Comparison of Computational and Experimental U-Velocity Profile;

Experimental L1=101.6 mm, Computational L1=143.9 mm, L2=50.8 mm;

Profile at Filter Center

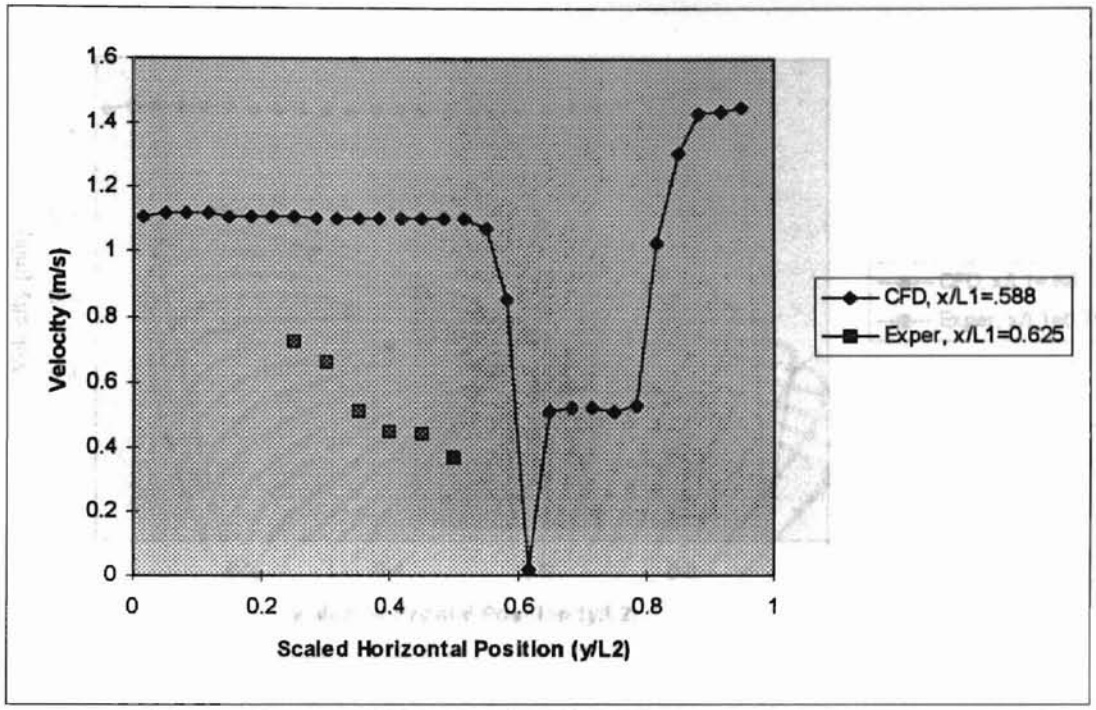

Figure 5.20 Comparison of Computational and Experimental U-Velocity Profile; Experimental L1=101.6 mm, Computational L1=143.9 mm, L2=50.8 mm; Profile 12.7 mm (0.5 in) Downstream of Filter Center

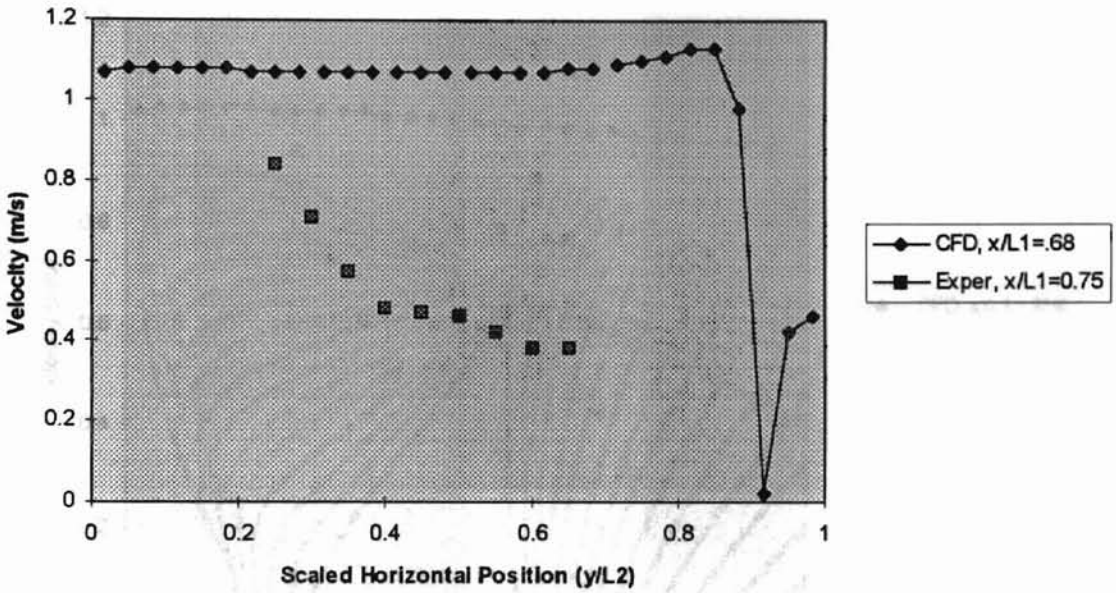

Figure 5.21 Comparison of Computational and Experimental U-Velocity Profile;

Experimental L1=101.6 mm, Computational L1=143.9 mm, L2=50.8 mm;

Profile 25.4 mm (1.0 in) Downstream of Filter Center

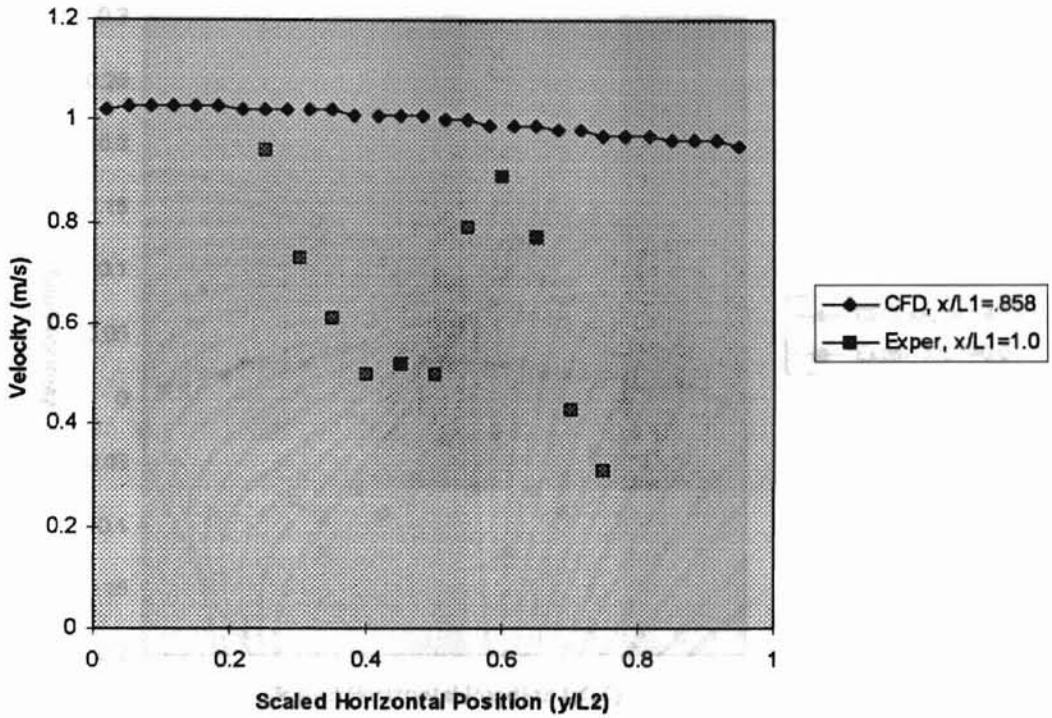

Figure 5.22 Comparison of Computational and Experimental U-Velocity Profile;

Experimental L1=101.6 mm, Computational L1=143.9 mm, L2=50.8 mm;

Profile 50.8 mm (2.0 in) Downstream of Filter Center

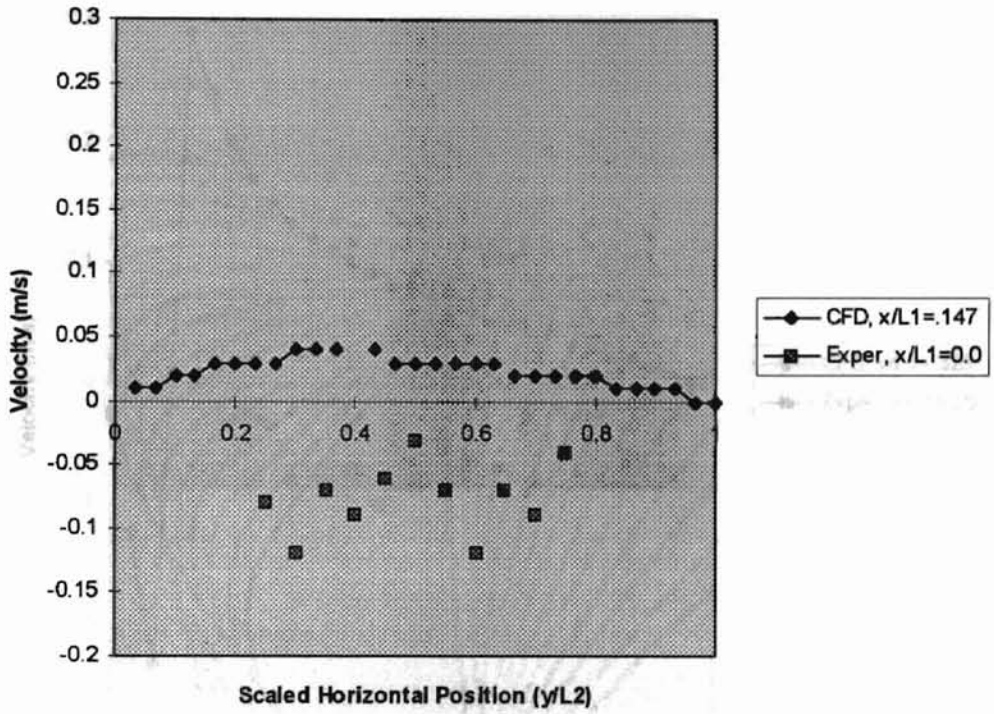

Figure 5.23 Comparison of Computational and Experimental V-Velocity Profile;

Experimental L1=101.6 mm, Computational L1=143.9 mm, L2=50.8 mm;

Profile 50.8 mm (2.0 in) Upstream of Filter Center

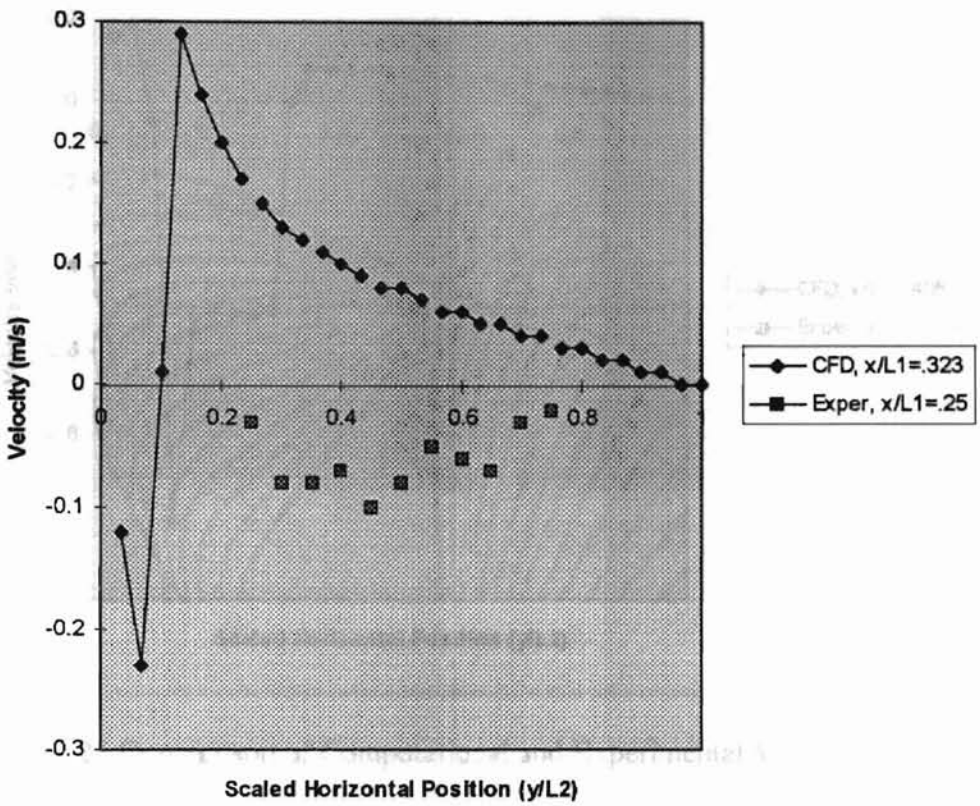

Figure 5.24 Comparison of Computational and Experimental V-Velocity Profile; Experimental L1=101.6 mm, Computational L1=143.9 mm, L2=50.8 mm; Profile 25.4 mm (1.0 in) Upstream of Filter Center

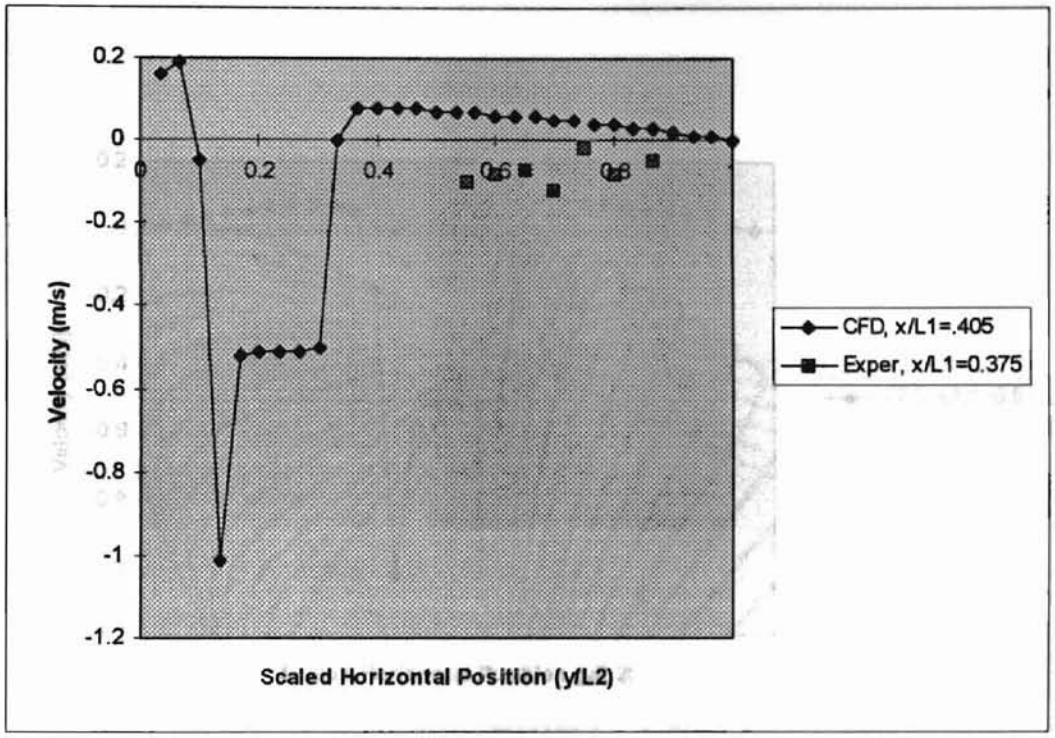

Figure 5.25 Comparison of Computational and Experimental V-Velocity Profile; Experimental L1=101.6 mm, Computational L1=143.9 mm, L2=50.8 mm; Profile 12.7 mm (0.5 in) Upstream of Filter Center

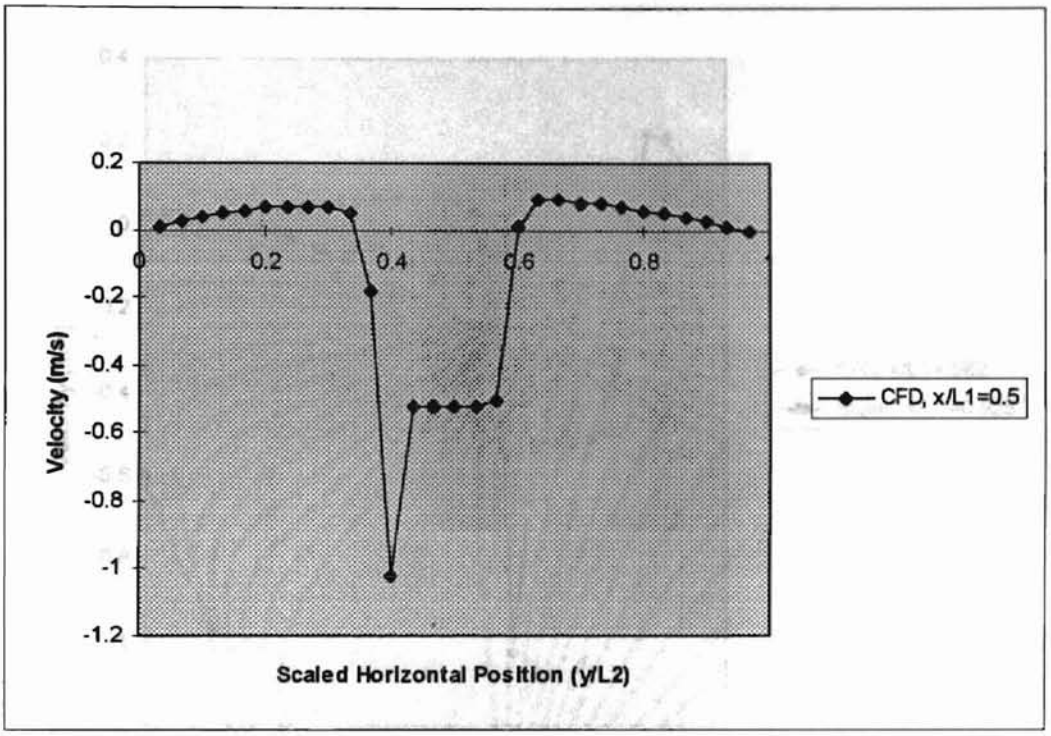

Figure 5.26 Computational V-Velocity Profile;

L1=143.9 mm, L2=50.8 mm, Profile at Filter Center

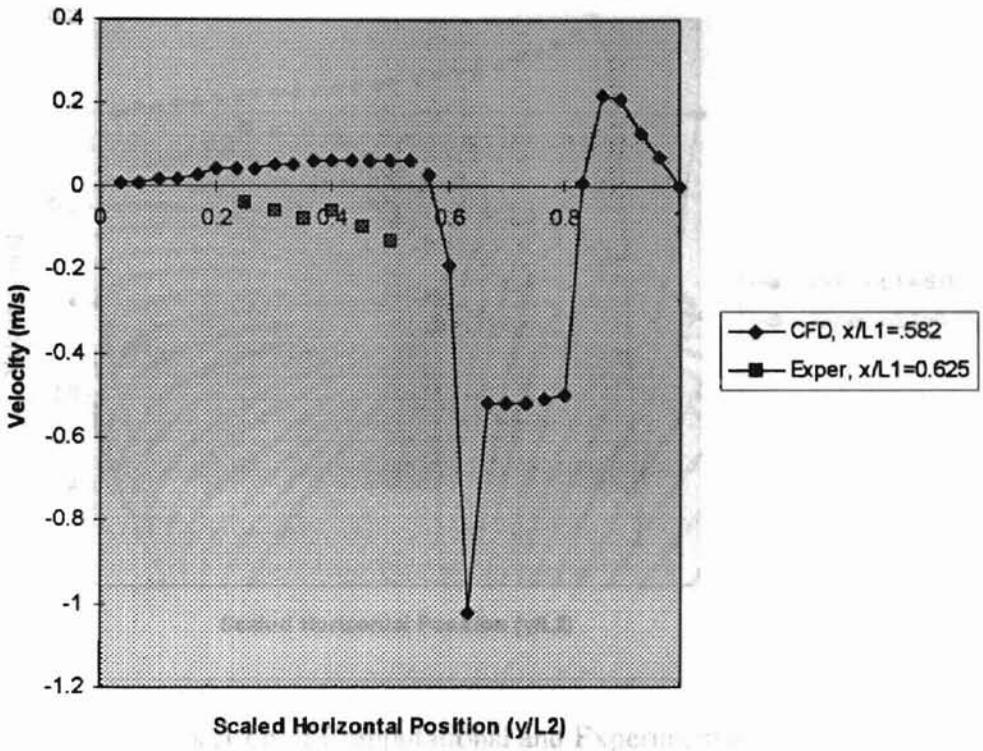

Figure 5.27 Comparison of Computational and Experimental V-Velocity Profile; Experimental L1=101.6 mm, Computational L1=143.9 mm, L2=50.8 mm; Profile 12.7 mm (0.5 in) Downstream of Filter Center

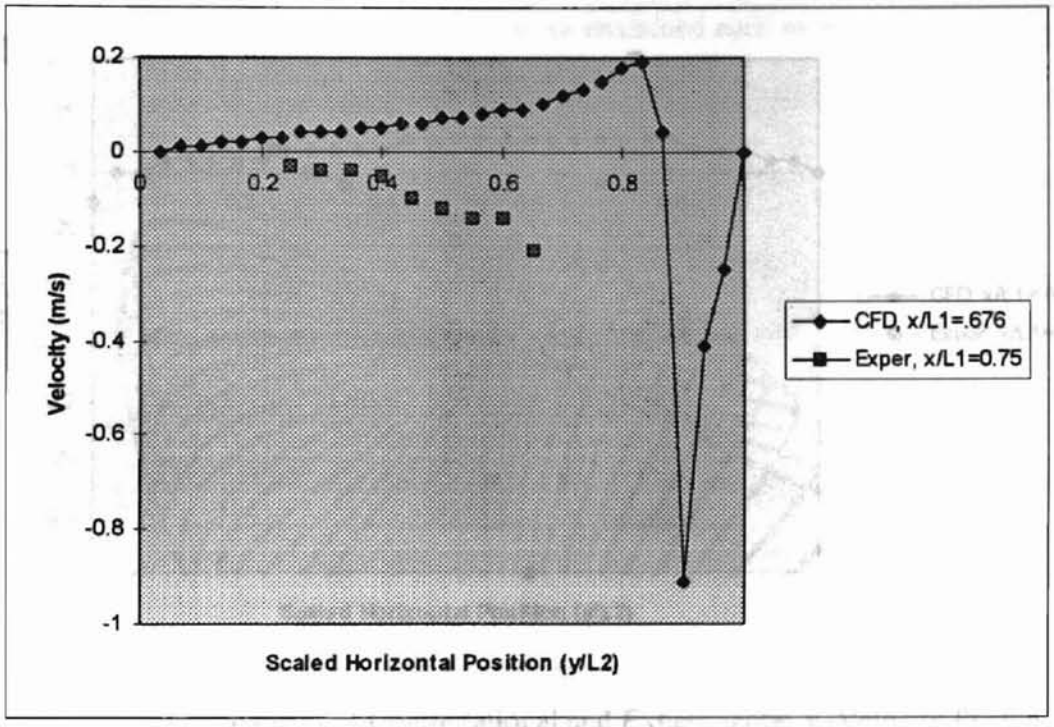

Figure 5.28 Comparison of Computational and Experimental V-Velocity Profile; Experimental L1=101.6 mm, Computational L1=143.9 mm, L2=50.8 mm; Profile 25.4 mm (1.0 in) Downstream of Filter Center

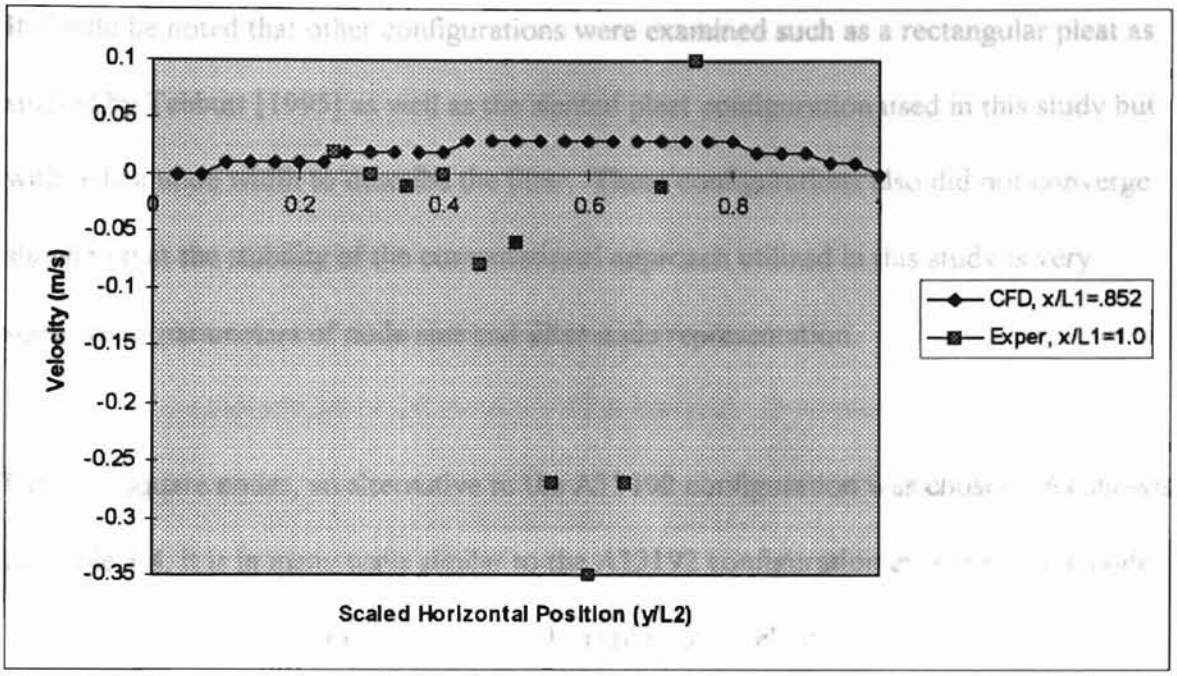

Figure 5.29 Comparison of Computational and Experimental V-Velocity Profile; Experimental L1=101.6 mm, Computational L1=143.9 mm, L2=50.8 mm; Profile 50.8 mm (2.0 in) Downstream of Filter Center

5.2.8 A13192 Configuration Results

Despite multiple attempts, the pressure solution for the A13192 configuration did not converge. Parametrics on the configuration showed that the ratio of the lengths of the node element seemed to be the cause of the nonconvergence. The ratio is 3.0 mm to 0.15 mm. This ratio was driven by the small pleat angle for this configuration. Other parametrics were completed on the A13192 configuration in an attempt for convergence. These included changing the permeability, time increment and node size. Of these, changing the node size to a 0.15 mm x 0.15 mm square created a convergence.

It should be noted that other configurations were examined such as a rectangular pleat as studied by Tebbutt [1995] as well as the slanted pleat configuration used in this study but with only a node width to describe the filter. These configurations also did not converge showing that the stability of the computational approach utilized in this study is very sensitive to parameters of node size and filter node representation.

Utilizing square nodes, an alternative to the A13192 configuration was chosen. As shown by Table 3.4, it is in many ways similar to the A13192 configuration except that the node size is 0.15 mm x 0.15 mm creating a much smaller flow field of 7.5 mm x 1.5 mm. Even so, the time for solution convergence for this case was approximately 150 hours. It was found that the pressure drop through the filter for this configuration was 80 Pa which is significantly smaller than the 180 Pa found in the experiment. However, due to the large discrepancy in the size of the two domains, it is not believed that the flow field for the alternative A13912 configuration can be directly compared to the experimental results.

CHAPTER VI

DISCUSSION

6.1 Analysis of Experiment

The experimental velocity data as provided by Figures 5.1 and 5.2, 5.3, and 5.4 describes the velocity characteristics of a flow near a filter medium. However, due to the nature of the LDV measurement system, some problems arose during the gathering of the data. Some of the data points described in Figures 4.7, 5.1, 5.2, 5.3, and 5.4 were determined to be questionable. The most obvious of these data points is the v-velocity for points 30 and 31. These values are given as zero which is incorrect. For these points, the blue beams that measure the horizontal or v-velocities were partially blocked by the filter due to the constricted area and a slight bending of the filter paper due to the pressure.

One other problem noticed was the poor velocity histograms for several of the data points downstream of the filter. Possible causes of this could be the absorption of the PSL particles by the filter or perhaps a turbulent swirl created by the filter interface with the test housing. Measurement locations with these poor histograms include points 12, 43, 46, 53, 54, 55, 56, and 57 with all but the first downstream of the filter. Data gathering at these locations was slow due to the low rate of PSL particles passing through the probe volume. The validity of these measurements were determined to be questionable.

Another one of the odd trends noticed in the results was that the flow downstream of the filter was measured at a much slower velocity than the flow upstream of the filter as

illustrated by Figure 5.1. Within a duct flow, this would seem to violate the principle of continuity. However, it should be remembered that the flow was only measured within 12.7 mm (0.5 in.) of the ±y side walls. With a 50.8 mm (2 in.) duct, this allows only the inner 50% of the duct flow to be measured. Flow near the walls was not measured due to the interference of the laser beam and the side wall. However, for the flow downstream of the filter, Figures 5.21 and 5.22 show an increasing u-velocity in the direction of the -y duct wall. Extrapolation of this trend would show high velocity flows in the region of the -y duct wall that could satisfy continuity and therefore explain the low velocities found in the duct center. However, without actual measurements, this can not be confirmed.

6.2 Comparison between Computational and Experimental Data

Many differences were noted when comparing the results between the computational and experimental data. The strongest difference between the two sets of data is the acceleration and deceleration of the flow within the upstream and downstream crevasses formed by the filter. An examination of the u-velocity in Figures 5.16 through 5.29 show that the flow in the computational simulation accelerated into the constricting crevasse upstream of the filter while the flow in the experiment decelerated into the same constriction. Likewise, in the crevasse downstream of the filter, the computational results showed a flow with a high velocity in the constricted region that decelerates as it moves through the expanding crevasse. The experimental data showed a flow that is accelerating as it moves downstream through the expansion.

Opposite tendencies were also noted with the horizontal or v-velocity data. With the computational data, the flow was directed in the +y-direction in both the upstream and downstream crevasses while the experimental data showed a distinct -y-direction for the flow in both the upstream and downstream crevasses.

One possible explanation of these opposite trends is described by the simple one-dimensional analysis in Section 1.5.1. For a contracting porous one-dimensional duct, it can be easily seen from the flow rate equation, Eq. (1.14), that if the ratio of the decreasing flow rate is less than the ratio of the decreasing area, the velocity will decrease even though the duct is contracting. This is what is indicated by the experimental data although not by the computational data. Opposite effects would be applicable for the downstream expanding crevasse. If the ratio of the increasing flow rate is greater than the ratio of the increasing area, then the flow will accelerate through the expansion. This is also indicated by the experimental data but not the computational data.

The computational trends of velocity acceleration within the upstream crevasse and deceleration in the downstream crevasse have been previously documented in past simulations such as those done by Tebbutt [1995]. For example, Tebbutt had found flow speeds up to 10 m/s in the constricted regions of both crevasses with an upstream flow inlet speed of 3.0 m/s. Although Cai [1993] had assumed unrealistic permeabilities on the order of 10^{-8} m^2, he had still found these same high speed trends in the constricted regions of the upstream and downstream crevasses.

However, in the analysis done by Chen et al., [1993], the velocity was shown to have accelerated to a maximum at the entrance of the pleat crevasse and then decelerate as the flow continued down the upstream crevasse. Downstream of the filter, the flow was seen to accelerate through the pleat crevasse reaching a maximum at the exit of the crevasse. These results were more similar to those found in the experiment than the results produced by Cai [1993] or Tebbutt [1995].

Other discrepancies between the computational modeling and the experiment was the indication of turbulence within the experiment although laminar flow was assumed in the modeling. Although the experiment was configured to create laminar flow, an examination of the turbulent intensity results in Figure 5.5 indicate the strong possibility of turbulent flow. The highest indications of turbulence were found to be in points 54, 55, 56 and 57 which indicate a possible swirl. However, if present, turbulence for the rest of the flow could have been induced by the induction at the duct inlet of the water vapor and PSL particles from the atomizer. It should be noted that the creation of turbulence would have a tendency to smooth out the velocity entering the upstream pleat crevasse which could possibly help explain the observed deceleration of the flow into the crevasse.

One of the assumptions of this study not previously investigated was the modeling of a thin 0.6 mm filter by a computational filter 10.8 mm thick with an adjustment in permeability and inertial resistance. An examination of Figure 5.15 shows that the velocity is affected by a changing filter thickness even though the permeability was adjusted to allow an equivalent pressure drop between the two cases. However, although the

magnitude varies between the two cases with the thicker filter creating greater velocity changes, the trends of acceleration within the upstream crevasse and deceleration in the downstream crevasse continued to hold for the computational data.

Of course, other explanations could be possible for the discrepancy between the experimental and computational results such as an air leak in the experiment. An air leak around the side of the filter would cause a decreasing volume flow in the upstream crevasse with a subsequent velocity drop.

However, what is certain is that the experimental results show that the experiment performed does not verify the computational simulation. These results do not necessarily imply that past filter velocity simulations were incorrect. However, they should show the need of experimental verification of computational simulations and cautious skepticism when reviewing data from simulations when they have not been verified.

CHAPTER VII

CONCLUSIONS AND RECOMENDATIONS

7.1 Conclusions

Several conclusions can be drawn from the results found in this analysis.

(1) The porosity strongly affects the pressure through the filter although not the velocity as shown by Figures 5.13 and 5.14. As shown by Eq (1.3), the porosity can be incorporated into the governing equation if the Darcian velocities are utilized and steady state conditions are assumed. It should be noted that in the parametrics performed for porosity, the inertial resistance was allowed to remain constant although it is known to be a function of porosity. Therefore, the actual effect of porosity on the results were not completely determined.

(2) The number of nodes utilized to represent the filter can strongly affect the pressure drop created by the filter medium. The use of two (2) nodes to describe the filter in the x and y directions is very inadequate. The use of six (6) or more nodes can describe the filter with better results.

(3) The values for permeability and inertial resistance can strongly affect the pressure drop through the filter medium. These values also affect velocity but much less so. Correct estimates for these values are necessary for an accurate filter analysis.

(4) The utilization of a thick filter simulation to describe the velocities induced by a thin filter is questionable. Although similar trends of acceleration and deceleration can be seen through different simulated filter media of different thickness, the velocity magnitudes were not found to be the same.

(5) The experiment completed in this analysis did not verify the computational simulation. The results of the simulation including the acceleration in the upstream crevasse and deceleration in the downstream crevasse is similar to the results found in previous analyses. However, the experimental data indicated an opposite effect of deceleration within the upstream crevasse and acceleration within the downstream crevasse. Possible explanations of this discrepancy include the simulated thick filter approach, the interaction between the simulation of filter and non-filter nodes, an overly strong assumption of laminar flow in the simulation or a leak or other unforeseen difficulty in the experiment.

(6) The method of using porous flow and nonporous flow governing equations utilized in the simulations for this computational study is unstable for some geometric configurations.

7.2 Recommendations

Although the experiment described in this analysis did not adequately verify the computational simulation, the results for this analysis suggested several directions for future filter simulation and experimentation.

(1) An experiment should be created that uses the same scale for the filter medium as the external flow. This experiment in this analysis utilized a filter medium 0.6 mm thick. A foam filter with a thickness on the order of centimeters could be utilized to properly scale the flow through the filter medium and the external flow.

(2) The use of hot wire probes could be utilized to measure the flow near the filter. The use of an LDV to measure velocity data near the filter is limited due to the interference of the filter and the laser beam. Although access, two component measurement and calibration is difficult, the hot wire probes could possibly measure the velocity very near a filter described in this experiment or the velocity near a standard A13192 air filter.

(3) Other methods of modeling porous flow problems should be investigated. Chief among these could be a finite-element simulation. Investigation of this method to determine solution stability should be completed.

REFERENCES

Brown, R.C. (1993): *Air Filtration: An Integrated Approach to the Theory and Applications of Fibrous Filters*, Pergamon Press, Oxford.

Cai, Q. (1993): "A Study of Air Filter Flow By Computational Fluid Dynamics", M.S. Thesis, School of Mechanical & Aerospace Engineering, Oklahoma State U., Stillwater, OK.

Canabal III, F. (1992): "A Two-Dimensional Navier-Stokes Equations Solver for Environmental and Thermal Control Engineering Problems", M.S. Thesis, The Department of Mechanical Engineering, The University of Alabama in Huntsville, Huntsville, AL.

Chen D., Pui, D., and Liu, Y.H. (1993): *A Numerical Study and Optimization of Pleated Gas Filters*, Particle Technology Laboratory, Proceedings of the 1993 Institute of the Environmental Sciences, Annual Technical Meeting, pp. 414-422.

Chung, T.J. (1994): *Introduction To Continuum Mechanics*, Department of Mechanical and Aerospace Engineering, The University of Alabama in Huntsville.

Duran, R. (1995): "Improvement of Flow Uniformity and Modeling of Filtration Efficiencies for Automotive Air Filter Test Housings", M.S. Thesis, School of Mechanical & Aerospace Engineering, Oklahoma State U., Stillwater, OK.

Gurumoothy, V. (1990): Computational Fluid Dynamics of an Air Induction System, M.S. Thesis, Dept. of Mechanical Engineering, U. of Rhode Island.

Hinze, J.O. (1975): Turbulence, McGraw Hill, New York.

Hirt, C.W., Nichols, B.D., and Romero, N.C. (1975): "SOLA- A Numerical Solution Algorithm for Transient Fluid Flows", Los Alamos Scientific Laboratory Report LA-5852, Los Alamos Scientific Laboratory at the U. of California, Los Alamos

Lilley, D.G. (1992): *Computational Fluid Dynamics*, Dept of Mechanical & Aerospace Engineering, Oklahoma State U., Stillwater, OK.

Liu, G. (1995): "Velocity Measurements and CFD Predictions of Flow Redistribution Through Air Filters", M.S. Thesis, School of Aerospace & Mechanical Engineering, Oklahoma State U., Stillwater, OK.

Newman, R. (1994): "Uniformity of Airflow in Automotive Air Filter Test Housings and Its Effect on the Efficiency of Fibrous Filters," M.S. Thesis, School of Mechanical & Aerospace Engineering, Oklahoma State U., Stillwater, OK.

Patankar, S.V. (1980): *Numerical Heat Transfer and Fluid Flow*, Hemisphere Publishing.

Sabnis, R.D. (1993): "Effects of Non-Uniform Airflow Through Filters on Filtration Efficiency", M.S. Thesis, School of Mechanical & Aerospace Engineering, Oklahoma State U., Stillwater, OK.

Tebbutt, C. B. (1995):"CFD Model of Flow Through Air Filter Pleats", M.S. Thesis, School of Mechanical & Aerospace Engineering, Oklahoma State U., Stillwater, OK.

Vafai, K. and Tien, C.L. (1980): "Boundary and Inertial Effects on Flow and Heat Transfer in Porous Media", *International Journal of Heat and Mass Transfer*, Vol. 24, pp.195-203.

White, F.M. (1991): *Viscous Fluid Flow*, 2nd ed., McGraw-Hill Inc,

APPENDIX A

EXPERIMENTAL CONFIGURATION RESULTS

*** Nodes between slashes indicate filter nodes**

U - VELOCITY

Horizontal position (y-value) of columns in millimeters

-.84	.846	2.54	4.23	5.92	7.62	9.31	11.0	12.7	14.3	16.0	17.7
19.4	21.1	22.8	24.5	26.2	27.9	29.6	31.3	33.0	34.7	36.4	38.1
39.7	41.4	43.1	44.8	46.5	48.2	49.9	51.6				

Row 1 x=0.0 mm

1.00	1.00	1.00	1.00	1.00	1.00	1.00	1.00	1.00	1.00	1.00	1.00
1.00	1.00	1.00	1.00	1.00	1.00	1.00	1.00	1.00	1.00	1.00	1.00
1.00	1.00	1.00	1.00	1.00	1.00	1.00	1.00				

Row 2 x=1.69 mm

-1.00	1.00	1.00	1.00	1.00	1.00	1.00	1.00	1.00	1.00	1.00	1.00
1.00	1.00	1.00	1.00	1.00	1.00	1.00	1.00	1.00	1.00	1.00	1.00
1.00	1.00	1.00	1.00	1.00	1.00	1.00	-1.00				

Row 3 x=3.38 mm

-.99	.99	1.00	1.00	1.00	1.00	1.00	1.00	1.00	1.00	1.00	1.00
1.00	1.00	1.00	1.00	1.00	1.00	1.00	1.00	1.00	1.00	1.00	1.00
1.00	1.00	1.00	1.00	1.00	1.00	-1.00					

Row 4 x=5.08 mm

-.99	.99	.99	.99	.99	.99	1.00	1.00	1.00	1.00	1.00	1.00
1.00	1.00	1.00	1.00	1.00	1.00	1.00	1.00	1.00	1.00	1.00	1.00
1.00	1.00	1.00	1.01	1.01	1.01	1.00	-1.00				

Row 5 x=6.77 mm

-.99	.99	.99	.99	.99	.99	.99	.99	1.00	1.00	1.00	1.00
1.00	1.00	1.00	1.00	1.00	1.00	1.00	1.00	1.00	1.00	1.01	1.01
1.01	1.01	1.01	1.01	1.01	1.01	1.00	-1.00				

Row 6 x=8.46 mm

-.98	.98	.99	.99	.99	.99	.99	.99	.99	.99	1.00	1.00
1.00	1.00	1.00	1.00	1.00	1.00	1.00	1.00	1.01	1.01	1.01	1.01
1.01	1.01	1.01	1.01	1.01	1.00	-1.00					

Row 7 x=10.16 mm

-.98	.98	.99	.99	.99	.99	.99	.99	.99	.99	.99	1.00
1.00	1.00	1.00	1.00	1.00	1.00	1.00	1.01	1.01	1.01	1.01	1.01
1.01	1.01	1.01	1.01	1.01	1.01	-1.01					

Row 8 x=11.85 mm

-.98	.98	.98	.98	.99	.99	.99	.99	.99	.99	.99	1.00
1.00	1.00	1.00	1.00	1.00	1.00	1.01	1.01	1.01	1.01	1.01	1.01
1.01	1.01	1.01	1.01	1.01	1.01	-1.01					

Row 9 x=13.54 mm

-.98	.98	.98	.98	.98	.98	.99	.99	.99	.99	.99	.99
1.00	1.00	1.00	1.00	1.00	1.01	1.01	1.01	1.01	1.01	1.01	1.01
1.01	1.01	1.01	1.01	1.01	1.01	-1.01					

Row 10 x=15.24 mm

-.97	.97	.98	.98	.98	.98	.98	.99	.99	.99	.99	.99
1.00	1.00	1.00	1.00	1.00	1.01	1.01	1.01	1.01	1.01	1.01	1.01
1.02	1.02	1.02	1.02	1.02	1.01	-1.01					

Row 11 x=16.93 mm

-.97	.97	.97	.98	.98	.98	.98	.98	.99	.99	.99	.99
1.00	1.00	1.00	1.00	1.01	1.01	1.01	1.01	1.01	1.01	1.01	1.02
1.02	1.02	1.02	1.02	1.02	1.01	-1.01	-1.06				

Row 12 x=18.62 mm

-.96	.96	.97	.97	.97	.98	.98	.98	.98	.99	.99	.99
1.00	1.00	1.00	1.00	1.01	1.01	1.01	1.01	1.01	1.02	1.02	1.02
1.02	1.02	1.02	1.02	1.02	1.02	1.02	-1.02				

Row 13 x=20.32 mm

-.96	.96	.96	.97	.97	.97	.97	.98	.98	.99	.99	.99
1.00	1.00	1.00	1.00	1.01	1.01	1.01	1.01	1.02	1.02	1.02	1.02
1.02	1.02	1.02	1.02	1.02	1.02	1.02	-1.02				

Row 14 x=22.01 mm

-.95	.95	.96	.96	.96	.97	.97	.98	.98	.98	.99	.99
1.00	1.00	1.00	1.01	1.01	1.01	1.01	1.02	1.02	1.02	1.02	1.02
1.02	1.02	1.02	1.03	1.03	1.03	1.02	-1.02				

Row 15 x=23.70 mm

-.95	.95	.95	.96	.96	.96	.97	.97	.98	.98	.99	.99
1.00	1.00	1.00	1.01	1.01	1.01	1.02	1.02	1.02	1.02	1.02	1.02
1.03	1.03	1.03	1.03	1.03	1.03	1.02	-1.02				

Row 16 x=25.40 mm

-.94	.94	.94	.95	.95	.96	.96	.97	.98	.98	.99	.99
1.00	1.00	1.01	1.01	1.01	1.02	1.02	1.02	1.02	1.02	1.03	1.03
1.03	1.03	1.03	1.03	1.03	1.03	1.03	-1.03				

Row 17 x=27.09 mm

-.93	.93	.94	.94	.95	.95	.96	.97	.97	.98	.99	.99
1.00	1.00	1.01	1.01	1.01	1.02	1.02	1.02	1.03	1.03	1.03	1.03
1.03	1.03	1.03	1.03	1.03	1.03	1.03	-1.03				

Row 18 x=28.78 mm

-.92	.92	.92	.93	.94	.95	.96	.96	.97	.98	.99	.99
1.00	1.01	1.01	1.01	1.02	1.02	1.02	1.03	1.03	1.03	1.03	1.03
1.03	1.04	1.04	1.04	1.04	1.04	1.03	-1.03				

Row 19 x=30.48 mm

-.90	.90	.91	.92	.93	.94	.95	.96	.97	.98	.99	1.00
1.00	1.01	1.01	1.02	1.02	1.02	1.03	1.03	1.03	1.03	1.04	1.04
1.04	1.04	1.04	1.04	1.04	1.04	1.04	-1.04				

Row 20 x=32.17 mm

-.88	.88	.89	.90	.92	.93	.95	.96	.97	.98	.99	1.00
1.01	1.01	1.02	1.02	1.02	1.03	1.03	1.03	1.04	1.04	1.04	1.04
1.04	1.04	1.04	1.04	1.04	1.04	1.04	-1.04				

Row 21 x=33.86 mm

-.86	.86	.87	.89	.91	.93	.94	.96	.97	.99	.99	1.00
1.01	1.02	1.02	1.02	1.03	1.03	1.03	1.04	1.04	1.04	1.04	1.04
1.04	1.05	1.05	1.05	1.05	1.05	1.04	-1.04				

Row 22 x=35.56 mm

-.82	.82	.84	.87	.90	.92	.94	.96	.98	.99	1.00	1.01
1.01	1.02	1.03	1.03	1.03	1.04	1.04	1.04	1.04	1.04	1.05	1.05
1.05	1.05	1.05	1.05	1.05	1.05	1.05	-1.05				

Row 23 x=37.25 mm

-.77	.77	.80	.85	.89	.92	.95	.97	.98	1.00	1.01	1.01
1.02	1.03	1.03	1.03	1.04	1.04	1.04	1.05	1.05	1.05	1.05	1.05
1.05	1.05	1.05	1.06	1.06	1.06	1.05	-1.05				

Row 24 x=38.94 mm

-.68	.68	.76	.83	.89	.93	.96	.98	.99	1.01	1.02	1.02
1.03	1.03	1.04	1.04	1.04	1.05	1.05	1.05	1.05	1.05	1.05	1.06
1.06	1.06	1.06	1.06	1.06	1.06	1.05	-1.05				

Row 25 x=40.64 mm

-.51	.51	.72	.83	.90	.94	.97	.99	1.01	1.02	1.03	1.03
1.04	1.04	1.04	1.05	1.05	1.05	1.05	1.06	1.06	1.06	1.06	1.06
1.06	1.06	1.06	1.06	1.06	1.06	1.06	-1.06				

```
Row 26 x=42.33 mm
  -.14   .14   .76   .88   .94   .98  1.00  1.02  1.03  1.03  1.04  1.04
  1.05  1.05  1.05  1.05  1.06  1.06  1.06  1.06  1.06  1.06  1.06  1.07
  1.07  1.07  1.07  1.07  1.07  1.07  1.06 -1.06
Row 27 x=44.02 mm
  -.13   .13 \ .38   .94  1.00  1.02  1.03  1.04  1.05  1.05  1.05  1.05
  1.06  1.06  1.06  1.06  1.06  1.06  1.06  1.07  1.07  1.07  1.07  1.07
  1.07  1.07  1.07  1.07  1.07  1.07  1.07 -1.07
Row 28 x=45.72 mm
  -.24   .24   .24 \ .60  1.06  1.08  1.07  1.07  1.07  1.07  1.07  1.07
  1.07  1.07  1.07  1.07  1.07  1.07  1.07  1.07  1.07  1.07  1.07  1.07
  1.08  1.08  1.08  1.08  1.08  1.08  1.07 -1.07
Row 29 x=47.41 mm
  -.36   .36   .36   .35 \ .78  1.12  1.11  1.10  1.09  1.08  1.08  1.08
  1.08  1.07  1.07  1.07  1.07  1.07  1.08  1.08  1.08  1.08  1.08  1.08
  1.08  1.08  1.08  1.08  1.08  1.08  1.08 -1.08
Row 30 x=49.16 mm
  -.48   .48   .47   .45   .44 \ .91  1.14  1.13  1.11  1.10  1.09  1.09
  1.08  1.08  1.08  1.08  1.08  1.08  1.08  1.08  1.08  1.08  1.08  1.08
  1.09  1.09  1.09  1.09  1.09  1.09  1.08 -1.08
Row 31 x=50.8 mm
  -.61   .61   .61   .54   .50   .49 \ .99  1.14  1.12  1.11  1.10  1.10
  1.09  1.09  1.09  1.09  1.09  1.09  1.09  1.09  1.09  1.09  1.09  1.09
  1.09  1.09  1.09  1.09  1.09  1.09  1.09 -1.09
Row 32 x=52.49 mm
  -.72 \ .72   .80   .63   .55   .51   .52 \1.02  1.13  1.12  1.11  1.10
  1.10  1.10  1.09  1.09  1.09  1.09  1.09  1.09  1.09  1.09  1.09  1.09
  1.10  1.10  1.10  1.10  1.10  1.10  1.09 -1.09
Row 33 x=54.18 mm
 -1.94  1.94 \ .11   .58   .55   .53   .51   .53 \1.03  1.12  1.12  1.11
  1.10  1.10  1.10  1.10  1.09  1.09  1.09  1.10  1.10  1.10  1.10  1.10
  1.10  1.10  1.10  1.10  1.10  1.10  1.10 -1.10
Row 34 x=55.88 mm
 -1.89  1.89  1.23 \ .03   .53   .53   .52   .51   .53 \1.03  1.12  1.11
  1.11  1.10  1.10  1.10  1.10  1.10  1.10  1.10  1.10  1.10  1.10  1.10
  1.11  1.11  1.11  1.11  1.11  1.11  1.10 -1.10
Row 35 x=57.57 mm
 -1.66  1.66  1.46  1.06 \ .02   .51   .52   .52   .52   .53 \1.03  1.11
  1.11  1.11  1.10  1.10  1.10  1.10  1.10  1.10  1.10  1.11  1.11  1.11
  1.11  1.11  1.11  1.11  1.12  1.12  1.11 -1.11
Row 36 x=59.26 mm
 -1.50  1.50  1.43  1.30   .99 \ .02   .51   .52   .52   .52   .53 \1.04
  1.11  1.11  1.11  1.11  1.11  1.11  1.11  1.11  1.11  1.11  1.11  1.11
  1.12  1.12  1.12  1.12  1.12  1.12  1.12 -1.12
Row 37 x=60.96 mm
 -1.40  1.40  1.37  1.31  1.23   .95 \ .02   .51   .52   .52   .52   .53
 \1.04  1.11  1.11  1.11  1.11  1.11  1.11  1.11  1.11  1.11  1.12  1.12
  1.12  1.12  1.13  1.13  1.13  1.13  1.12 -1.12
Row 38 x=62.65 mm
 -1.33  1.33  1.32  1.29  1.25  1.18   .92 \ .02   .51   .52   .52   .52
   .53 \1.04  1.11  1.11  1.11  1.11  1.11  1.11  1.12  1.12  1.12  1.12
  1.13  1.13  1.13  1.13  1.14  1.14  1.13 -1.13
Row 39 x=64.34 mm
 -1.28  1.28  1.28  1.26  1.23  1.21  1.15   .90 \ .02   .51   .52   .52
   .52   .53 \1.04  1.11  1.11  1.11  1.11  1.12  1.12  1.12  1.13  1.13
  1.13  1.14  1.14  1.14  1.14  1.15  1.14 -1.14
Row 40 x=66.04 mm
 -1.25  1.25  1.25  1.24  1.22  1.20  1.18  1.13   .89 \ .02   .51   .52
   .52   .52   .53 \1.04  1.11  1.11  1.12  1.12  1.12  1.13  1.13  1.13
  1.14  1.14  1.15  1.15  1.15  1.15  1.15 -1.15
```

```
Row 41 x=67.73 mm
 -1.22  1.22  1.23  1.22  1.20  1.19  1.17  1.16  1.11  1.88  \.02  1.51
   .52   .52   .52   .53 \1.04  1.11  1.12  1.12  1.12  1.13  1.13  1.14
  1.14  1.15  1.15  1.16  1.16  1.16  1.16 -1.16
Row 42 x=69.42 mm
 -1.20  1.20  1.21  1.20  1.19  1.18  1.17  1.16  1.14  1.10  1.87  \.02
   .51   .52   .52   .52   .53 \1.04  1.12  1.12  1.13  1.13  1.14  1.14
  1.15  1.16  1.16  1.17  1.17  1.17  1.17 -1.17
Row 43 x=71.12 mm
 -1.19  1.19  1.19  1.19  1.18  1.17  1.16  1.15  1.14  1.13  1.09  1.86
  \.02   .51   .52   .52   .52   .53 \1.04  1.12  1.13  1.13  1.14  1.15
  1.16  1.16  1.17  1.18  1.18  1.19  1.18 -1.18
Row 44 x=72.81 mm
 -1.17  1.17  1.18  1.17  1.17  1.16  1.15  1.15  1.14  1.13  1.12  1.09
   .86  \.02   .51   .52   .52   .52   .53 \1.04  1.13  1.14  1.14  1.15
  1.16  1.17  1.18  1.19  1.20  1.20  1.20 -1.20
Row 45 x=74.50 mm
 -1.16  1.16  1.17  1.16  1.16  1.15  1.15  1.14  1.13  1.13  1.12  1.12
  1.08   .85 \ .02   .51   .52   .52   .52   .53 \1.04  1.14  1.15  1.16
  1.17  1.18  1.19  1.20  1.21  1.22  1.21 -1.21
Row 46 x=76.20 mm
 -1.15  1.15  1.16  1.15  1.15  1.15  1.14  1.14  1.13  1.13  1.12  1.12
  1.11  1.08   .85 \ .02   .51   .52   .52   .52   .53 \1.04  1.15  1.16
  1.17  1.19  1.20  1.22  1.23  1.24  1.24 -1.24
Row 47 x=77.89 mm
 -1.14  1.14  1.15  1.14  1.14  1.14  1.13  1.13  1.13  1.12  1.12  1.11
  1.11  1.11  1.07   .85 \ .02   .51   .52   .52   .52   .53 \1.04  1.16
  1.18  1.19  1.21  1.23  1.25  1.26  1.26 -1.26
Row 48 x=79.58 mm
 -1.13  1.13  1.14  1.14  1.13  1.13  1.13  1.13  1.12  1.12  1.12  1.11
  1.11  1.11  1.10  1.07   .85 \ .02   .51   .52   .52   .52   .53 \1.04
  1.18  1.20  1.23  1.25  1.28  1.29  1.29 -1.29
Row 49 x=81.28 mm
 -1.13  1.13  1.13  1.13  1.13  1.13  1.12  1.12  1.12  1.11  1.11  1.11
  1.11  1.10  1.10  1.10  1.07   .85 \ .02   .51   .52   .52   .52   .53
 \1.04  1.20  1.24  1.27  1.31  1.33  1.33 -1.33
Row 50 x=82.97 mm
 -1.12  1.12  1.12  1.12  1.12  1.12  1.12  1.12  1.11  1.11  1.11  1.11
  1.10  1.10  1.10  1.10  1.10  1.07   .85  \.02   .51   .52   .52   .52
   .53 \1.04  1.24  1.30  1.35  1.38  1.39 -1.39
Row 51 x=84.66 mm
 -1.11  1.11  1.12  1.12  1.12  1.11  1.11  1.11  1.11  1.11  1.10  1.10
  1.10  1.10  1.10  1.10  1.10  1.10  1.07   .85 \ .02   .51   .52   .52
   .51   .53 \1.03  1.31  1.43  1.44  1.45 -1.45
Row 52 x=86.36 mm
 -1.11  1.11  1.11  1.11  1.11  1.11  1.11  1.11  1.10  1.10  1.10  1.10
  1.10  1.10  1.10  1.10  1.10  1.10  1.10  1.07   .85 \ .02   .51   .51
   .51   .51   .52 \1.01  1.61  1.50  1.53 -1.53
Row 53 x=88.05 mm
 -1.10  1.10  1.11  1.11  1.10  1.10  1.10  1.10  1.10  1.10  1.10  1.10
  1.10  1.09  1.09  1.09  1.09  1.10  1.10  1.10  1.07   .85  \.02   .51
   .51   .51   .49   .49 \1.65  1.37  1.66 -1.66
Row 54 x=89.74 mm
 -1.10  1.10  1.10  1.10  1.10  1.10  1.10  1.10  1.10  1.09  1.09  1.09
  1.09  1.09  1.09  1.09  1.09  1.09  1.09  1.10  1.10  1.07   .85 \ .02
   .51   .51   .48   .40  1.53 \ .60  2.12 -2.12
Row 55 x=91.44 mm
 -1.09  1.09  1.10  1.10  1.09  1.09  1.09  1.09  1.09  1.09  1.09  1.09
  1.09  1.09  1.09  1.09  1.09  1.09  1.09  1.10  1.10  1.10  1.08   .87
  \.02   .52   .53   .56   .80   .48 \2.20 -2.20
```

```
Row 56 x=93.13 mm
 -1.09  1.09  1.09  1.09  1.09  1.09  1.09  1.09  1.09  1.09  1.09  1.08
  1.08  1.08  1.08  1.08  1.08  1.09  1.09  1.09  1.10  1.10  1.11  1.10
   .90  \.02   .54   .57   .60   .46  1.84\-1.84
Row 57 x=94.82 mm
 -1.08  1.08  1.09  1.09  1.09  1.08  1.08  1.08  1.08  1.08  1.08  1.08
  1.08  1.08  1.08  1.08  1.08  1.08  1.08  1.09  1.09  1.10  1.11  1.13
  1.13   .94 \ .02   .55   .59   .67  1.09 -1.09
Row 58 x=96.52 mm
 -1.08  1.08  1.08  1.08  1.08  1.08  1.08  1.08  1.08  1.08  1.08  1.08
  1.08  1.08  1.07  1.07  1.08  1.08  1.08  1.08  1.09  1.09  1.10  1.12
  1.14  1.15   .98 \ .03   .52   .58   .71  -.71
Row 59 x=98.21 mm
 -1.07  1.07  1.08  1.08  1.08  1.08  1.08  1.07  1.07  1.07  1.07  1.07
  1.07  1.07  1.07  1.07  1.07  1.07  1.07  1.07  1.08  1.08  1.09  1.10
  1.11  1.13  1.13   .98 \ .02   .42   .46  -.46
Row 60 x=99.90 mm
 -1.07  1.07  1.07  1.07  1.07  1.07  1.07  1.07  1.07  1.07  1.07  1.07
  1.07  1.07  1.06  1.06  1.06  1.06  1.06  1.06  1.07  1.07  1.07  1.07
  1.08  1.08  1.08  1.05   .89  \.01   .23  -.23
Row 61 x=101.6 mm
 -1.06  1.06  1.07  1.07  1.07  1.07  1.07  1.07  1.07  1.06  1.06  1.06
  1.06  1.06  1.06  1.06  1.06  1.06  1.06  1.05  1.05  1.05  1.05  1.05
  1.04  1.03  1.01   .97   .88   .65 \ .00   .00
Row 62 x=103.29 mm
 -1.06  1.06  1.06  1.06  1.06  1.06  1.06  1.06  1.06  1.06  1.06  1.06
  1.06  1.06  1.05  1.05  1.05  1.05  1.05  1.04  1.04  1.04  1.03  1.03
  1.01  1.00   .97   .91   .83   .67   .38  -.38
Row 63 x=104.98 mm
 -1.06  1.06  1.06  1.06  1.06  1.06  1.06  1.06  1.06  1.06  1.05  1.05
  1.05  1.05  1.05  1.05  1.04  1.04  1.04  1.04  1.03  1.03  1.02  1.01
   .99   .97   .94   .89   .82   .72   .60  -.60
Row 64 x=106.68 mm
 -1.05  1.05  1.06  1.06  1.06  1.06  1.06  1.05  1.05  1.05  1.05  1.05
  1.05  1.05  1.04  1.04  1.04  1.04  1.03  1.03  1.02  1.01  1.01   .99
   .98   .95   .92   .88   .83   .77   .72  -.72
Row 65 x=108.37 mm
 -1.05  1.05  1.05  1.05  1.05  1.05  1.05  1.05  1.05  1.05  1.05  1.05
  1.04  1.04  1.04  1.04  1.03  1.03  1.03  1.02  1.01  1.01  1.00   .98
   .97   .95   .92   .89   .85   .82   .79  -.79
Row 66 x=110.06 mm
 -1.04  1.04  1.05  1.05  1.05  1.05  1.05  1.05  1.05  1.04  1.04  1.04
  1.04  1.04  1.03  1.03  1.03  1.02  1.02  1.01  1.01  1.00   .99   .98
   .96   .94   .92   .90   .87   .85   .83  -.83
Row 67 x=111.76 mm
 -1.04  1.04  1.05  1.05  1.05  1.05  1.04  1.04  1.04  1.04  1.04  1.04
  1.04  1.03  1.03  1.03  1.02  1.02  1.01  1.01  1.00   .99   .98   .97
   .96   .95   .93   .91   .89   .88   .87  -.87
Row 68 x=113.45 mm
 -1.04  1.04  1.04  1.04  1.04  1.04  1.04  1.04  1.04  1.04  1.04  1.03
  1.03  1.03  1.03  1.02  1.02  1.02  1.01  1.00  1.00   .99   .98   .97
   .96   .95   .93   .92   .91   .90   .89  -.89
Row 69 x=115.14 mm
 -1.04  1.04  1.04  1.04  1.04  1.04  1.04  1.04  1.04  1.03  1.03  1.03
  1.03  1.03  1.02  1.02  1.02  1.01  1.01  1.00  1.00   .99   .98   .97
   .96   .95   .94   .93   .92   .91   .91  -.91
Row 70 x=116.84 mm
 -1.03  1.03  1.04  1.04  1.04  1.04  1.04  1.03  1.03  1.03  1.03  1.03
  1.03  1.02  1.02  1.02  1.01  1.01  1.00  1.00   .99   .99   .98   .97
   .96   .96   .95   .94   .93   .93   .92  -.92
```

Row 71 x=118.53 mm
-1.03 1.03 1.04 1.04 1.03 1.03 1.03 1.03 1.03 1.03 1.03 1.03
1.02 1.02 1.02 1.01 1.01 1.01 1.00 1.00 .99 .99 .98 .97
.97 .96 .95 .95 .94 .94 .93 -.93
Row 72 x=120.22 mm
-1.03 1.03 1.03 1.03 1.03 1.03 1.03 1.03 1.03 1.03 1.02 1.02
1.02 1.02 1.02 1.01 1.01 1.00 1.00 1.00 .99 .99 .98 .97
.97 .96 .96 .95 .95 .94 .94 -.94
Row 73 x=121.92 mm
-1.03 1.03 1.03 1.03 1.03 1.03 1.03 1.03 1.03 1.02 1.02 1.02
1.02 1.02 1.01 1.01 1.01 1.00 1.00 1.00 .99 .99 .98 .98
.97 .97 .96 .96 .95 .95 .95 -.95
Row 74 x=123.61 mm
-1.02 1.02 1.03 1.03 1.03 1.03 1.03 1.03 1.02 1.02 1.02 1.02
1.02 1.01 1.01 1.01 1.01 1.00 1.00 .99 .99 .99 .98 .98
.97 .97 .97 .96 .96 .96 .95 -.95
Row 75 x=125.30 mm
-1.02 1.02 1.03 1.03 1.03 1.03 1.02 1.02 1.02 1.02 1.02 1.02
1.02 1.01 1.01 1.01 1.00 1.00 1.00 .99 .99 .99 .98 .98
.98 .97 .97 .97 .96 .96 .96 -.96
Row 76 x=127.00 mm
-1.02 1.02 1.03 1.03 1.02 1.02 1.02 1.02 1.02 1.02 1.02 1.02
1.01 1.01 1.01 1.01 1.00 1.00 1.00 .99 .99 .99 .98 .98
.98 .97 .97 .97 .97 .97 .96 -.96
Row 77 x=128.69 mm
-1.02 1.02 1.02 1.02 1.02 1.02 1.02 1.02 1.02 1.02 1.02 1.01
1.01 1.01 1.01 1.01 1.00 1.00 1.00 .99 .99 .99 .98 .98
.98 .98 .97 .97 .97 .97 .96 -.96
Row 78 x=130.38 mm
-1.02 1.02 1.02 1.02 1.02 1.02 1.02 1.02 1.02 1.02 1.01 1.01
1.01 1.01 1.01 1.00 1.00 1.00 1.00 .99 .99 .99 .99 .98
.98 .98 .98 .97 .97 .97 .97 -.97
Row 79 x=132.08 mm
-1.02 1.02 1.02 1.02 1.02 1.02 1.02 1.02 1.02 1.02 1.01 1.01
1.01 1.01 1.01 1.00 1.00 1.00 1.00 .99 .99 .99 .99 .98
.98 .98 .98 .98 .97 .97 .97 -.97
Row 80 x=133.73 mm
-1.01 1.01 1.02 1.02 1.02 1.02 1.02 1.02 1.02 1.01 1.01 1.01
1.01 1.01 1.01 1.00 1.00 1.00 1.00 .99 .99 .99 .99 .98
.98 .98 .98 .98 .98 .98 .97 -.97
Row 81 x=135.46 mm
-1.01 1.01 1.02 1.02 1.02 1.02 1.02 1.02 1.02 1.01 1.01 1.01
1.01 1.01 1.01 1.00 1.00 1.00 1.00 .99 .99 .99 .99 .99
.98 .98 .98 .98 .98 .98 .97 -.97
Row 82 x=137.16 mm
-1.01 1.01 1.02 1.02 1.02 1.02 1.02 1.02 1.01 1.01 1.01 1.01
1.01 1.01 1.01 1.00 1.00 1.00 1.00 .99 .99 .99 .99 .99
.98 .98 .98 .98 .98 .98 .97 -.97
Row 83 x=138.85 mm
-1.01 1.01 1.02 1.02 1.02 1.02 1.02 1.02 1.01 1.01 1.01 1.01
1.01 1.01 1.00 1.00 1.00 1.00 1.00 .99 .99 .99 .99 .99
.98 .98 .98 .98 .98 .98 .97 -.97
Row 84 x=140.54 mm
-1.01 1.01 1.02 1.02 1.02 1.02 1.02 1.02 1.01 1.01 1.01 1.01
1.01 1.01 1.00 1.00 1.00 1.00 1.00 .99 .99 .99 .99 .99
.99 .98 .98 .98 .98 .98 .97 -.97
Row 85 x=142.24 mm
-1.01 1.01 1.02 1.02 1.02 1.02 1.02 1.01 1.01 1.01 1.01 1.01
1.01 1.01 1.00 1.00 1.00 1.00 1.00 .99 .99 .99 .99 .99
.99 .98 .98 .98 .98 .98 .97 -.97

Row 86 x=143.93 mm

-1.01	1.01	1.02	1.02	1.02	1.02	1.02	1.01	1.01	1.01	1.01	1.01
1.01	1.01	1.00	1.00	1.00	1.00	1.00	.99	.99	.99	.99	.99
.99	.98	.98	.98	.98	.98	.97	-.97				

Row 87 x=145.62 mm

-1.00	1.00	1.00	1.00	1.00	1.00	1.00	1.00	1.00	1.00	1.00	1.00
1.00	1.00	1.00	1.00	1.00	1.00	1.00	1.00	1.00	1.00	1.00	1.00
1.00	1.00	1.00	1.00	1.00	1.00	1.00	-1.00				

V - VELOCITY

Horizontal position (y-value) of columns in millimeters

0.0	1.6	3.3	5.0	6.7	8.4	10.1	11.8	13.5	15.2	16.9	18.6
20.3	22.0	23.7	25.4	27.0	28.7	30.4	32.1	33.8	35.5	37.2	38.9
40.6	42.3	44.0	45.7	47.4	49.1	50.8	52.4				

Row 1 x=-0.846 mm

.00	.00	.01	.01	.01	.01	.01	.01	.01	.02	.02	.02
.02	.02	.02	.02	.02	.02	.02	.02	.01	.01	.01	.01
.01	.01	.01	.00	.00	.00	.00	.00				

Row 2 x=0.846 mm

.00	.00	.01	.01	.01	.01	.01	.01	.01	.02	.02	.02
.02	.02	.02	.02	.02	.02	.02	.02	.01	.01	.01	.01
.01	.01	.01	.00	.00	.00	.00	.00				

Row 3 x=2.54 mm

.00	.00	.01	.01	.01	.01	.01	.01	.01	.02	.02	.02
.02	.02	.02	.02	.02	.02	.02	.02	.01	.01	.01	.01
.01	.01	.01	.00	.00	.00	.00	.00				

Row 4 x=4.23 mm

.00	.00	.00	.01	.01	.01	.01	.01	.01	.02	.02	.02
.02	.02	.02	.02	.02	.02	.02	.02	.01	.01	.01	.01
.01	.01	.01	.00	.00	.00	.00	.00				

Row 5 x=5.92 mm

.00	.00	.00	.01	.01	.01	.01	.01	.02	.02	.02	.02
.02	.02	.02	.02	.02	.02	.02	.02	.01	.01	.01	.01
.01	.01	.01	.00	.00	.00	.00	.00				

Row 6 x=7.62 mm

.00	.00	.01	.01	.01	.01	.01	.01	.02	.02	.02	.02
.02	.02	.02	.02	.02	.02	.02	.02	.02	.01	.01	.01
.01	.01	.01	.00	.00	.00	.00	.00				

Row 7 x=9.31 mm

.00	.00	.01	.01	.01	.01	.01	.02	.02	.02	.02	.02
.02	.02	.02	.02	.02	.02	.02	.02	.02	.01	.01	.01
.01	.01	.01	.01	.00	.00	.00	.00				

Row 8 x=11.00 mm

.00	.00	.01	.01	.01	.01	.02	.02	.02	.02	.02	.02
.02	.02	.02	.02	.02	.02	.02	.02	.02	.02	.01	.01
.01	.01	.01	.01	.00	.00	.00	.00				

Row 9 x=12.7 mm

.00	.00	.01	.01	.01	.01	.02	.02	.02	.02	.02	.02
.02	.02	.02	.02	.02	.02	.02	.02	.02	.02	.01	.01
.01	.01	.01	.01	.00	.00	.00	.00				

Row 10 x=14.39 mm

.00	.00	.01	.01	.01	.02	.02	.02	.02	.02	.02	.02
.03	.03	.02	.02	.02	.02	.02	.02	.02	.02	.02	.01
.01	.01	.01	.01	.00	.00	.00	.00				

Row 11 x=16.08 mm

.00	.00	.01	.01	.01	.02	.02	.02	.02	.03	.03	.03
.03	.03	.03	.03	.03	.02	.02	.02	.02	.02	.02	.01
.01	.01	.01	.01	.00	.00	.00	.00				

Row 12 x=16.08 mm

.00	.00	.01	.01	.02	.02	.02	.02	.03	.03	.03	.03
.03	.03	.03	.03	.03	.03	.02	.02	.02	.02	.02	.02
.01	.01	.01	.01	.00	.00	.00	.00				

Row 13 x=19.47 mm

.00	.01	.01	.01	.02	.02	.03	.03	.03	.03	.03	.03
.03	.03	.03	.03	.03	.03	.03	.02	.02	.02	.02	.02
.01	.01	.01	.01	.00	.00	.00	.00				

Row 14 x=21.16 mm

.00	.01	.01	.02	.02	.03	.03	.03	.03	.04	.04	.04
.04	.04	.03	.03	.03	.03	.03	.03	.02	.02	.02	.02
.02	.01	.01	.01	.01	.00	.00	.00				

Row 15 x=22.85 mm

.00	.01	.01	.02	.02	.03	.03	.04	.04	.04	.04	.04
.04	.04	.04	.04	.03	.03	.03	.03	.03	.02	.02	.02
.02	.01	.01	.01	.01	.00	.00	.00				

Row 16 x=24.55 mm

.00	.01	.02	.02	.03	.03	.04	.04	.04	.04	.04	.04
.04	.04	.04	.04	.04	.03	.03	.03	.03	.03	.02	.02
.02	.01	.01	.01	.01	.00	.00	.00				

Row 17 x=26.24 mm

.00	.01	.02	.03	.03	.04	.04	.05	.05	.05	.05	.05
.05	.05	.04	.04	.04	.04	.03	.03	.03	.03	.02	.02
.02	.01	.01	.01	.01	.00	.00	.00				

Row 18 x=27.94 mm

.00	.01	.02	.03	.04	.05	.05	.05	.06	.06	.06	.05
.05	.05	.05	.05	.04	.04	.04	.03	.03	.03	.03	.02
.02	.02	.01	.01	.01	.00	.00	.00				

Row 19 x=29.63 mm

.00	.02	.03	.04	.05	.06	.06	.06	.06	.06	.06	.06
.06	.06	.05	.05	.05	.04	.04	.04	.03	.03	.03	.02
.02	.02	.01	.01	.01	.00	.00	.00				

Row 20 x=31.32 mm

.00	.02	.04	.05	.06	.07	.07	.07	.07	.07	.07	.07
.06	.06	.06	.05	.05	.05	.04	.04	.04	.03	.03	.02
.02	.02	.01	.01	.01	.00	.00	.00				

Row 21 x=33.02 mm

.00	.03	.05	.06	.08	.08	.08	.08	.08	.08	.08	.07
.07	.06	.06	.06	.05	.05	.04	.04	.04	.03	.03	.03
.02	.02	.01	.01	.01	.00	.00	.00				

Row 22 x=34.71 mm

.00	.04	.07	.08	.10	.10	.10	.10	.09	.09	.09	.08
.07	.07	.07	.06	.06	.05	.05	.04	.04	.03	.03	.03
.02	.02	.02	.01	.01	.00	.00	.00				

Row 23 x=36.40 mm

.00	.05	.09	.11	.12	.12	.12	.11	.11	.10	.09	.09
.08	.07	.07	.06	.06	.05	.05	.05	.04	.04	.03	.03
.02	.02	.02	.01	.01	.00	.00	.00				

Row 24 x=38.10 mm

.00	.09	.14	.15	.15	.15	.14	.13	.12	.11	.10	.09
.09	.08	.07	.07	.06	.06	.05	.05	.04	.04	.03	.03
.03	.02	.02	.01	.01	.00	.00	.00				

```
Row 25 x=39.79 mm
   .00    .17    .21    .21    .19    .18    .16    .15   -.13  \-.12   -.11   -.10
   .09    .08    .08    .07    .06    .06    .05    .05    .04    .04    .03    .03
   .03    .02    .02    .01    .01    .00    .00    .00
Row 26 x=41.48 mm
   .00    .37    .32    .28    .24    .21    .18    .16   -.14   -.13  \-.11   -.10
   .09    .09    .08    .07    .07    .06    .06    .05    .05    .04    .04    .03
   .03    .02    .02    .01    .01    .00    .00    .00
Row 27 x=43.18 mm
   .00    .01 \ .40    .34    .28    .23    .20    .17    .15    .13   -.12  \-.11
   .10    .09    .08    .07    .07    .06    .06    .05    .05    .04    .04    .03
   .03    .02    .02    .01    .01    .00    .00    .00
Row 28 x=44.87 mm
   .00   -.12    .01 \ .36    .30    .24    .20    .18    .15    .13    .12    .11
   .10    .09    .08    .08    .07    .06    .06    .05    .05    .04    .04    .03
   .03    .02    .02    .01    .01    .00    .00    .00
Row 29 x=46.56 mm
   .00   -.12   -.23    .01 \ .29    .24    .20    .17    .15    .13    .12    .11
   .10    .09    .08    .08    .07    .06    .06    .05    .05    .04    .04    .03
   .03    .02    .02    .01    .01    .00    .00    .00
Row 30 x=48.26 mm
   .00   -.12   -.24   -.33    .01 \ .22    .19    .16    .14    .13    .12    .11
   .10    .09    .08    .08    .07    .07    .06    .05    .05    .04    .04    .04
   .03    .03    .02    .02    .01    .01    .00    .00
Row 31 x=49.95 mm
   .00   -.12   -.26   -.35   -.41    .01 \ .16    .15    .13    .12    .11    .10
   .10    .09    .08    .08    .07    .07    .06    .06    .05    .05    .04    .04
   .03    .03    .02    .02    .01    .01    .00    .00
Row 32 x=51.64 mm
   .00 \-.12   -.31   -.39   -.44   -.46    .00 \ .13    .12    .11    .11    .10
   .09    .09    .08    .08    .07    .07    .06    .06    .05    .05    .04    .04
   .03    .03    .02    .02    .01    .01    .00    .00
Row 33 x=53.34 mm
   .00 -1.21 \-.52   -.47   -.48   -.49   -.49    .00 \ .11    .10    .10    .09
   .09    .08    .08    .08    .07    .07    .06    .06    .05    .05    .04    .04
   .03    .03    .02    .02    .01    .01    .00    .00
Row 34 x=55.03 mm
   .00    .05 -1.08 \-.53   -.50   -.50   -.51   -.50    .00 \ .09    .09    .09
   .09    .08    .08    .07    .07    .07    .06    .06    .05    .05    .04    .04
   .03    .03    .02    .02    .01    .01    .00    .00
Row 35 x=56.72 mm
   .00    .23    .00  -1.02\-.52   -.51   -.51   -.51   -.50    .00 \ .09    .08
   .08    .08    .08    .07    .07    .07    .06    .06    .05    .05    .05    .04
   .04    .03    .02    .02    .01    .01    .00    .00
Row 36 x=58.42 mm
   .00    .16    .19   -.05 -1.01 \-.52   -.51   -.51   -.51   -.50    .00 \ .08
   .08    .08    .08    .07    .07    .07    .06    .06    .06    .05    .05    .04
   .04    .03    .03    .02    .01    .01    .00    .00
Row 37 x=60.11 mm
   .00    .10    .16    .15   -.09 -1.01 \-.52   -.51   -.51   -.51   -.50    .00
  \.08    .08    .07    .07    .07    .07    .06    .06    .06    .05    .05    .04
   .04    .03    .03    .02    .01    .01    .00    .00
Row 38 x=61.80 mm
   .00    .07    .12    .14    .12   -.11 -1.01 \-.52   -.51   -.52   -.52   -.50
   .00 \ .07    .07    .07    .07    .07    .07    .06    .06    .06    .05    .05
   .04    .04    .03    .02    .01    .01    .00    .00
Row 39 x=63.50 mm
   .00    .05    .08    .11    .12    .10   -.13 -1.01 \-.52   -.52   -.52   -.52
  -.50    .00 \ .07    .07    .07    .07    .07    .07    .06    .06    .05    .05
   .04    .04    .03    .02    .02    .01    .00    .00
```

```
Row 40 x=65.19 mm
   .00   .03   .06   .09   .10   .11   .08  -.15 -1.01 \-.52  -.52  -.52
  -.52  -.50   .00 \ .07   .07   .07   .07   .07   .07   .06   .06   .05
   .05   .04   .03   .03   .02   .01   .00   .00
Row 41 x=66.88 mm
   .00   .03   .05   .07   .08   .09   .10   .07  -.16 -1.02 \-.52  -.52
  -.52  -.52  -.50   .00 \ .07   .07   .07   .07   .07   .07   .06   .06
   .05   .04   .04   .03   .02   .01   .00   .00
Row 42 x=68.58 mm
   .00   .02   .04   .06   .07   .08   .09   .09   .06  -.17 -1.02 \-.52
  -.52  -.52  -.52  -.50   .01 \.08   .08   .08   .07   .07   .07   .06
   .06   .05   .04   .03   .02   .01   .00   .00
Row 43 x=70.27 mm
   .00   .02   .03   .05   .06   .07   .08   .08   .08   .05  -.17 -1.02
 \-.52  -.52  -.52  -.52  -.50   .01 \ .08   .08   .08   .08   .07   .07
   .06   .06   .05   .04   .03   .01   .00   .00
Row 44 x=71.96 mm
   .00   .01   .03   .04   .05   .06   .07   .07   .07   .07   .05  -.18
 -1.02 \-.52  -.52  -.52  -.52  -.50   .01 \ .09   .09   .08   .08   .08
   .07   .06   .05   .04   .03   .01   .00   .00
Row 45 x=73.66 mm
   .00   .01   .02   .03   .04   .05   .06   .06   .07   .07   .07   .04
  -.18 -1.02 \-.52  -.52  -.52  -.52  -.50   .01 \ .09   .09   .09   .09
   .08   .07   .06   .05   .03   .02   .00   .00
Row 46 x=75.35 mm
   .00   .01   .02   .03   .04   .05   .05   .06   .06   .07   .07   .07
   .04  -.18 -1.02\ -.52  -.52  -.52  -.52  -.50   .01 \ .10   .10   .10
   .09   .08   .07   .06   .04   .02   .00   .00
Row 47 x=77.04 mm
   .00   .01   .02   .03   .03   .04   .05   .05   .06   .06   .06   .07
   .06   .03  -.19 -1.02 \-.52  -.52  -.52  -.52  -.50   .01 \ .11   .11
   .11   .10   .09   .07   .05   .03   .00   .00
Row 48 x=78.74 mm
   .00   .01   .02   .02   .03   .04   .04   .05   .05   .06   .06   .06
   .06   .06   .03  -.19 -1.02 \-.52  -.52  -.52  -.52  -.50   .01  \.13
   .12   .12   .11   .09   .06   .03   .00   .00
Row 49 x=80.43 mm
   .00   .01   .01   .02   .03   .03   .04   .05   .05   .05   .06   .06
   .06   .06   .06   .03  -.19 -1.02 \-.52  -.52  -.52  -.52  -.50   .01
  \.15   .14   .13   .11   .08   .04   .00   .00
Row 50 x=82.12 mm
   .00   .01   .01   .02   .03   .03   .04   .04   .05   .05   .05   .06
   .06   .06   .06   .06   .03  -.19 -1.02 \-.52  -.52  -.52  -.51  -.50
   .01  \.18   .17   .15   .10   .05   .00   .00
Row 51 x=83.82 mm
   .00   .01   .01   .02   .02   .03   .04   .04   .04   .05   .05   .06
   .06   .06   .06   .06   .06   .03  -.19 -1.02\ -.52  -.52  -.52  -.51
  -.50   .01 \ .22   .21   .13   .07   .00   .00
Row 52 x=85.51 mm
   .00   .01   .01   .02   .02   .03   .03   .04   .04   .05   .05   .05
   .06   .06   .06   .06   .07   .06   .04  -.18 -1.02\ -.52  -.52  -.52
  -.51  -.49   .02 \ .32   .14   .08   .00   .00
Row 53 x=87.20 mm
   .00   .01   .01   .02   .02   .03   .03   .04   .04   .04   .05   .05
   .06   .06   .06   .06   .07   .07   .07   .04  -.18 -1.02 \-.52  -.52
  -.52  -.51  -.49   .03 \ .00   .13   .00   .00
Row 54 x=88.90 mm
   .00   .01   .01   .02   .02   .03   .03   .04   .04   .04   .05   .05
   .05   .06   .06   .06   .07   .07   .07   .07   .04  -.18 -1.02 \-.53
  -.53  -.53  -.52  -.43  -.31 \ .45   .00   .00
```

```
Row 55 x=90.59 mm
   .00    .01    .01    .02    .02    .02    .03    .03    .04    .04    .05    .05
   .05    .06    .06    .06    .07    .07    .07    .07    .07    .04   -.18  -1.04
 \-.54   -.56   -.61   -.77   -.04    .09   \.00    .00
Row 56 x=92.28 mm
   .00    .00    .01    .01    .02    .02    .03    .03    .04    .04    .05    .05
   .05    .06    .06    .07    .07    .07    .08    .08    .08    .08    .05   -.19
 -1.07 \-.56   -.57   -.58   -.38   -.36    .00 \  .00
Row 57 x=93.98 mm
   .00    .00    .01    .01    .02    .02    .03    .03    .04    .04    .05    .05
   .05    .06    .06    .07    .07    .08    .08    .08    .09    .09    .09    .06
  -.17  -1.09\  -.57   -.55   -.54   -.76    .00    .00
Row 58 x=95.67 mm
   .00    .00    .01    .01    .02    .02    .03    .03    .04    .04    .04    .05
   .05    .06    .06    .07    .07    .08    .08    .09    .10    .10    .11    .12
   .11   -.10  -1.05 \-.53   -.46   -.37    .00    .00
Row 59 x=97.36 mm
   .00    .00    .01    .01    .02    .02    .03    .03    .04    .04    .04    .05
   .05    .06    .06    .07    .07    .08    .09    .09    .10    .12    .13    .15
   .18    .19    .04   -.91 \-.41   -.25    .00    .00
Row 60 x=99.06 mm
   .00    .00    .01    .01    .02    .02    .03    .03    .03    .04    .04    .05
   .05    .06    .06    .07    .07    .08    .09    .10    .11    .12    .14    .17
   .20    .25    .30    .24   -.63 \-.22    .00    .00
Row 61 x=100.75 mm
   .00    .00    .01    .01    .02    .02    .02    .03    .03    .04    .04    .05
   .05    .06    .06    .07    .07    .08    .09    .10    .11    .13    .14    .17
   .21    .25    .32    .39    .40   -.24   \.00    .00
Row 62 x=102.44 mm
   .00    .00    .01    .01    .02    .02    .02    .03    .03    .04    .04    .05
   .05    .06    .06    .07    .07    .08    .09    .10    .11    .12    .14    .17
   .20    .23    .28    .34    .40    .38    .00    .00
Row 63 x=104.14 mm
   .00    .00    .01    .01    .02    .02    .02    .03    .03    .04    .04    .04
   .05    .05    .06    .06    .07    .08    .09    .10    .11    .12    .14    .15
   .18    .20    .23    .26    .27    .22    .00    .00
Row 64 x=105.83 mm
   .00    .00    .01    .01    .01    .02    .02    .03    .03    .03    .04    .04
   .05    .05    .06    .06    .07    .08    .08    .09    .10    .11    .12    .14
   .15    .17    .18    .19    .17    .12    .00    .00
Row 65 x=107.52 mm
   .00    .00    .01    .01    .01    .02    .02    .03    .03    .03    .04    .04
   .05    .05    .05    .06    .07    .07    .08    .09    .09    .10    .11    .12
   .13    .14    .14    .14    .11    .07    .00    .00
Row 66 x=109.22 mm
   .00    .00    .01    .01    .01    .02    .02    .02    .03    .03    .04    .04
   .04    .05    .05    .06    .06    .07    .07    .08    .09    .09    .10    .11
   .11    .11    .11    .10    .08    .04    .00    .00
Row 67 x=110.91 mm
   .00    .00    .01    .01    .01    .02    .02    .02    .03    .03    .03    .04
   .04    .05    .05    .05    .06    .06    .07    .07    .08    .08    .09    .09
   .09    .09    .09    .08    .06    .03    .00    .00
Row 68 x=112.60 mm
   .00    .00    .01    .01    .01    .02    .02    .02    .03    .03    .03    .04
   .04    .04    .05    .05    .05    .06    .06    .07    .07    .07    .08    .08
   .08    .07    .07    .06    .04    .02    .00    .00
Row 69 x=114.30 mm
   .00    .00    .01    .01    .01    .01    .02    .02    .02    .03    .03    .03
   .04    .04    .04    .05    .05    .05    .06    .06    .06    .06    .07    .07
   .07    .06    .06    .05    .03    .02    .00    .00
```

Row 70 x=115.99 mm

.00 .00 .01 .01 .01 .01 .02 .02 .02 .03 .03 .03
.03 .04 .04 .04 .05 .05 .05 .05 .06 .06 .06 .06
.05 .05 .04 .04 .03 .01 .00 .00

Row 71 x=117.68 mm

.00 .00 .01 .01 .01 .01 .02 .02 .02 .02 .03 .03
.03 .03 .04 .04 .04 .04 .05 .05 .05 .05 .05 .05
.05 .04 .04 .03 .02 .01 .00 .00

Row 72 x=119.38 mm

.00 .00 .00 .01 .01 .01 .01 .02 .02 .02 .02 .03
.03 .03 .03 .04 .04 .04 .04 .04 .04 .04 .04 .04
.04 .04 .03 .02 .02 .01 .00 .00

Row 73 x=121.07 mm

.00 .00 .00 .01 .01 .01 .01 .02 .02 .02 .02 .02
.03 .03 .03 .03 .03 .04 .04 .04 .04 .04 .04 .04
.03 .03 .03 .02 .01 .01 .00 .00

Row 74 x=122.76 mm

.00 .00 .00 .01 .01 .01 .01 .01 .02 .02 .02 .02
.02 .03 .03 .03 .03 .03 .03 .03 .03 .03 .03 .03
.03 .02 .02 .02 .01 .01 .00 .00

Row 75 x=124.46 mm

.00 .00 .00 .01 .01 .01 .01 .01 .01 .02 .02 .02
.02 .02 .02 .03 .03 .03 .03 .03 .03 .03 .03 .03
.02 .02 .02 .01 .01 .00 .00 .00

Row 76 x=126.15 mm

.00 .00 .00 .00 .01 .01 .01 .01 .01 .01 .02 .02
.02 .02 .02 .02 .02 .02 .02 .03 .02 .02 .02 .02
.02 .02 .01 .01 .01 .00 .00 .00

Row 77 x=127.84 mm

.00 .00 .00 .00 .01 .01 .01 .01 .01 .01 .01 .02
.02 .02 .02 .02 .02 .02 .02 .02 .02 .02 .02 .02
.02 .01 .01 .01 .01 .00 .00 .00

Row 78 x=129.54 mm

.00 .00 .00 .00 .01 .01 .01 .01 .01 .01 .01 .01
.01 .02 .02 .02 .02 .02 .02 .02 .02 .02 .02 .02
.01 .01 .01 .01 .01 .00 .00 .00

Row 79 x=131.23 mm

.00 .00 .00 .00 .00 .01 .01 .01 .01 .01 .01 .01
.01 .01 .01 .01 .02 .02 .02 .02 .02 .01 .01 .01
.01 .01 .01 .01 .00 .00 .00 .00

Row 80 x=132.92 mm

.00 .00 .00 .00 .00 .00 .01 .01 .01 .01 .01 .01
.01 .01 .01 .01 .01 .01 .01 .01 .01 .01 .01 .01
.01 .01 .01 .01 .00 .00 .00 .00

Row 81 x=134.62 mm

.00 .00 .00 .00 .00 .00 .00 .01 .01 .01 .01 .01
.01 .01 .01 .01 .01 .01 .01 .01 .01 .01 .01 .01
.01 .01 .01 .00 .00 .00 .00 .00

Row 82 x=136.31 mm

.00 .00 .00 .00 .00 .00 .00 .00 .00 .01 .01 .01
.01 .01 .01 .01 .01 .01 .01 .01 .01 .01 .01 .01
.01 .01 .00 .00 .00 .00 .00 .00

Row 83 x=138.00 mm

.00 .00 .00 .00 .00 .00 .00 .00 .00 .00 .00 .00
.01 .01 .01 .01 .01 .01 .01 .01 .01 .01 .01 .01
.00 .00 .00 .00 .00 .00 .00 .00

Row 84 x=139.70 mm

.00 .00 .00 .00 .00 .00 .00 .00 .00 .00 .00 .00
.00 .00 .00 .00 .00 .00 .00 .00 .00 .00 .00 .00
.00 .00 .00 .00 .00 .00 .00 .00

Row 85 x=141.39 mm

.00	.00	.00	.00	.00	.00	.00	.00	.00	.00	.00	.00
.00	.00	.00	.00	.00	.00	.00	.00	.00	.00	.00	.00
.00	.00	.00	.00	.00	.00	.00	.00				

Row 86 x=143.08 mm

.00	.00	.00	.00	.00	.00	.00	.00	.00	.00	.00	.00
.00	.00	.00	.00	.00	.00	.00	.00	.00	.00	.00	.00
.00	.00	.00	.00	.00	.00	.00	.00				

Row 87 x=144.78 mm

.00	.00	.00	.00	.00	.00	.00	.00	.00	.00	.00	.00
.00	.00	.00	.00	.00	.00	.00	.00	.00	.00	.00	.00
.00	.00	.00	.00	.00	.00	.00	.00				

APPENDIX B

EXPERIMENTAL DERIVATION OF INERTIAL RESISTANCE AND PERMEABILITY

Tebbutt [1995] determined experimentally the values of K and b for the Purolator A13192 filter. The values utilized in this study were determined in a similar experiment and are fairly close to those derived by Tebbutt.

The theoretical base for the experiment is derived from the extended form of Darcy's equation.

$$\nabla P = -\frac{\mu}{K}\mathbf{V}_D - \frac{b\rho}{2}(\mathbf{V}_D \cdot \mathbf{V}_D)\frac{\mathbf{V}_D}{|\mathbf{V}_D|} \qquad (1.3)$$

For a filter within a finite area duct, this equation is integrated over the thickness and width of the filter to produce an algebraic equation describing the pressure drop through the filter.

$$\Delta P = \frac{\mu t}{KA}Q + \frac{b\rho}{2A^2}Q^2 \qquad (B.1)$$

In this equation t is the medium thickness, A is the medium face area normal to the flow, Q is the flow rate, P is the pressure, K is the medium permeability, and b is the inertial resistance. The equation is in the form of a polynomial.

$$\Delta P = mQ + nQ^2 \qquad (B.2)$$

$$m = \frac{\mu t}{KA} \qquad (B.3)$$

$$n = \frac{b\rho t}{2A^2} \qquad \text{(B.4)}$$

By measuring the pressure drop through the filter at varying flow rates, the constants a and b can be determined with the method of least-squares. From these, the permeability and inertial resistance can be determined since the other variables of medium thickness, cross sectional area, air viscosity and density are known.

The experiment used a duct 50.8 mm x 254 mm and 864 mm long as illustrated in Figure 1.3. This experimental duct was driven by a 40 hp induction blower through a series of PVC tubing. A manometer was used to measure the pressure difference upstream and downstream of the filter medium using static pressure taps. At varying flow rates, the pressure drop through the test housing was measured without the filter. The blower was then adjusted to provide different flow rates with the filter inserted. The flow rate was measured by a TSI flow meter. This flow meter measures a standard volumetric flow rate which can be converted to a true volumetric and mass flow rate if one knows the local air density. The pressure was recorded at these varying rates.

Flow Rate (m^3/sec)	Pressure Drop (Pascals)
.0176	271
.0208	330
.0242	405
.0255	412
.0323	576
.0337	594
.0370	683
.0387	723
.0401	760

Table B.1 Filter Constant Experimental Results

From these values, a least square curve fit was created to determine the constants a and b. From these values the permeability and inertial resistance were determined to be 6.72e-11 m^2 and 81833 m^{-1}, respectively. These values for permeability and inertial resistance can be compared to those derived by Tebbutt [1995] which are 7.4e-11 m^2 and 68000 m^{-1}, respectively.

VITA

Wayne Gimlin

Candidate for the Degree of

Master of Science

Thesis: VERIFICATION OF CFD PREDICTIONS FOR AIRFLOW VELOCITY AND PRESSURE THROUGH AN AIR FILTER

Major Field: Mechanical Engineering

Biographical:

Personal Data: Born in Edmond, Oklahoma on June 22, 1967, son of Richard W. Gimlin and Joanne M. Gimlin

Education: Received a Bachelor of Science Degree from the University of Oklahoma, Norman, Oklahoma in Aerospace Engineering in May 1989. Attended the University of Alabama in Huntsville, Huntsville, Alabama for graduate mechanical engineering classes. Completed the requirements for the Master of Science degree with a major in Mechanical Engineering at Oklahoma State University in July 1997.

Experience: Employed by the National Aeronautics and Space Administration in Huntsville, Alabama from May 1989 to May 1995 as an aerospace engineer. From May 1995 to May 1996, worked as a graduate research assistant on the Oklahoma State University Filtration Project. Employed from May 1996 to present as a mechanical engineer at Tinker Air Force Base, Oklahoma.

Professional Membership: None